Soy–Polypropylene Biocomposites

for

Automotive Applications

by

Barbara Elisabeth Güttler

A thesis
presented to the University of Waterloo
in fulfillment of the
thesis requirement for the degree of
Master of Applied Science
in
Chemical Engineering

Waterloo, Ontario, Canada, 2009

AUTHOR'S DECLARATION

I hereby declare that I am the sole author of this thesis. This is a true copy of the thesis, including any required final revisions, as accepted by my examiners.

I understand that my thesis may be made electronically available to the public.

.....

ABSTRACT

For the automotive sector, plastics play the most important role when designing interior and exterior parts for cars. Currently, most parts are made from petroleum-based plastics but alternatives are needed to replace environmentally harmful materials while providing the appropriate mechanical performance and preferably reduce the cost for the final product.

The objective of this work was to explore the use of soy flakes as natural filler in a composite with polypropylene and to investigate the mechanical properties, water absorption and thermal behaviour. For a better understanding of the filler, the soy flakes were characterized extensively with analytical and microscopic methods.

Two types of soy fillers were investigated, soy flakes, provided by Bunge Inc., with a 48 wt-% protein content and an industrial soy based filler with 44 wt-% protein content and provided by Ford.

The size of the soy flakes after milling was mainly between 50 and 200 µm and below 50 µm for the industrial filler. The aspect ratio for all filler was below 5. The soy flakes were used after milling and subjected to two pre-treatment methods: (1) one hour in a 50 °C pH 9 water solution in a 1 : 9 solid-liquid ratio; (2) one hour in a 50 °C pH 9 1M NaCl solution in a 1 : 9 solid-liquid ratio. A control filler, without pre-treatment was considered. The soy flakes were also compared to an industrial soy based filler provided by Ford (soy flour (Ford)). The thermogravimetric analysis showed an onset of degradation at 170 °C for the treated filler (IS_{H_2O} and IS_{NaCl}) and 160 °C for the untreated filler.

The biocomposites formulation consisted of 30 wt-% filler, and polypropylene with/without 0.35 wt-% anti-oxidant Irganox 1010 and with/without the addition of MA-PP as coupling agent. All biocomposites were compounded in a mini-extruder, pressed into bars by injection moulding and tested subsequently.

The mechanical properties of the biocomposites are promising. An increase of the E-modulus was observed when compared to pure polypropylene. The addition of MA-PP as coupling agent increased the yield strength of the biocomposites. When pure polypropylene and the biocomposites were compared no difference could be seen for their yield strength.

The thermal behaviour deduced from differential scanning calorimetry, revealed a similar behaviour for the biocomposites and the pure polypropylene. Only the samples treated in the presence of NaCl and without a coupling agent, appear to have a slightly higher degree of crystallinity. The melt flow index was slightly increased for the biocomposites containing soy flakes pre-treated with NaCl and decreased for biocomposites containing the soy flour.

The water absorption behaviour of the biocomposites was quite similar at the beginning with a slightly lower absorption for the materials with coupling agent. After three months, all samples except the ones treated with water showed a weight loss that can be due to the leaching of the water soluble components in the untreated filler and the NaCl treated filler.

In conclusion, soy flakes represent an attractive filler when used in a polypropylene matrix if an aqueous alkaline pre-treatment is performed. The aqueous alkaline extraction also leads to the recovery of the proteins that can be used in food products while the remaining insoluble material is used for the biocomposites, avoiding the competition with the use of soy for food products.

ACKNOWLEDGEMENTS

I would like to express my sincerest thanks to my supervisor Dr. Christine Moresoli. She has been a fantastic advisor by providing great guidance and simply being a wonderful person throughout my time here. Also, I would like to express my great thanks to my co-supervisor Dr. Leonardo C. Simon for his constructive advice and guidance along the way.

I am very grateful to my thesis committee members Dr. Ali Elkamel and Dr. Raymond L. Legge for their acceptance to be the reader of my thesis.

Funding from OCE (Ontario Center of Excellence) and OSG (Ontario Soybean Growers) for this project is gratefully acknowledged.

I would like to thank Bunge Inc. for providing the soy flakes and A. Schulman for providing the polypropylene. A special thanks to Joseph Emili (ATS Scientific Inc.) for kindly providing the Retsch ZM 200 mill.

Furthermore, I want to thank my colleagues especially Paula Kapustan Krüger, Zena Sin-Nga Ng, Ramila Peiris, Dr. C. Ravindra Reddy, Amirpouyan Sardashti, and Dr. Sang-Young Anthony Shin for their great support and for very constructive discussions.

Specially, I want to thank Daryl Enstone (University of Waterloo, Department of Biology), Mark Gijzen (Agriculture and Agri-Food Canada), and Dr. Carol A. Peterson (University of Waterloo, Department of Biology) who were a great help by analyzing the microscopic soybean structures.

Thanks to Soy 20/20 for kindly providing me with very useful information on the economics side of soybean agriculture.

Mein besonderer Dank gilt meinen Eltern, Elisabeth und Michael, und meinen Geschwistern Bernadette, Katharina, Johannes und Michaela. Vielen Dank für Euer Verständnis und Eure Unterstützung.

Finally, I want to thank my friends, especially Katja, Saskia, Patricia, Beate and Brian who supported me not only through this time but particularly showed a great understanding and confidence in me.

Thanks to everyone who prayed for me.

TABLE OF CONTENTS

LIST OF FIGURES

LIST OF TABLES

ABBREVIATIONS

Abbreviation	
E	Strain
σ	Stress
λ	Wave length
µg	Microgram
µl	Microliter
µm	Micrometer
ADF	Acid detergent fiber
ADM	Archer Daniels Midland Company
AE	Alkaline extraction
ASTM	American Society for Testing and Materials
°C	Degrees Celsius
C	Complete break (Izod Impact Test)
CAD or C$	Canadian Dollar
cm	Centimetre
cm^3	Cubic meter
Co.	Corporation
DIN	Deutsches Institut für Normung/German Institute for Standardization
DSC	Differential scanning Calorimetry
e.g.	Exempli gratia/for example
EDX/EDS	Energy dispersive X-ray spectroscopy
et al.	Et alii/and others
etc.	et cetera/and so forth
eV	Electron volt
FDA	Food and Drug Administration
FESEM	Field emission scanning electron microscopy
FET	Field effect transistor
g	Gram
GmbH	Gesellschaft mit beschränkter Haftung/limited liability corporation
GPa	Giga Pascal
H	Hinge (Izod Impact Test)
i.e.	Id est/ that is
Inc.	Incorporation
IPN	Interpenetrating network
IS	Insoluble soy
ISO	International Organization for Standardization
kg	Kilogram
l	Liter
LCA	Life cycle assessment
M	Molar

m	Meter
m^2	Square meter
MA-PP	Maleic anhydride polypropylene
MCA	Multi channel analyzer
MFI	Melt flow index
min	Minute
MJ	Mega Joule
ml	Milliliter
Mm	Millimeter
MPa	Mega Pascal
N	Newton
n	Number (of tests)
NDF	Neutral detergent fiber
Nm	Newton meter
nm	Nanometer
OEM	Original Equipment Manufacturer
P	Partial break (Izod Impact Test)
PA	Pascal
PAGE	Polyacrylamide gel electrophoresis
PC	Personal computer
PE	Polyethylene
pH	Power of hydrogen
PHA	Polyhydroxyalkanoic acid
PHB	Polyhydroxybutyrate
pI	Isoelectric point
PLA	Poly lactic acid
PP	Polypropylene
PS	Polystyrene
PVA	Poly(vinyl alcohol)
PVDF	Poly(vinylidene) fluoride
rpm	Rounds per minute
S	Svedberg constant
SD	Standard deviation
SDS	Sodium dodecyl sulphate
SEM	Scanning electron microscope
SF	Soy flakes
SPC	Soy protein concentrate
SPE	Soy protein extract
SPI	Soy protein isolate
TDF	Total dietary fiber
T_g	Glass transition temperature
T_m	Melt temperature

TGA	Thermogravimetric analysis
US	United States
Wt	Weight
XRF	X-ray fluorescence

1 INTRODUCTION: OBJECTIVE AND MOTIVATION

The research and development on biocomposites is of increasing interest in many areas where plastics are commonly used. Biocomposites can have advantages such as reduction in weight and cost when compared to the plastics currently used but also can offer an opportunity for recycling. The number of publications on biocomposites has nearly doubled within a two year period. In 2005, 203 published papers on biocomposites were identified using Scholars Portal Search. Two years later, in 2007, there were 369 published papers. This shows the exponential interest in biocomposites and promises an increasing market for biocomposites.

One major application for composites containing materials from natural sources is the automotive sector. Worldwide, the changes in the environmental and the political situation affect the use of cars and their manufacture. Over the past decade, car companies producing for the North American market have focused on cars for customers looking for spacious and affordable cars. Thus, the technology and materials were developed for cars that were massive and heavy which are associated with high fuel consumption. This situation is no longer viable. The automotive sector for the North American market will need to invest in new technologies for lighter materials and more efficient engines. Natural fillers offer a promising avenue for the development of composite materials that will result in weight reduction, decrease in cost and facilitate the waste management of cars.

The challenges in developing alternative materials for the automotive sector reside in the need for materials that are very durable and possess appropriate mechanical properties. Recent studies have shown that biofibers and biological particles, such as wheat straw, hemp and flax, can significantly decrease the weight of the material in comparison to glass fiber composites while maintaining the mechanical properties. It is expected that the weight of a car made from biocomposites could be reduced by at least 50 %. Also, biofibers are generally considered a waste and represents an abundant material which can significantly reduce the price of the biocomposite material. Finally, the degradability of biocomposites represents another advantage when compared to glass fiber composites.

Soybean represents an attractive natural material which is grown in South-western Ontario. Once the oil has been extracted, the residual material, the defatted soy flake containing protein and cellulosic, can be used as animal feed or undergo further processing to recover

the protein. In this study, the defatted soy flake is considered as filler or reinforcement particles in a polypropylene matrix for automotive applications. The first part of the thesis involved the characterization of the soy flakes. The second part of the thesis, considered a pre-treatment of the soy flakes for the removal of proteins. The third and last part of the thesis focused on the development of the composite formulation, and the evaluation of the mechanical and thermal properties of the biocomposites.

This document starts with a literature review on biocomposites (Chapter 2). The equipment, materials and methods employed in this study are described in Chapter 3. The results and discussion are presented in Chapter 4 and focus on the soy flakes and the biocomposite formulation, preparation and testing. The last chapter, Chapter 5, presents the conclusion and recommendations for this work.

2 LITERATURE REVIEW

This chapter deals with the theoretical background on composites from biobased materials. It provides definition of the technical terms used in this thesis and explains in detail recent research work reported by other researchers in the literature.

2.1 APPLICATIONS

In a broad sense a composite is any material that is made of more than one component. Polymer composites are made from a combination of different polymers, or a combination of polymers with other types of material. There are mainly two different types of polymer composites: fiber-reinforced and particle reinforced.

Biocomposites are applicable in many different areas such as furniture for the garden and house, parts for cars and technical devices, and also products for medicine and nanotechnology. Depending on the type of application the biocomposite needs to be developed and tested with focus on the requirements for certain uses. Because the main application for the biocomposite developed during this project is for automotive applications, this section will focus mainly on the use of biocomposites in vehicles.

Natural fibers used in the automotive sector are mostly wood, cellulose, flax, jute, sisal, hemp, and kenaf fibers. Depending on the car part the amount of the fibers varies between 20 and 90 wt-%. Matrices for the biocomposites can be thermosets (e.g. polyester) or thermoplastics (e.g. polypropylene). Most matrices used so far are petroleum-based. An in depth discussion of biobased resins is out of the scope of this document. Table 2-3 presents a list for the year 2006 of automotive manufacturers, also known as original equipment manufacturer (OEM), and the vehicle models that used biocomposites in various exterior and interior applications. Figure 2-1 shows two examples of cars where biocomposites were used for certain parts.

Table 2-1 presents the quantity of natural fibers used in the European Union published by Karus et al. including a forecast for the year 2010 (Karus, Kaup 2002). According to that data up to 100,000 tonnes of natural fibers per year will be used only in the European Union. The authors referred to a study published by Kline & Company about natural fiber composites in North America where an increase in use was predicted from US$ 155 million

to US$ 1,380 million from the year 2000 to the year 2005 (Karus, Kaup 2002). An overview about the quantity of natural fibers used in different car parts is given in

Table 2-2.

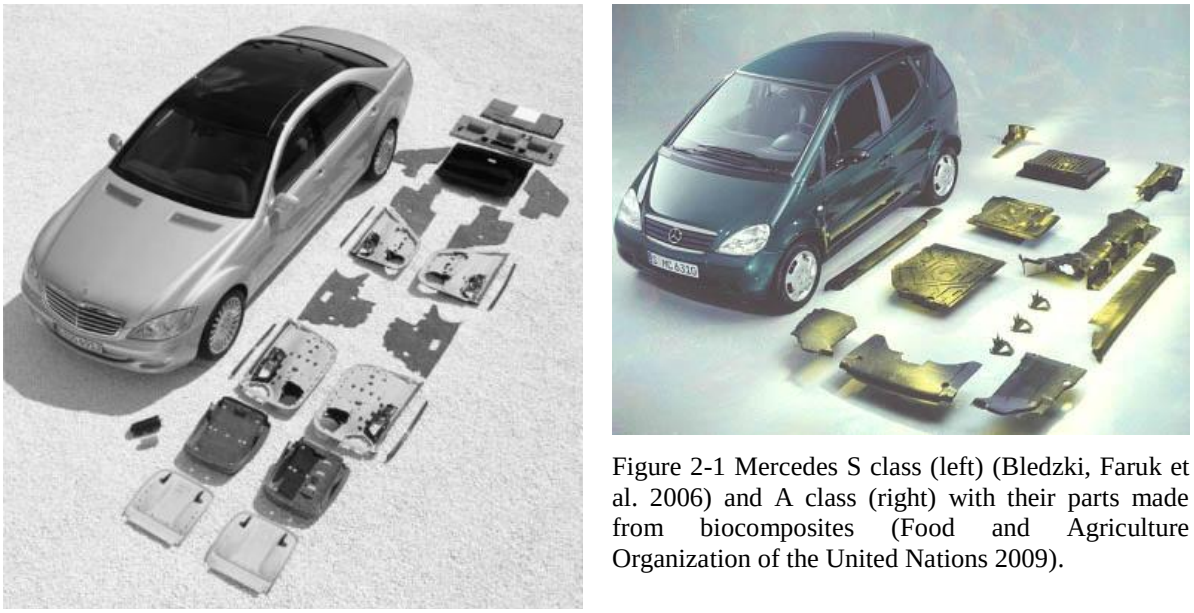

Figure 2-1 Mercedes S class (left) (Bledzki, Faruk et al. 2006) and A class (right) with their parts made from biocomposites (Food and Agriculture Organization of the United Nations 2009).

Table 2-1 Use of natural fibers in the European Union 1996-2010 in tonnes/year (composites, excluding seat upholstery) (Karus, Kaup 2002).

Fiber	1996	1999	2000	2005 (forecast)	2010 (forecast)
Flax	2,100	15,900	20,000		
Hemp	0	1,700	3,500		
Jute	1,100	2,100	1,700		
Sisal	1,100	500	100		
Kenaf	0	1,100	2,000		
Coconut fiber	0	0	1,000		
Total	4,300	21,300	28,300	50,000-70,000	> 100,000

Table 2-2 Typical weight of natural fibers used in automotive components (Bledzki, Faruk et al. 2006).

Automotive component	Typical weight of fiber [kg]
Front door liners	1.2 – 1.8
Rear door liners	0.8 – 1.5
Boot liners	1.5 – 2.5
Parcel shelves up to	2
Seat backs	1.6 – 2
Sunroof sliders up to	0.5
NVH material min	0.5
Headliners average	2.5

In the year 2002, 685,000 tonnes of biofiber composites with a market value of US$ 775 million were used the European and North American market. The main part (two-thirds) of the biocomposites are applicable in many different areas such as furniture for garden and house, parts for cars and technical devices, and also products for medicine and nanotechnology. Depending on the type of application, the biocomposite needs to be developed and tested with a focus on the requirements for certain uses. Because the main application for the biocomposite developed during this project is for automotive applications, this section will focus mainly on the use of biocomposites in vehicles.

The reasons for the use of biocomposites in automotive industry are that they are economical and environmental. A car made with biocomposites can be significantly lighter and thus result in reduced fuel consumption and carbon dioxide emissions. According to Bledzki et al. (Bledzki, Faruk et al. 2006) a car made from biocomposites containing 50 kg of natural fibers can result in a weight reduction of about 10 kg compared to the use of glass-fiber composites. Natural fillers are abundant and often considered as by-product or waste-product during the harvest or processing of plants. This makes natural fillers inexpensive and attractive to reducing the cost of biocomposites based on natural fibers. Briefly, fibers and fillers can be classified according to aspect ratio: fibers have high aspect ratio (mostly higher than 10); fillers have low aspect ratio (mostly lower than 5).

Table 2-3 Automotive manufacturers, models, and components using biofibers (Bledzki, Faruk et al. 2006).

Automotive Manufacturer	Model	Application
Audi	A2, A3, A4, A4 Avant, A6, A8, Roadstar, Coupe	Seat back, side and back door panel, boot lining, hat rack, spare tire lining
BMW	3, 5 and 7 series and others	Door panels, headliner panel, boot lining, seat back
Daimler-Chrysler	A, C, E, S class	Door panels, windshield/dashboard, business table, pillar cover panel
	A class, Travego bus	Exterior under body protection trim
	M class	Instrument panel
	S class	27 parts (43 kg) manufactured from biofibers
Fiat	Punto, Brava, Marea, Alfa Romeo 146, 156	
Ford	Mondeo CD 162, Focus	Door panels, B-pillar, boot liner
Opel	Astra, Vectra, Zafira	Headliner panel, door panels, pillar cover panel, instrument panel
Peugeot	New 406	
Renault	Clio	
Rover	Rover 2000 and others	Insulation, rear storage shelf/panel
Saab		Door panels
SEAT		Door panels, seat back
Volkswagen	Golf A4, Passat Variant, Bora	Door panel, seat back, boot lid finish panel, boot liner
Volvo	C70, V70	
Mitsubishi	Space star	Door panels
	Colt	Instrument panels

2.2 BIOCOMPOSITES: DEFINITIONS

Fowler and his colleagues define composites as: "Composites consist of two (or more) distinct constituents or *phases*, which when married together result in a material with entirely different properties from those of the individual components." (Fowler, Hughes et al. 2006).

A classification scheme for composites is presented in Figure 2-2 and gives a brief overview about the main types of reinforcements which will be explained later.

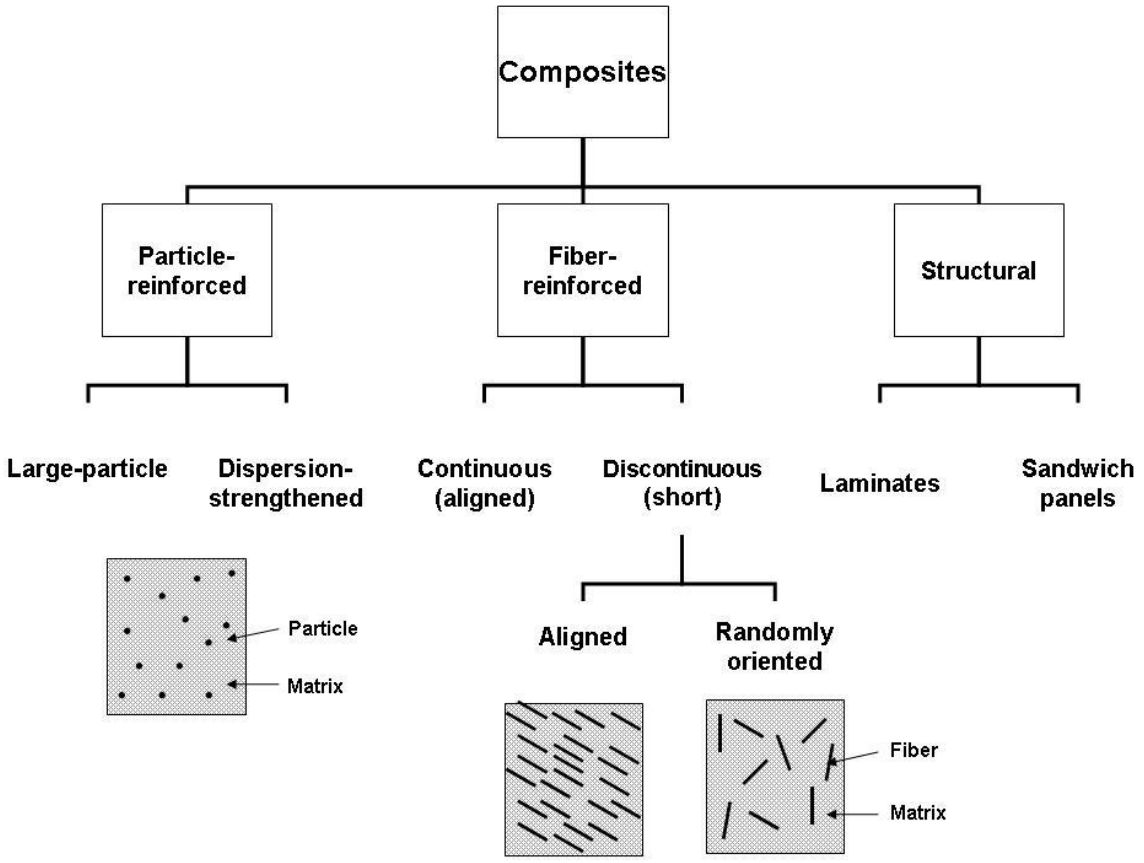

Figure 2-2 Classification scheme for the types of composites (Callister 1996) modified.

In order to call a composite "biobased" or "biocomposite" the following definitions need to be considered:

According to the ASTM standards, biobased materials are materials that contain "carbon based compound(s) in which the carbon comes from contemporary (non-fossil) biological sources."(ASTM International 2008f)

Compared the ASTM definition of biobased materials with their definition of biobased products, a "product generated by blending or assembling biobased materials, either exclusively or in combination with non-biobased materials, in which the biobased material is present as a quantifiable portion of the total product mass of the product."(ASTM International 2008f), the biocomposite from polypropylene and soy flakes can be considered as biobased product, thus a biocomposite.

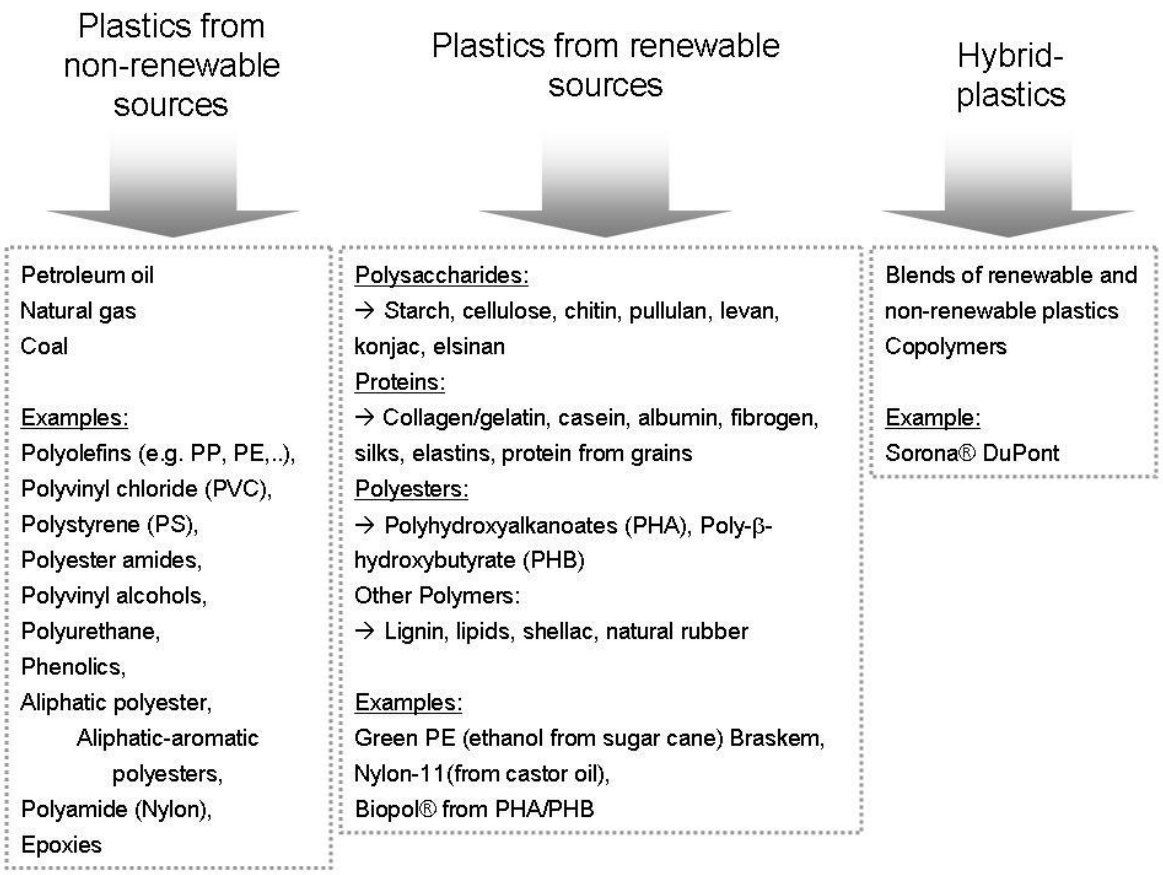

Figure 2-3 Overview about different types of plastics in regards to their sources (Mohanty, Misra et al. 2002, Progelhof, Throne 1993, Netravali, Chabba 2003) modified.

Usually, composites consist of a polymeric matrix and reinforcement. At least one of the components has to be biobased in order to call the final composite a biocomposite. Typical matrices grouped regarding their sources are shown in Figure 2-3. Each of it could function as a matrix in a biocomposite but also a blend of more than one could be used. Renewable plastics are made from natural sources that are obtained from plants or animals or their products. Non-renewable plastics are made from fossil or synthetic sources that can be problematic if supply is limiting. Depending on the sources of the monomers and the polymerization method the plastic can be biodegradable or recyclable. A biodegradable plastic implies the microbial degradation by bacteria and fungi. Polymers like PHA and PHB are made from materials produced by bacteria and can be decomposed by them. Recyclable plastics only imply the possibility of reuse when suitable facilities are available that are also able to separate types of plastic and process them for a new, recycled designation. Biodegradable plastics are used in applications such as compostable bags or grocery and gardening packaging. Because of the inferior balance of properties, especially

of PHA and PHB plastics, petroleum-based plastics are often preferred for applications such as automotive parts.

Filler materials can be classified in the same categories as matrices: biobased and non-biobased. Typical examples for non-biobased filler used in composites are carbon black and calcium carbonate. Biobased and biodegradable fillers are generally particulate materials that originate from stems, leaves or seeds (Figure 2-10). Further details about biobased filler materials are given in Sections 2.3 and 2.3.4.

2.3 BIOCOMPOSITES: COMPOSITION

Biocomposites or natural fiber composites are an alternative to some inorganic composites based on fiber (glass-reinforced composites) or filler (calcium carbonate filled composites). An advantage of natural fiber composites is that they can deliver similar performance but with reduced weight. In some cases they can be 25 – 30 % stronger for the same weight. An overview about the components of biocomposites is shown in Figure 2-4 (Mohanty, Misra et al. 2002).

Around 1941, Henry Ford began experimenting with biocomposites. Initially he started using compressed soybeans to produce composite plastic-like components. Many research projects have shown that natural fibers have very good sound absorption efficiency and are more shatter resistant (Bledzki, Faruk et al. 2006, Mohanty, Misra et al. 2002, Saheb, Jog 1999, Garcia, Garmendia et al. 2008, Holbery, Houston 2006). The energy management during impact (such as in the case of a car accident) for natural fibers is better in comparison to the use of glass fiber in automotive parts. The mass of the car using natural fiber composites is lower and thus it reduces the energy needed for production by of the material by 80 % and the energy (fuel) needed to run the car proportional to the weight savings (Mohanty, Misra et al. 2002).

Beside the synthetically produced polymers that are used as matrices for many kinds of composites there are also biologically produced polymers such as polyhydroxybutyrate (PHB). An overview about the most common polymers is presented in Figure 2-3. PHB is a polyhydroxyalkanoic acid (PHA), a polymer belonging to the polyesters class that was first isolated and characterized in 1925 by French microbiologist Maurice Lemoigne. PHA represent a complex class of storage polyesters which can be produced by micro-organisms (Gram-positive and Gram-negative bacteria such as *Bacillus megaterium* or *Alcaligenes eutrophus* as well as by some Archaea) apparently in response to conditions of

physiological stress (Rehm, Steinbüchel 1999). The polymer is primarily a product of carbon assimilation (from glucose or starch) and is employed by micro-organisms as a form of energy storage to be metabolized when other common energy sources are not available. Microbial biosynthesis of PHB starts with the condensation of two molecules of acetyl-CoA to give acetoacetyl-CoA which is subsequently reduced to hydroxybutyryl-CoA. This latter compound is then used as a monomer to polymerize PHB (Steinbüchel 2002). The bacteria-produced polyester (Biopol®) was processed and its properties tested after reinforcing with wood cellulose. The cellulose fibers improved the strength and stiffness of PHB. The composite obtained was very brittle (Mohanty, Misra et al. 2000). An "All-Cellulose Composite", where matrix and filler is cellulose was described by Nishino et al. This biodegradable composite showed advantage attributed to reduced interfacial energy between the fiber and the matrix (Nishino, Matsuda et al. 2004).

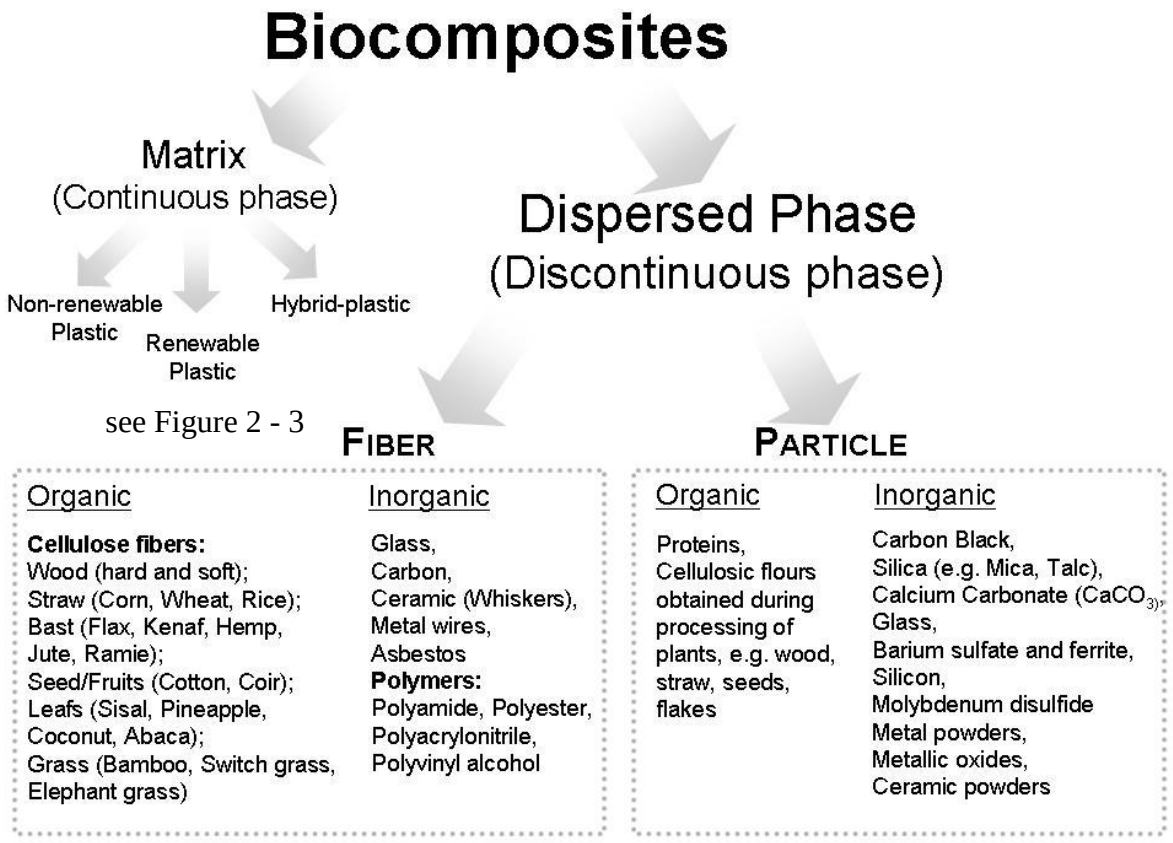

Figure 2-4 Overview about possible biocomposite components.

2.3.1 FIBER AS REINFORCEMENT

Fiber-reinforced composites are materials in which a fiber made of one material is embedded in another material. Any material which can reinforce the properties of the composite can be used as a fiber. Depending on the application of the composite there are different treatments of the reinforcements. Biological and chemical composition as well as particle size (nanocomposites) and formation are important parameter of the fiber which can have a significant effect on the composite. Fiber-reinforced composites can take diverse forms such as continuous bundles of fibers, woven fabrics and chopped fibers.

In Figure 2-2 is a schematic of the structures of fiber and particle reinforced composites. Fiber reinforced materials can be continuous aligned or discontinuous, randomly orientated or aligned due to use of short fibers. In comparison to metals, polymers generally possess about 100 times lower moduli and about 5 times lower strengths. The use of particles or fibers as reinforcements can improve the stiffness and strength of the composites and thus expand the application of plastics. Some examples of non-biobased fibers used primarily for reinforcement are glass fibers, carbon fibers and oriented polymeric fibers (McCrum, Buckley et al. 1990). Successful reinforced polymers are fiber-reinforced plastic (epoxy resin in which are embedded continuous Kevlar and carbon reinforcing fibres), carbon-fibre reinforced polymer (nylon), Fiberglas^{TM}, and reinforced material at several different levels (carbon black with polymer, rigid cords) (McCrum, Buckley et al. 1990). An overview about natural fibers is given in Figure 2-10. Natural Fibers are grouped into three types: seed hair (e.g. cotton), bast fibers (e.g. ramie, jute, flax), and leaf fibers (e.g. sisal, abaca), depending upon the source (Saheb, Jog 1999). Another classification of natural/biofibers is shown in Figure 2-5.

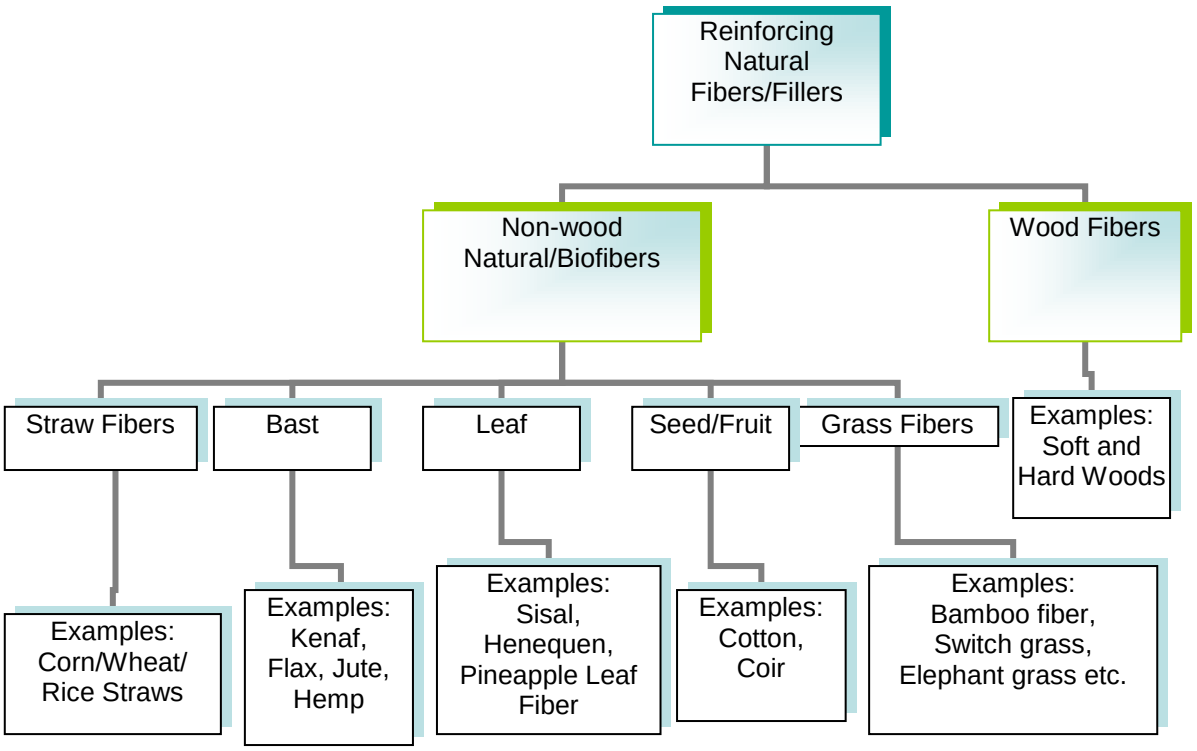

Figure 2-5 Classification of natural/biofibers (Mohanty, Misra et al. 2002) adapted.

The properties of some common natural fibers are presented in Table 2-5 as well as of glass fiber. The tensile strength of glass fiber is much higher than that of natural fibers even though the modulus is of the same order. However, when the specific modulus (modulus/specific gravity) of natural fibers is considered, the natural fibers show values which are comparable to or better than those of glass fibers (Saheb, Jog 1999). For comparison the specific density of the filler material used in this study is presented in Table 2-4.

Table 2-4 Specific density of the filler, obtained through gas pycnometry analysis, carried out by Porous Materials, Inc. (PMI), Ithaca, NY, USA.

	IS_{H_2O}	**IS_{NaCl}**	**Soy Flakes (Bunge)**	**Soy Flour (Ford)**
Specific density	1.6550	1.3743	1.4379	1.3366
SD (n = 10)	0.05683113	0.07152630	0.13172906	0.03477930
Volume [ml]	0.58120	0.53900	0.34460	0.55427
SD (n = 10)	0.01945822	0.02728451	0.03126304	0.01405450

Table 2-5 Properties of natural fibers and E-glass fiber used in fiber-reinforced composites (Brouwer 2000) (* tensile strength strongly depends on type of fibre, being a bundle or a single filament); **(Saheb, Jog 1999).

	Density [g/cm^3]	Tensile strength* [10^{6}N/m^2]	E-modulus [GPa]	Specific gravity**	Specific modulus**	Specific density [E/density]	Elongation at failure [%]	Moisture absorption [%]	Price raw [US$/kg] (mat/fabric)
Cotton	1.51	400	12			8	3-10	8-25	1.5-2-2
Abaca	1.5	980	N/A			N/A	N/A	N/A	1.5-2.5
Sisal	1.33	600-700	38	1.3	22	29	2-3	11	0.6-0.7
Coir	1.25	220	6			5	15-25	10	0.25-0.5
Ramie	1.5	500	44			29	2	12-17	1.5-2.5
Jute	1.46	400-800	10-30	1.3	38	7-21	1.8	12	0.35 (1.5/0.9-2)
Hemp	1.48	550-900	70			47	1.6	8	0.6-1.8 (2/4)
Flax	1.4	800-1500	60-80	1.5	50	26-46	1.2-1.6	7	1.5 (2/4)
Pineapple**	N/A	170 MPa	62	1.56	40	N/A	N/A	N/A	N/A
Sunhemp**	N/A	389 MPa	35	1.07	32	N/A	N/A	N/A	N/A
E-glass	2.55	2400	73	2.5	28	29	3	-	1.3 (1.7/3.8)

2.3.2 PARTICLES AS REINFORCEMENT

Non-biobased particles which are used for reinforcing polymer composites are minerals, ceramics, metals or amorphous materials such as carbon black. A filler should have a low aspect ratio and can be added to a polymer matrix for a variety of functions. The addition of fillers can affect physical, mechanical, thermal or electrical properties and cost. The most commonly used general purpose fillers are clays, silicates, talcs, carbonates, asbestos fines and paper. It is possible fillers can also act as pigments, e.g., carbon black, chalk and titanium dioxide or act as a lubricant, e.g. graphite and molybdenum disulfide. By using magnetic materials as fillers magnetic properties can be obtained. Metallic fillers are used to increase specific gravity or impart higher thermal and electrical conductivity.

The particles can be used to increase the modulus of the matrix, to decrease the permeability of the matrix and to decrease the ductility of the matrix. Particles are specially

used to decrease the cost of composites. The word filler is generally associated with a low cost material that is added to the formulation primarily to decrease cost. However some fillers can contribute to the improvement of certain properties, those are known as functional fillers. A very popular filler used as a reinforcement particle is carbon black when used in natural rubber/caoutchouc. It is mainly derived from aromatic oil in petroleum or from natural gas (Jong 2007).

Making particle reinforced composites is much easier and less costly than making fiber reinforced thermoplastic composites. With polymeric matrices, the particles are more easily added to the polymer melt in an extruder or injection moulding apparatus during polymer processing. Inorganic (non-biobased) fillers do not have a hydrocarbon basis in their chemical structure. Inorganic substances used as fillers are minerals, ceramics and metals. Some examples for inorganic filler are silica (SiO_2), titania, alumina, calcium carbonate ($CaCO_3$), aluminium hydroxide, strontium carbonate ($SrCO_3$), clay, talk and mica. Biobased particles used as fillers can be any kind of plant material or by-product during the processing of plant materials that has a shape which is particle-like. Most plant materials are milled to flour like particles and used as filler in composites.

2.3.3 THE MATRIX: POLYPROPYLENE

In fiber or particle reinforced composites the matrix is the material in which the dispersed phase (fiber or particle) is embedded (Figure 2-2). There are common polymer matrices used in composites, they can be classified in thermoplastics, thermosets or elastomers. Thermoplastics can be melted during processing, which is convenient when recycling. Thermosets are processed by transforming a viscous liquid into a rigid polymer upon polymerization; they cannot be melted after the polymerization. Polyethylene (PE) and polypropylene (PP) belong to a group of polymers known as polyolefins, the synthetic polymer with the largest volume of applications. Polypropylene because of its high-volume, low-cost has been produced in large quantities and widely used in fabrication of automotive parts since 1959. Polypropylene is a obtained by polymerization of propene. The most common polymerization method for manufacturing polypropylene is the Ziegler-Natta system introduced in the early 1950s', metallocene catalysts were introduced in the late 1980s' and today they contribute to a minor fraction of the total polypropylene manufacturing. Polypropylene (Figure 2-6 a) belongs to the thermoplastics and has a semi-crystalline crystalline (isotactic or syndiotactic) or amorphous (atactic) morphology. The melting temperature of polypropylene is at 176 °C (100 % isotactic) and the glass transition temperature at -20 °C (Progelhof, Throne 1993, McCrum, Buckley et al. 1990). At

temperatures below -20 °C (T_g) polypropylene is brittle. A classification scheme for the characteristics of the polymer molecules is shown in Figure 2-7.

a) 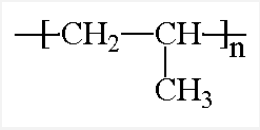

b) 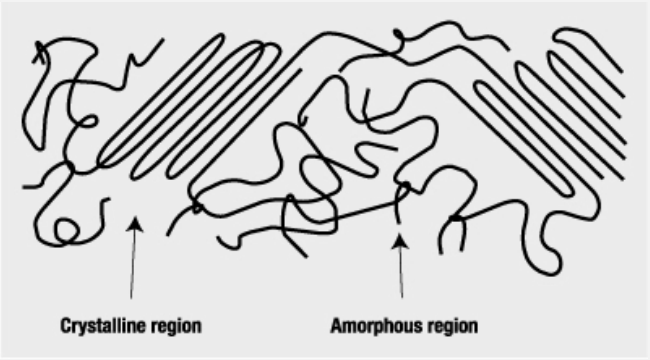

Figure 2-6 a) Structure of polypropylene and b) Crystalline and amorphous regions after polymerization (Rosner 2001).

The density of semi-crystalline polypropylene is between 0.9 – 0.91 g/cm^3 (homopolymer). The elastic modulus for polypropylene is between 1.05 – 2.10 GPa (homopolymer). Total burning of polypropylene without additives produces CO_2 and water. The calorific value of polypropylene is 43.5 MJ/kg which shows a high amount of energy. The energy consumption for producing of the feedstock (pellets) is about 80 MJ/kg. Polypropylene has good mechanical properties, low density, durability, resistance to X-rays, low water permeability, relatively good impact resistance (when modified with copolymers) and good temperature resistance up to 135 °C. It also has good properties in terms of electrical isolation. These properties, the low cost and easy processing allows a large variety of uses: various household items, plastic packaging, automobile parts, batteries, (garden) furniture, syringes, bottles and appliances.

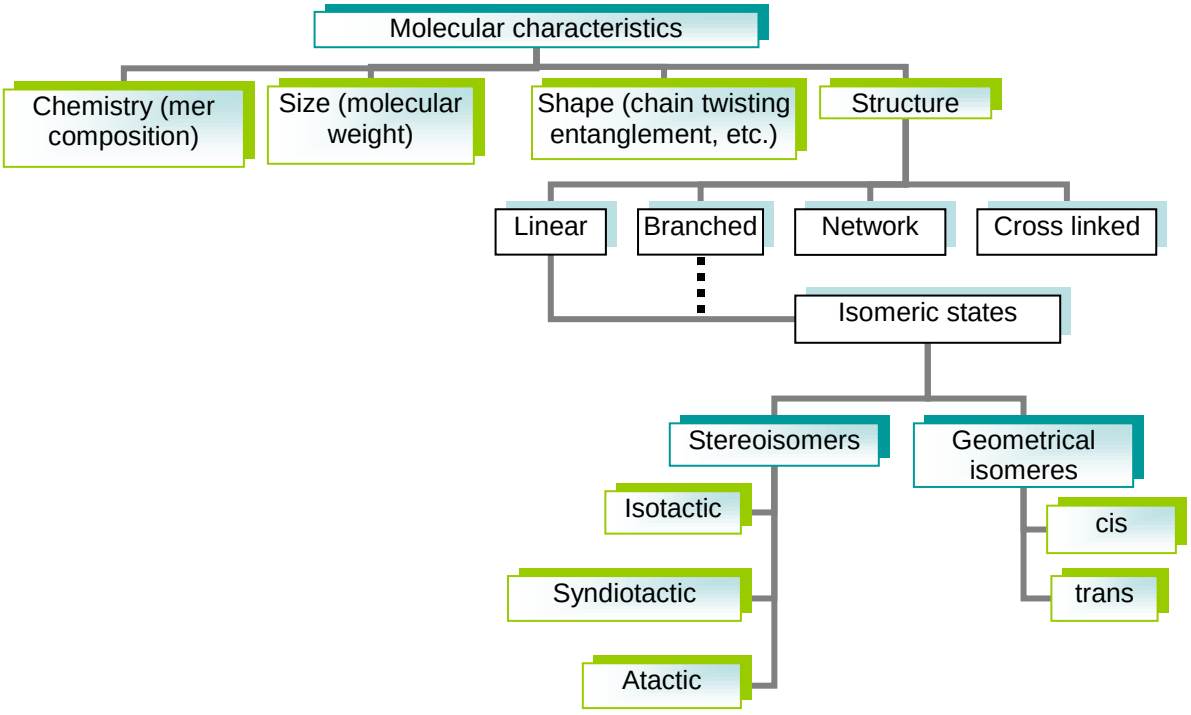

Figure 2-7 Classification scheme for the characteristics of polymer molecules (Callister 1996) adapted.

2.3.4 THE FILLER: SOY

Soybeans (Figure 2-8) belong to the Leguminosae (legumes) family and are characterized by a high protein content. Therefore, they have a wide use as ingredient in many foods. During the harvest and the processing of soy plants there are several by-products with potential use in biocomposites. The processing of soy products and their uses are shown in Figure 2-9.

From the perspective of renewable materials and environmental reasons, soy protein and other soybean products have been investigated as a component in plastics and adhesives, but have been rarely investigated as a reinforcement component in elastomers (Jong 2007). Dried soy plastics have a 50 % higher modulus than that of currently used epoxy engineering plastics. Reduction of water sensitivity by soy protein plastic by using certain techniques has led to new uses in higher moistures environments. The final product resulted in improved biodegradable plastics having a high degree of flowability for easy processing, high tensile strength and water resistance (Mohanty, Misra et al. 2000).

The main bioconstituents of biopolymers in plants are cellulose, hemicelluloses, pectin and lignin. Different fractions are present in each part of the plant or in different species. Coir for example contains a very high amount of lignin and a low amount of cellulose (Mohanty, Misra et al. 2000). The use of soybean stock-based nanofibers has been reviewed by B. Wang (Wang, Sain 2007). By chemo-mechanical treatment cellulose nanofibers were extracted and used as reinforcements in poly(vinyl alcohol) (PVA) and polyethylene (PE). Cellulose nanofibers have a theoretical stiffness of up to 130 GPa and strength up to 7 GPa. The mechanical performance is comparable to materials such as glass fibers or carbon fibers (Wang, Sain 2007).

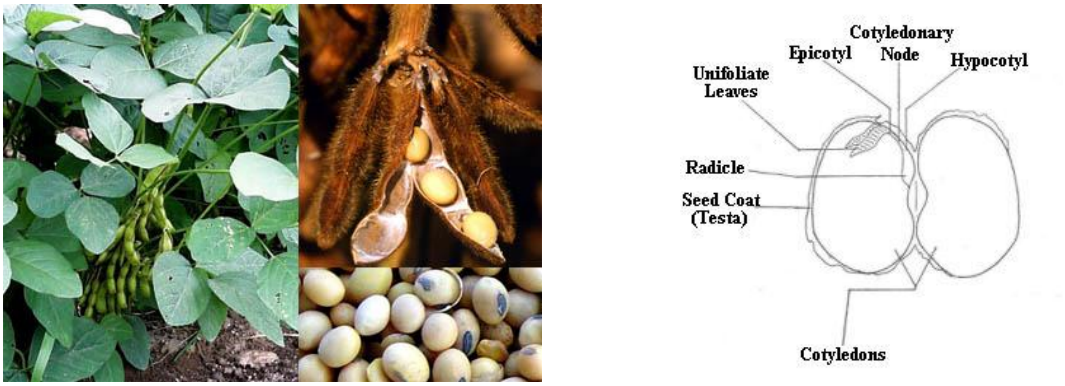

Figure 2-8 Soybean plant and soybeans (left) (Kennislink 2009); schematic draw of a bean with its components (right).

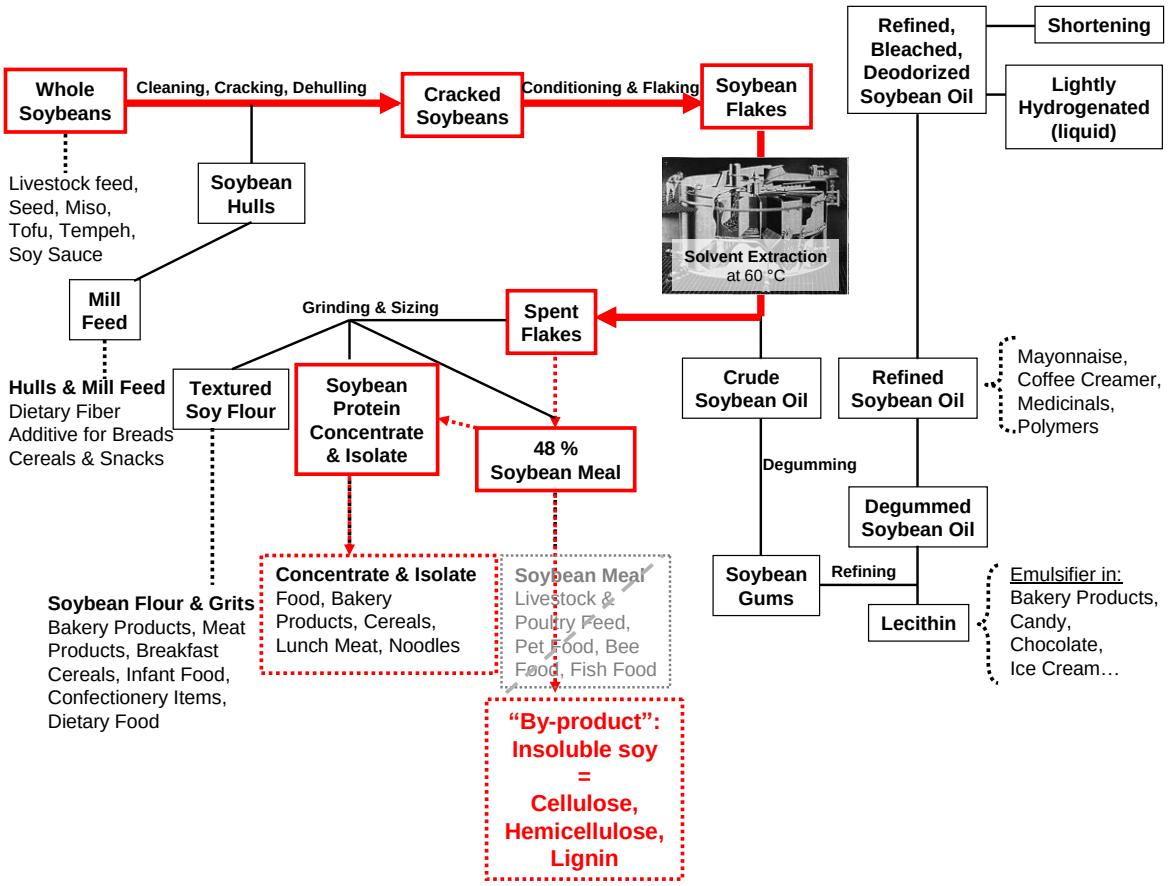

Figure 2-9 Soybean processing with the process for defatted soy flakes (spent flakes) and their further processing to obtain insoluble soy (IS) highlighted ((National Soybean Research Laboratory), modified. Products are highlighted to illustrate the current use of soybean meal.

SOY HULLS

Soy hulls are usually toasted to destroy their urease activity and ground to the desirable particle size. The soybean hull is high in fiber (73 wt-%) and low in protein (9.4 wt-%). The protein is highly degradable, while the cell wall is low in lignin and highly digestible. Ground hulls are often sold as soy mill feed. This feed contains some meal so the protein content may equal 12 to 14 wt-%. Soy hulls are very palatable and are typically used to increase bulk in rations of fine texture. They are a good source of digestible fiber, but not as desirable as effective fiber. The maximum level of incorporation in dairy cattle rations should be 20 - 25 % of the dry matter (Ng 2008).

SOY PROTEINS

Soy proteins have adhesive properties. In the year 2000 not even 0.5 % of the available soy protein was used in manufactured product applications, such as in the automotive sector Mohanty, Misra et al. 2000). Paetau investigated soy protein concentrates (SPC) and isolates (SPI) with respect to their preparation and processing conditions for making biodegradable plastics. The optimal pH was at the isoelectric point ~4.5 (Paetau, Chen et al. 1994). The soy protein was treated with different acids depending on the required final properties. After compression moulding at different moisture levels and moulding temperatures the properties were measured (yield strength, elongation, Young's modulus and water absorption). The material obtained from SPC and SPI were brittle and rigid with similar values in tensile strength, yield strength and elongation. The water absorption of the specimens from SPC was higher than those of plastics from SPI. Sue et al. tested, amongst other properties, the mechanical behaviour of engineered soy (from soy protein) and compared to the Young's modulus and storage modulus with those of epoxy and polycarbonate. The authors also compared the properties of moisturized and dried soy plastics. Dry soy plastic possessed a significantly higher value for the Young's modulus (4.4 GPa), whereas epoxy with 3 GPa and polycarbonate with 2.1 GPa was below that value (Sue, Wang et al. 1997). Wang et al. prepared bio–composites from SPI and cellulose whiskers where the soy protein served as matrix for the cellulose reinforcement (Wang, Cao et al. 2006, Vaz, Mano et al. 2002). Also Vaz et al. used soy protein isolates as a matrix which they reinforced with ceramic filler. Wang and Vaz used glycerol for the plasticization. Both showed improved mechanical properties for their SPI materials. Soy protein isolates (SPI) and soy protein concentrates (SPC) were also used to make biofilms and biodegradable plastic films (Schmidt, Giacomelli et al. 2005, Swain, Rao et al. 2005, Das, Routray et al. 2008).

SOY FLAKES

Soy flakes are an abundant by-product from the isolation process of soy protein and contains mainly soy protein and cellulose. The cost of soy flakes is much lower than that of extracted and purified proteins, and is usually used as animal feed. Zhang et al. used soy flakes, called "soy dreg", to produce a biodegradable plastic. The group used glycerol as plasticizer and glutaraldehyde as cross-linker. After compression-moulding the material was tested for tensile strength of the soy dreg plastic with 6.8 wt-% glutaraldehyde and was found to be 14.5 MPa. A coating of the soy dreg plastic sheets based on castor-oil-based polyurepolyurethane/nitrochitosan interpenetrating network (IPN) resulted in a significantly higher strength and water resistance of the sheets with a tensile strength of 24.6 MPa in the

dry state and 9.8 MPa in the wet state. The sheets were also put in a special medium with microorganisms and the soy dreg plastic was found to be fully biodegradable (Zhang, Chen et al. 2003). A rubber composite using spent soy flakes as reinforcement was developed by Jong producing a material with increased tensile strength at break and toughness (Jong 2007).

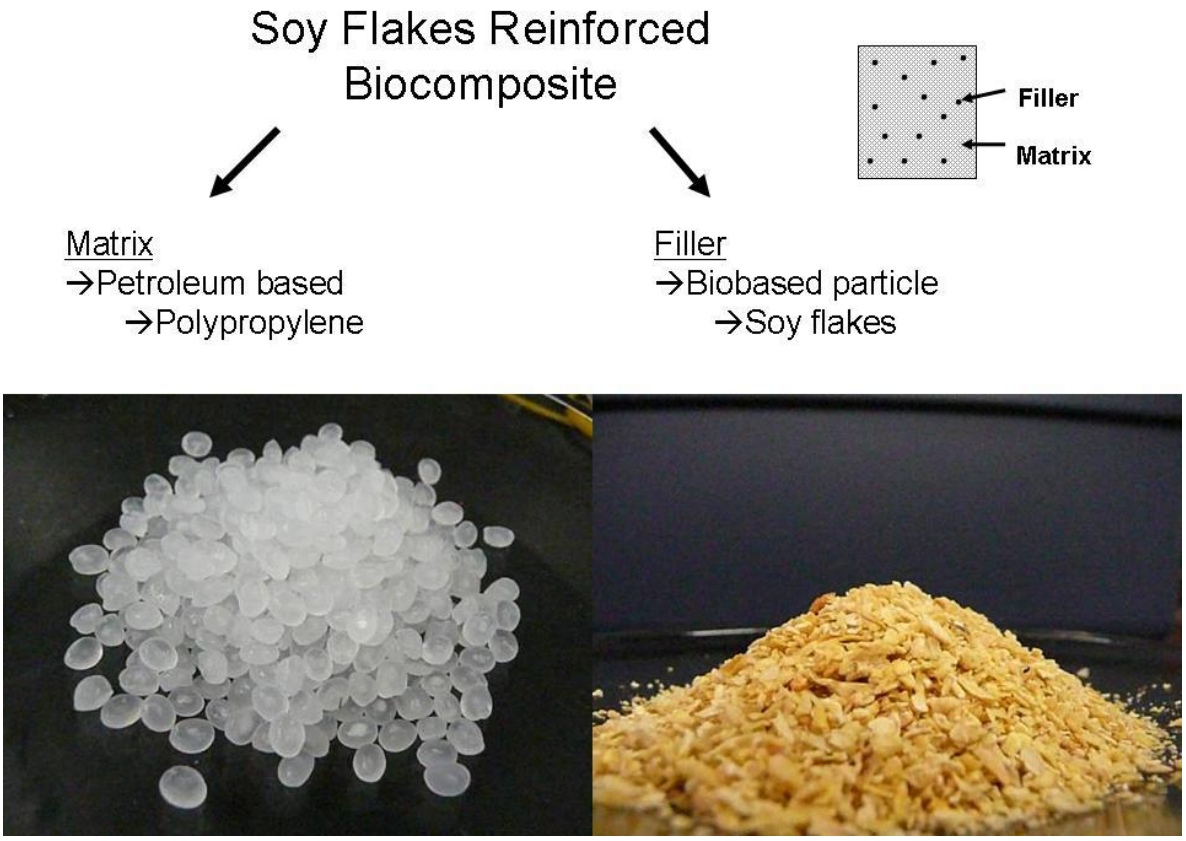

Figure 2-10 Components of soy flake reinforced biocomposites.

SOYBEAN MEAL

Soybean meal is the most commonly used plant protein supplement. It is the residual product at the end of the oil extraction process from soybeans. Oil can be extracted mechanically or via the utilization of solvents. The use of solvents is the most efficient and common technique resulting in a meal that contains about 48 wt-% crude protein. Typically, mill feed (ground soy-hulls) will be blended with this meal to produce the more common 44 wt-% crude protein soybean meal. There is also an expeller or old processed soybean meal that contains 42 wt-% crude protein and 5 wt-% oil. Soybean meal has a very high nutritional value and has a modest content of rumen undegradable protein (RUP). The

amino acid methionine is the most restrictive component to milk protein synthesis in soybean meal.

In Table 2-6 and Table 2-7 the composition of soybeans, defatted soy flour, SPC, and SPI according to Solae (Nguyen) and AMD (Archer Daniels Midland Company 2004 - 2005), two of the biggest soybean producers in Canada, is presented. The composition is susceptible to changes depending on breed type and processing. Soybeans used for the extraction of oil will contain a higher amount of oil and soybeans used for the extraction of proteins will contain a higher amount of proteins.

COMPOSITION OF SOY MATERIAL

Depending on the breed of soybean, the protein and the fat content can vary. Soybean breeds used for the extraction of proteins are higher in protein content where soybeans used for the extraction of oil are higher in fat. Table 2-6 shows a typical composition of soybeans and Table 2-7 shows the composition of different products from soybean processing which are used in the food industry.

Table 2-6 Composition of soybeans according to Solae (Nguyen).

Component	Details
40 % Protein	Phytic acid, trypsin inhibitors, Bowman-Birk inhibitor, globulins, phenolics
15 % Mono- & Oligosaccharids	Succhrose, raffinose, stachyose
15 % Dietary fibers	Soluble and insoluble fiber
20 % Oil	Lecithin, sterols, vitamin E
10 % Other	Moisture and ash

The soy flakes, provided by Bunge Inc., contain about 48 % protein according to the company. The insoluble carbohydrates can be cellulose, hemicellulose, and pectin. The containing sugar in soybeans is succhrose, raffinose, and stachyose. The pure ash content for soybeans is usually around 6 % and the fat content of the defatted soy flakes is below 1 %.

Table 2-7 Composition of different soybean products from ADM and Solae (*based on SUPRO®670 and FXP H0219D); TDF = total dietary fiber.

Soybean product	Composition	
Defatted soy flakes [ADM]	53 %	Protein (N x 6.25)
	9 %	Moisture
	3 %	Fat
	18 %	Total dietary fiber
	30 %	Carbohydrates (incl. TDF)
Soy protein concentrate (SPC) [ADM]	68 – 72 %	Protein (N x 6.25)
	6 – 9 %	Moisture
	3 – 4 %	Fat
	19 – 20 %	Total dietary fiber
	20 – 21 %	Carbohydrates (incl. TDF)
Soy protein isolate (SPI) [ADM]	82 – 90 %	Protein (N x 6.25)
	6 – 7 %	Moisture
	4 – 5.5 %	Fat
	5 – 8 %	Ash
	5.3 – 7.4	pH
Soy protein isolate (SPI)*[Solae]	> 90 %	Protein (N x 6.25)
	5.5 – 6 %	Moisture
	1 – 5.5 %	Fat
	5 – 6 %	Ash
	7.2 – 7.7	pH

VALUE AND SIGNIFICANCE FOR THE NORTH AMERICAN MARKET

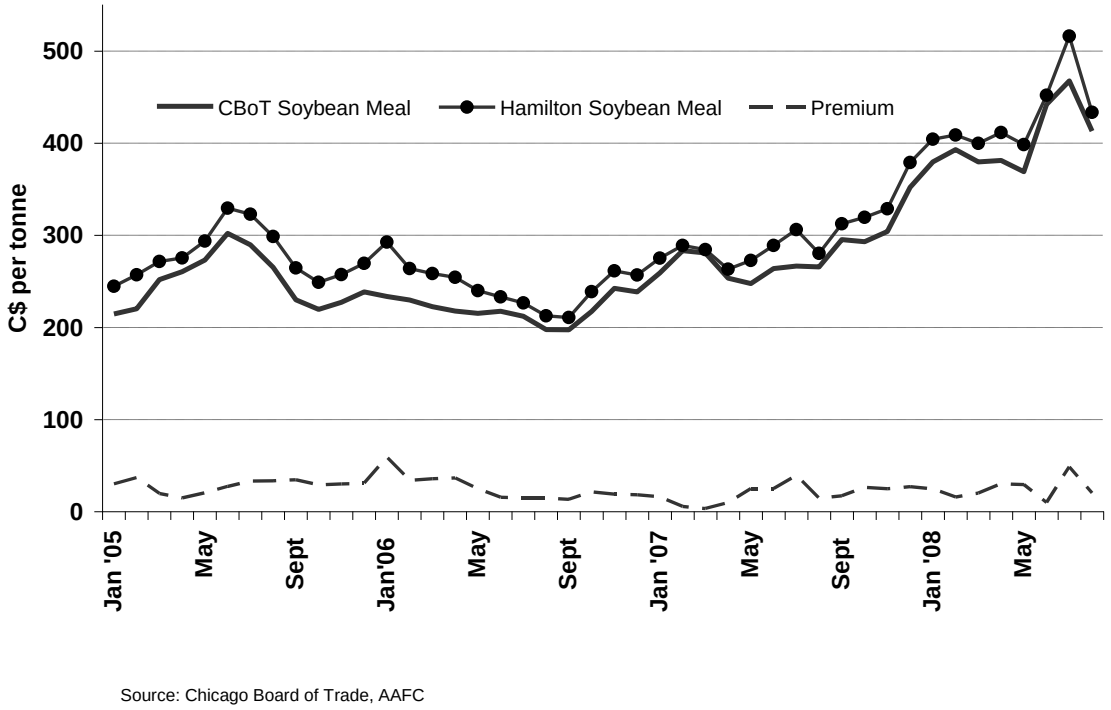

Source: Chicago Board of Trade, AAFC

Figure 2-11 Soybean meal prices determined using the Chicago Board of Trade (CBOT) price for in-store Decatur 48 % protein (Soy 20/20 8/2008).

In Figure 2-12 the seven largest soybean growers are presented with their share of produced soybeans. In Canada 90 wt-% of the soy meal is produced in Hamilton and Windsor, Ontario; and 80 wt-% of the soybean is sold as soybean meal. All facilities in Canada have the capacity to produce 1.7 million tonnes of soybean meal per year (Soy 20/20 8/2008). Factors affecting the price of soybean meal are: increased production of renewable fuel, soybean crushing capacity expansion, exchange rate volatility, soybean production and livestock industry dynamics (Soy 20/20 8/2008).

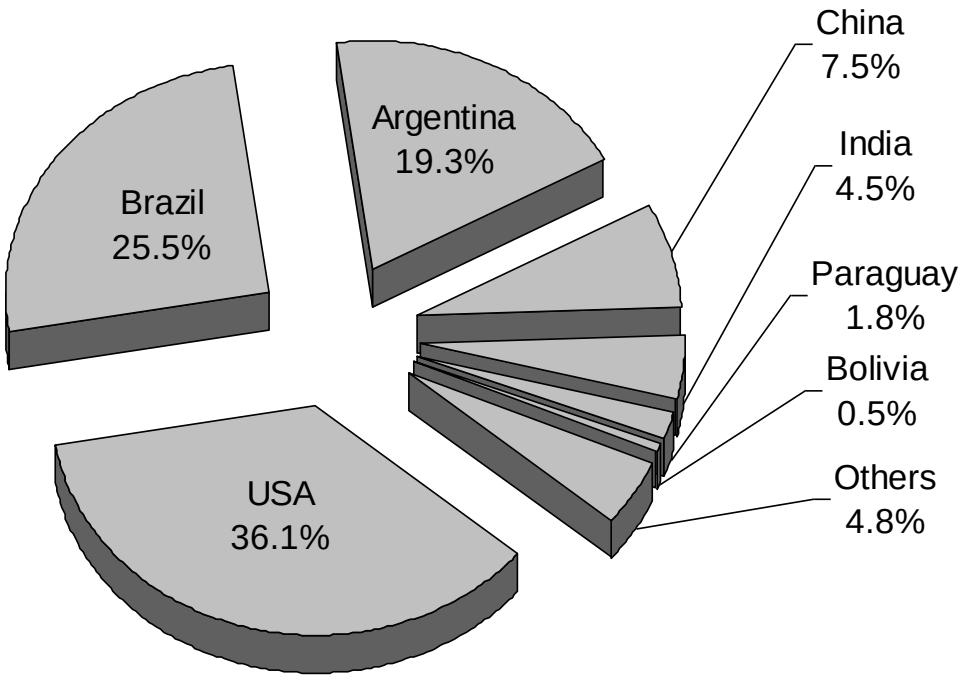

Figure 2-12 World soybean producer of a total amount of 223,270,000 tonnes soybeans in 2008/2009 according to USDA (USDA, 2008).

2.3.5 ADDITIVES

Additives in bioplastic composites are used to fulfill specific needs during manufacturing or to improve properties during the life time of the materials. Additives commonly used are coupling agents, antioxidants, stabilizers, pigments, lubricants or biocides. Biocides in bioplastics and biocomposites may be more relevant than in other composites due to their ability to inhibit the growth of different microorganisms (bacteria, fungi) responsible for biological deterioration of the materials.

COUPLING AGENTS

A coupling agent is a chemical substance which is able to react at the interface between the dispersed phase (fiber or filler) and the matrix. In some instances it is also possible to covalently bind an inorganic filler or fiber to organic resins. This promotes a stronger interaction at the interface. Bataille and his colleagues have shown that the treatment of fibers with coupling agents can improve significantly the interfacial adhesion and therefore the mechanical properties of the composites (Bataille, Ricard et al. 1989).

It is often reported that natural fibers based on cellulose have hydrophilic surface properties and therefore inherent incompatibilities with hydrophobic thermoplastics, like polyolefins for example. This leads usually to poor interfacial adhesion when dispersing cellulose based materials in polyethylene or propylene. The use of maleic anhydride grafted polyolefin as a coupling agent was found to be one of the most efficient for composites using cellulose based materials (fiber or filler) and polyolefin matrixes. Composites were produced by the melting mixing method with maleic anhydride grafted polypropylene (MA-PP) as compatibilizer and the mechanical properties of the composites improved drastically. The mechanism is attributed to stronger interfacial adhesion caused by esterification between anhydride groups of MA-PP and hydroxyl groups of cellulose (Qiu, Zhang et al. 2005). The preparation of biocomposites using coupling agents can be executed in two ways. The first way is a pre-treatment of the natural fibers with maleated polymer; then the further processing steps are the same as with untreated fibers. The second way is to combine the fibers with maleic anhydride during the extrusion processing; the polymer matrix and maleic anhydride can be added with peroxide initiator in one-step processing to get the compatibilized biocomposite product for further compression moulding/injection moulding (Mohanty, Misra et al. 2002).

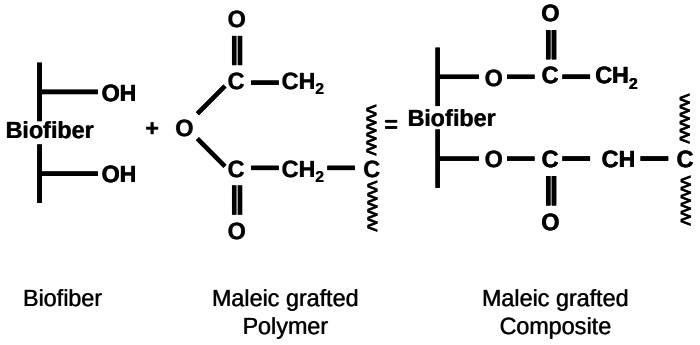

Figure 2-13 Chemical structure of maleic anhydride grafted fiber and biopolymer (Mohanty, Misra et al. 2002) modified.

ANTI-OXIDANTS

Plastic generally ages rapidly under the effects of light, oxygen and heat, leading to loss of strength, stiffness of flexibility, discoloration, scratching, and loss of gloss. Antioxidants, light stabilizers and fluorescent whitening agents can help to combat these effects. There are primary and secondary antioxidants. Antioxidants used for polyolefins are usually a phenolic antioxidants combined with a phosphorus based melt processing stabilizer that

react as H - donor (radical interceptor) and –COOH decomposer (Choosing an antioxidant: some of the basics. 2005). Unlike hindered amines, anti-oxidants are not regenerated in the stabilization process which means that plastics with antioxidants are subject to aging and thus lose their initial properties over time.

Ciba® IRGANOX® 1010

Irganox 1010 is the commercial name of pentaerythrityl tetrakis-[3-(3,5-di-tert-butyl-4-hydroxyphenyl) propionate], a primary phenolic based antioxidant. It hinders thermally induced oxidation of the polymers and protects against overbake yellowing by terminating free radicals in conventional solvent-based and powder coating systems. The chemical structure of Irganox is shown in Figure 2-14.

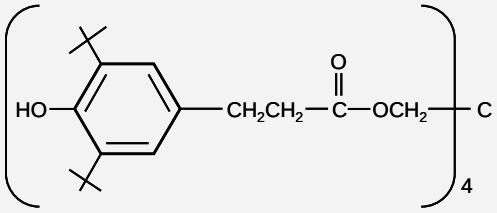

Figure 2-14 Chemical structure of the antioxidant Irganox 1010 (Kimura, Yoshikawa et al. 2000).

2.4 COMPOSITE PROCESSING

2.4.1 FILLER TREATMENT: ALKALINE EXTRACTION

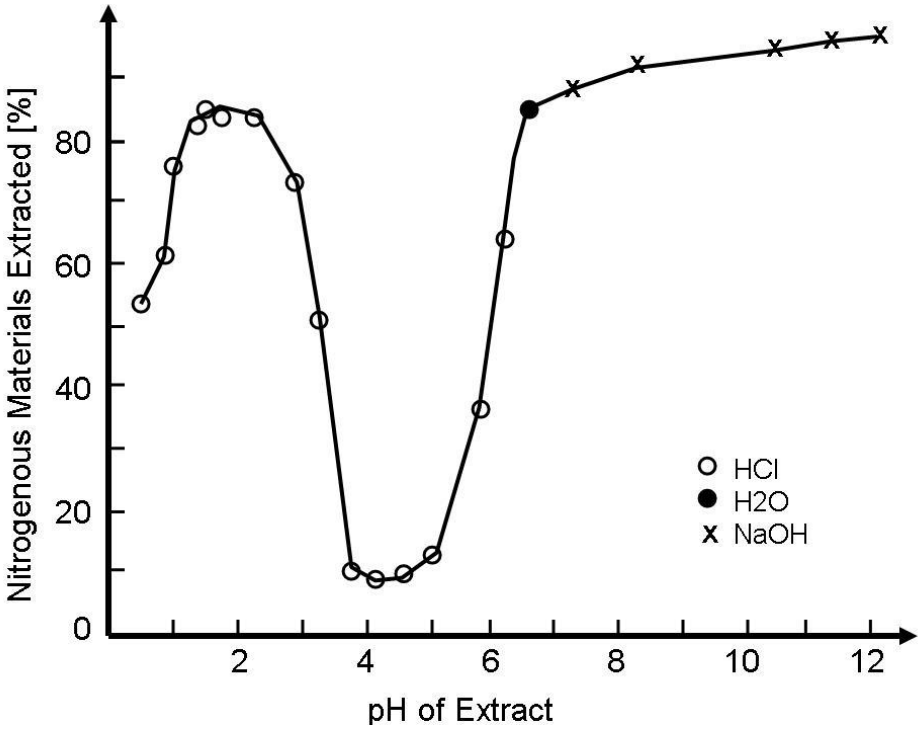

Figure 2-15 Extractability of proteins in defatted soybean meal as a function of pH (Wolf 1970) adapted.

Proteins are polypeptide chains consisting of amino acids. They are bounded together by different forces such as hydrogen bonding, disulfide bridges, and electrostatic interactions. Most of them are very sensitive to temperature and pH extremes which would result in denaturation. Because the processing temperature of polypropylene has to be above 170 °C the proteins would start denaturation and decomposition, thus resulting in development of gas (bubbles) during preparation of composites by melt mixing.

About 48 wt-% of the soy flakes (provided by Bunge Inc.) are proteins which are widely used in the food industry as an ingredient for texture and defensibility. Soy proteins have a high nutritional value as well as positive health effects (isoflavones). Because of an already established market, the price for soy proteins is much higher than for the remaining by-products. Thus, there is an increased interest in increasing the efficiency of extraction during protein production. Another use for the proteins is in producing protein films or adhesives (Kumar, Choudhary et al. 2002, Tkaczyk, Otaigbe et al. 2001, Liu, Misra et al.

2005). For some industrial applications the extraction of the proteins does not need follow FDA restrictions.

The solubility profile of soy protein is shown in Figure 2-15. The solubility of the proteins depends mainly on the pH of the solution. The charge and the solubility of the proteins changes with changing pH. The solubility reaches a minimum at the isoelectric point. The salt concentration also affects the charge and solubility of the proteins. For the alkaline extraction of the soy proteins the conditions from literature vary slightly but in general there are three factors: a) the temperature at which the extraction is conducted, b) the pH of the solution and c) the solid/liquid ratio of the preparation. This method is widely used because it is inexpensive and easy to conduct with a high throughput. Protein extraction in an ethanol solution or by enzymatic treatment was not considered in this study because these methods would increase significantly the complexity of the process and the costs.

2.4.2 EXTRUSION

Extrusion has the role of melting the plastic and to compound it with the fibers, fillers, colorants and additives. The extruder usually has one or two screws rotating inside a heated barrel. Depending on the speed of the screw and the screw configuration and geometry the material will be retained for longer in the system and thus has a longer exposure to the high temperature. A higher speed causes a higher shear which could have a negative impact on the dispersed phase; excessive shear can change the size and shape of the particles, particularly affecting fibers.

2.4.3 INJECTION MOULDING

There are several techniques to transform plastic materials into the shape required for the final application. The most common one is by injection moulding. The machine itself can have different ways to plasticize the material but also different gates to feed the plasticized material into the mould. The apparatus can have, for example, a rotation screw or a pestle to transfer the molten plastic into the mould. The most common types of gates used in injection moulding are sprue gate, pin gate, edge gate, ring gate, diaphragm gate, fan gate, film gate, and tab gate (McCrum, Buckley et al. 1990). Depending on the mould, the type and number of gates are chosen to obtain an even flow and fill up the mould uniformly. The cooling process causes contraction of the moulding. The volume contractions by cooling down polyethylene from 190 °C to 20 °C is about 18 %, and for polystyrene 7 % by a start temperature of 195 °C. This can lead to voids in the moulded parts and excessive sink

marks after the cooling process if the pressure and temperature is not controlled and maintained over the whole injection moulding process.

2.5 COMPOSITE TESTING

When a material is used as an automotive part certain requirements need to be met. For mechanical properties some of the most important parameters are the E-modulus, yield strength and the impact. Further requirements in the performance are changes due to weathering, e.g. exposure to different environmental conditions.

2.5.1 FLEXURAL MODULUS

To investigate the stiffness of a plastic the flexural modulus or tensile strength can be used. The flexural performance can be tested by using three-point-bending as described in the ASTM standard method D 790 - 07 (ASTM International 2008g). When force is applied onto a specimen a typical stress/strain curve can be obtained and analyzed with regards to the mechanical performance of the material. This method requires only a simple apparatus that applies stress under controlled conditions. A schematic drawing of a three-point-bending test and a stress/strain diagram is presented in Figure 2-16. The characteristics of the curve display the areas of elastic and plastic deformation. The point between elastic and plastic deformation identifies the maximal force that can be applied until a material deforms permanently. The slope of the tangent drawn through the linear curve represents the modulus of elasticity or E-modulus and the point of breakage is called elongation at break or ultimate tensile strength. Figure 2-17 shows some typical stress/strain curves which refer to different mechanical classifications such as soft and weak, hard and brittle, hard and strong, soft and tough, and hard and tough.

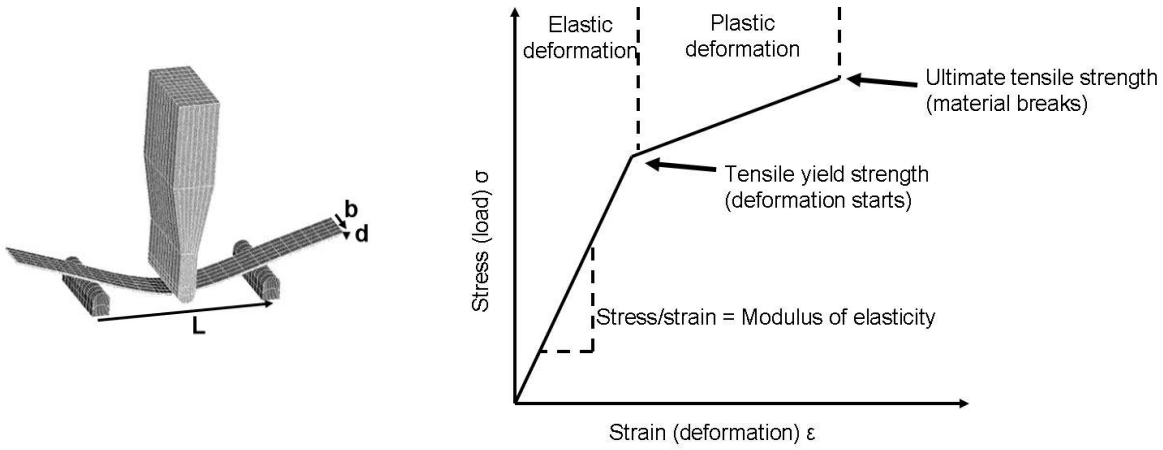

Figure 2-16 Flexural test: Schematic drawing of a three – point – bending (left). Typical stress/strain diagram of an ordinary metal. Until the tensile yield strength is reached the material shows an elastic behaviour (Ryhänen 1999) adapted (right).

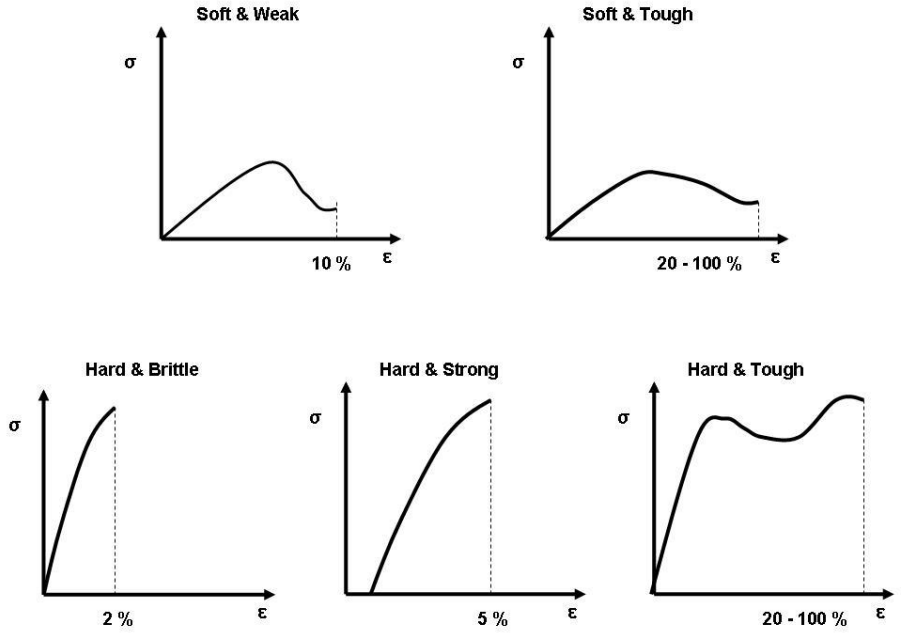

Figure 2-17 Classification of engineering stress-strain curves for polymers. Σ = applied stress, ε = resulting strain (Progelhof, Throne 1993), adapted.

2.5.2 IZOD IMPACT

The Izod impact test is named after the English engineer Edwin Gilbert Izod, who published his work "Testing brittleness of steel" in 1903. This mechanical failure test is described in the ASTM standard method D 256 – 06 a and determines the resistance of a plastic by using a pendulum swing. The specimen is fixed into a clamping vice in 180° and the pendulum hits the notched sample and creates a stress concentration that enhances a brittle fracture. The Izod impact strength is reported in J/m which is the energy absorbed per unit of (specimen) width or per unit of cross-sectional area under the notch (ASTM International 2008d).

2.5.3 WATER ABSORPTION

This property plays a very important role when the final application of the composite is in environments with moisture or water, for example parts which are directly exposed to precipitation. Biological materials have the characteristic to absorb moisture from the surrounding area because of their hydrophilic nature (hydroxyl groups)(Marcovich, Reboredo et al. 1998). The main components in most plants are cellulose, hemicellulose, and lignin. Depending on the structure of the components the water uptake can change. Amorphous structures of cellulose will take-up more water than crystalline ones because their various hydroxyl groups are easily accessible (Arbelaiz, Fernández et al. 2005). Lignin is considered as protection against hydrothermal degradation because of its hydrophobic structure and should show a lower water uptake then amorphous cellulose (Espert, Vilaplana et al. 2004). Rana et al. showed that the use of compatibilizer could decrease the water absorption which was attributed to the ester linkage of the hydrophilic – OH groups with acid anhydrides (Rana, Mandal et al. 1998). According to Ton-That and Jungnickel, who studied the water diffusion into transcrystalline layers on polypropylene, the diffusion of water is selectively passing through the amorphous phase of semicrystalline materials (Ton-That, Jungnickel 1999).

2.5.4 THERMOGRAVIMETRIC ANALYSIS (TGA)

Thermogravimetric analysis can be used to determine the thermal stability of the filler material. A schematic diagram is shown in Figure 2-18 (left) where the sample was placed on a balance arm in a closed chamber. A second arm with a reference weight connected to the balance is also placed in that chamber. The chamber can be filled with an inert gas, such as helium or nitrogen, or with oxygen to simulate a combustion of the material. The

chamber is heated at a set rate of °C/min beginning with a low initial temperature up to 600 °C, or higher. The temperature range depends on the material and also could be set isothermal so that the temperature is kept stable over a set time. Over the heating exposure, the weight of the sample is compared with the reference weight and the difference is recorded by a computer connected to the balance. A typical output of the analysis is a plot with the weight loss over temperature (Figure 2-18, right). The first derivative of this curve provides information about the onset of degradation and the area under the peak is equal to the weight lost during the degradation process.

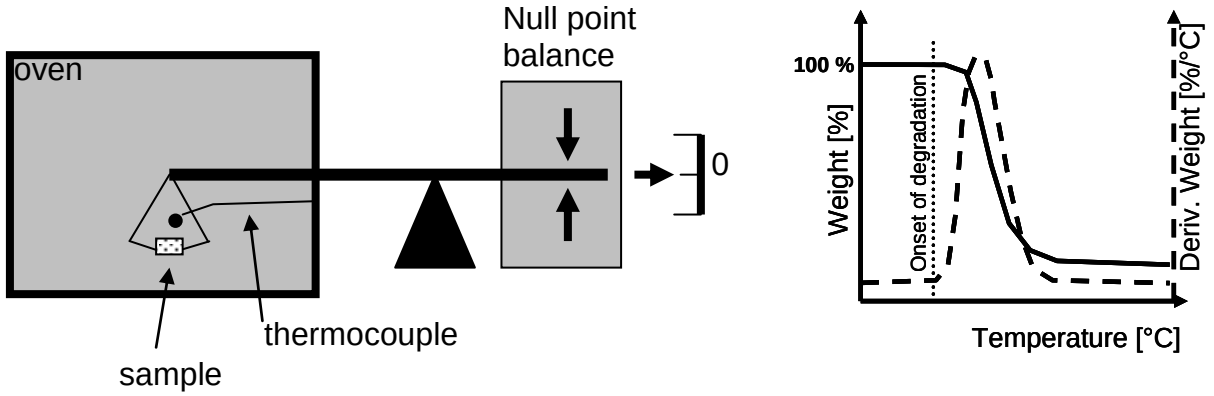

Figure 2-18 Schematic diagram of a horizontal thermobalance, (Ehrenstein, Riedel et al.) adapted (left). Graph of a typical thermal degradation as a function of temperature (right).

2.5.5 DIFFERENTIAL SCANNING CALORIMETRY (DSC)

Differential scanning calorimetry is an essential tool for investigating thermal transitions of a polymer and to obtain information about the glass transition, melting and crystallisation as well as their corresponding temperatures (Progelhof, Throne 1993). The glass transition temperature (T_g) describes the change in the character of a polymer from a brittle to a rubbery state which occurs before the melting and appears as a drop in heat flow in the DSC diagram. The melting point (T_m) is the temperature peak when a polymer is heated and its state changes from rubbery to liquid. This change involves a release of energy which appears in the DSC diagram as an increase in heat flow. In comparison to the melting point the crystallization point is found when a material is cooled down and the liquid state changes into the solid state by forming crystals. The structure of the crystals depends on the cooling rate and the material which undergoes the crystallization. The melting and crystallization peaks represent first-order thermodynamic phase transitions. The point of the glass transition is a second-order thermodynamic phase transition and can be identified from the slope of the curve (Progelhof, Throne 1993). The area under the peak represents

the energy needed to crystallize the composite which in turn can be used to determine the degree of crystallization of the polymer. The crystallinity represents the ratio of the crystalline part of the polymer to its amorphous region. A schematic drawing illustrating the crystalline and amorphous regions is shown in Figure 2-6 b).

During the DSC test the material is heated along with a reference at a constant rate and the temperatures of both are kept the same by individually and independent heat input. The input of heat is measured very precisely and plotted versus temperature. Because the heating rate is constant the heat input used in J/s or Watts. A typical plot is shown in Figure 2-19 where the melting and crystallization event appears as a peak. Its area represents the amount of energy of each phase transition and depends on the event. The crystallinity of a material depends on many different factors that will affect the mechanical properties. A material of high crystallinity, for example, will have a very brittle performance.

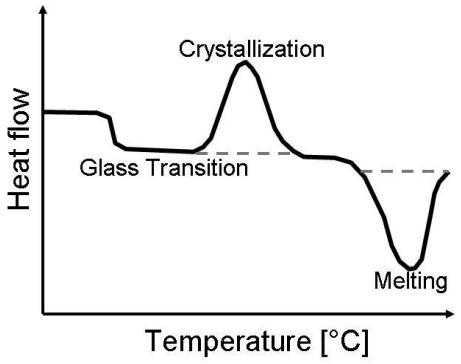

Figure 2-19 Typical plot from differential scanning calorimetry (DSC) with glass transition, crystallization, and melting regions.

2.5.6 FIELD-EMISSION SCANNING ELECTRON MICROSCOPY (FESEM)

A scanning electron microscope (SEM) is a high resolution microscope which uses a beam of electrons instead of visible light to investigate the morphological characteristics of the sample surface. The main differences between light and electron microscopy are the wavelengths of the beams which varies by a factor of many thousands ($\lambda_{\text{visible light}}$ = 400–700 nm; $\lambda_{\text{electron}}$ = Planck's constant/momentum of the electron). Electron microscopy offers a much higher resolution and thus it is possible to obtain images with a resolution of up to 2 nm. The magnetic fields are used to focus the beam of electrons and to control

magnification. It is necessary to decrease the pressure to at least 10^{-2} Pa to operate an electron microscope. An example for an electron microscope is the Field Emission Scanning Electron Microscope (FESEM). The main difference in a FESEM to other electron microscopes is the production of the electron beam. The FESEM (Figure 2-20) works in a high vacuum (10^{-5} - 10^{-7} Pa). The electrons are generated by a field emission source and accelerated in a field gradient. The beam passes through the electromagnetic lenses and focuses onto the specimen. As a result of this bombardment, different types of electrons are emitted from the specimen (Figure 2-21). The secondary electrons will be caught by a detector and an image of the sample surface is constructed by comparing the intensity of these secondary electrons to the scanning primary electron beam. Finally the black and white image is displayed on a monitor. For non-conductive materials it is necessary to fix the specimen on conductive tape and coat it with an electron dense material such as gold or carbon.

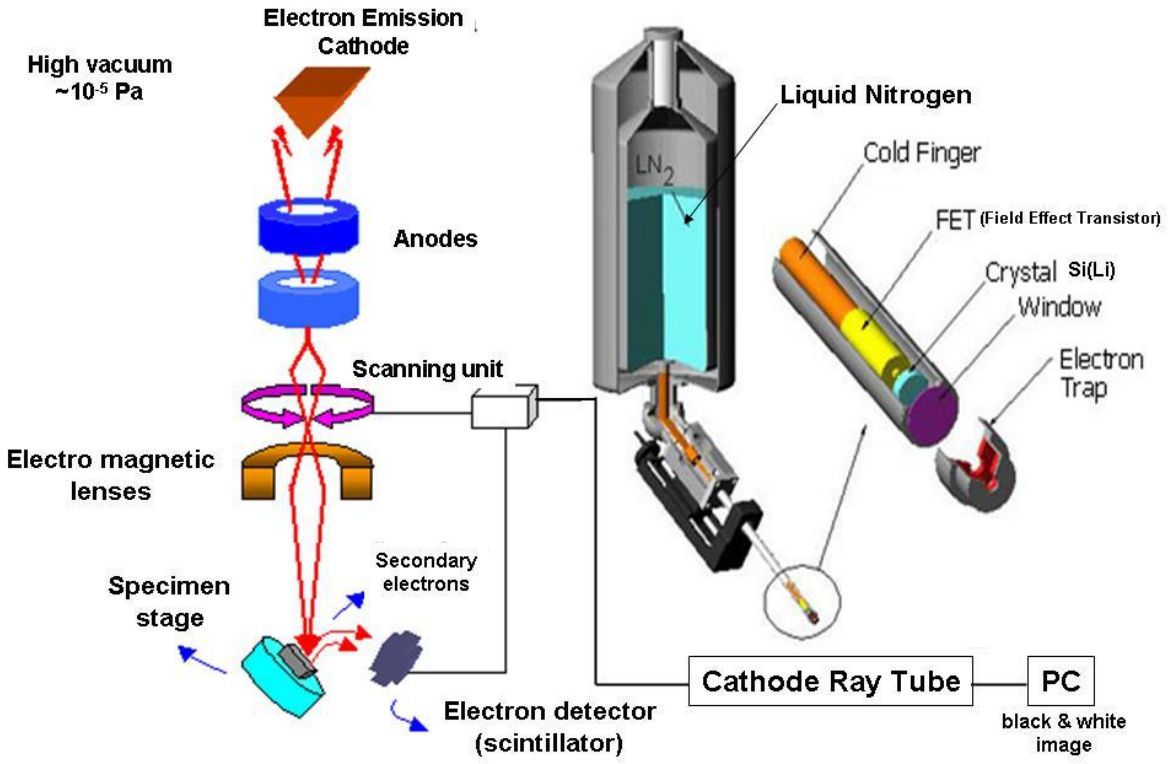

Figure 2-20 Scheme of a Field Emission Scanning Electron Microscope (NEW MEXICO TECH 2007) with Energy Dispersive X-ray detector (Advanced Analysis Technologies 2005) modified.

In 1950 it was found out that it is possible to obtain information about composition, crystal structure, and orientation of a solid specimen by analysing the emitted X-rays during the scanning electron microscopy. The Energy Dispersive X-ray Spectroscopy (EDX or EDS) is a microanalysis technique used to identify and quantify the composition based on the chemical elements. Microanalysis can be performed on a very small amount of material. The determination of the wavelength and energy is used to obtain information about the chemical of elements in the sample. In the X-ray spectrum each element has its own characteristic peak and therefore EDX is a convenient technique for element mapping and determination of material compositions.

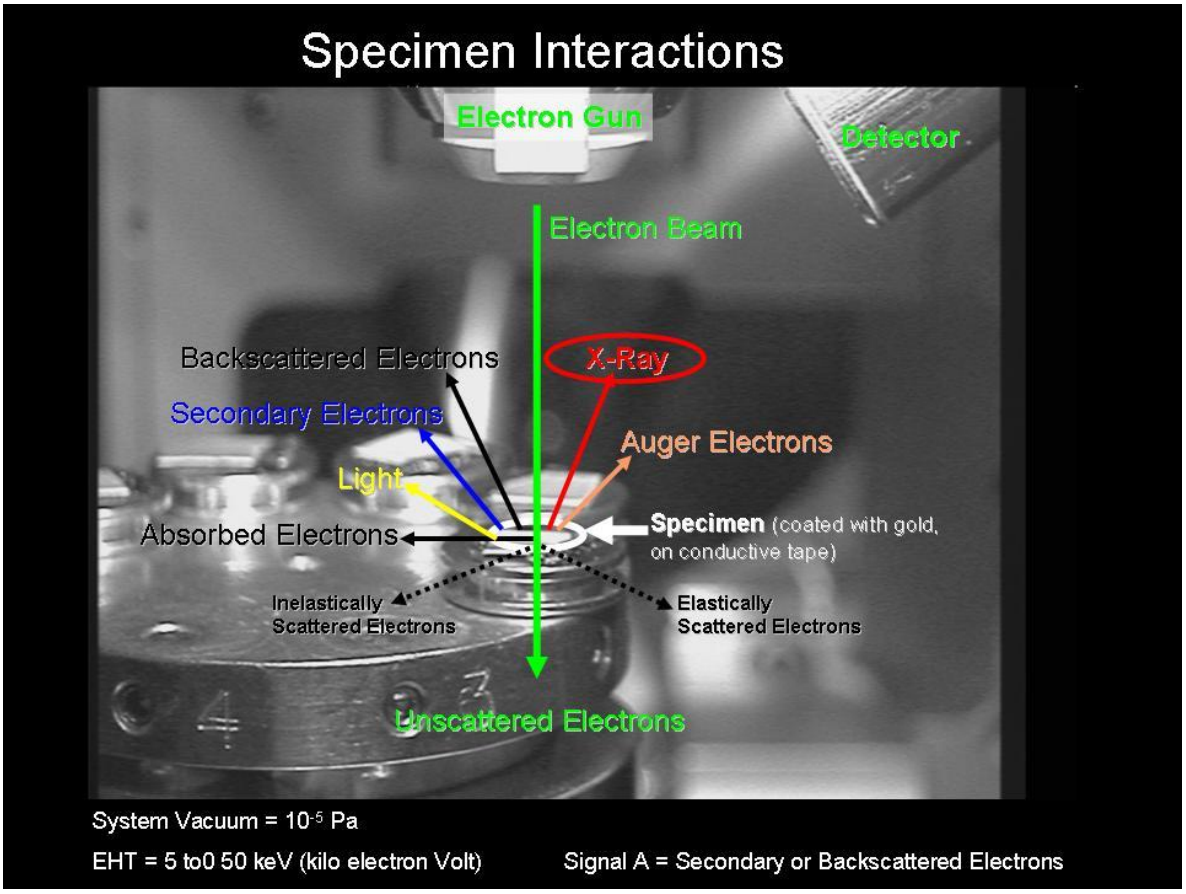

Figure 2-21 Specimen interactions during scanning electron microscopy.

X-ray radiation takes place when an electron has received extra energy, e.g. due to a collision with an electron of the primary beam (bombardment of a specimen in electron microscope). As this is an unstable situation, the electron will fall back into is original orbit; the extra energy is released in the form of an X-ray quantum; this is determined by the position in the orbit and the fall back of the orbit.

Each element has its characteristic X-ray emission. This is displayed in a certain peak position on the spectrum which is corresponding to the possible transition in its electron shell. The emitted wavelength depends on the nature of the atoms in the specimen. Elements in an EDX spectrum are identified based on the energy content of the X-rays emitted by their electrons as these electrons transfer from a higher-energy shell to a lower-energy one. To detect X-rays, different detectors can be attached on the SEM and connected to a computer. The detector is controlled by the computer. The Electron Dispersive Analysis uses Solid State and Silicon (e.g. Si(Li) or Si(Ge)) X-ray Detectors and Multi-Channel Analyzer (MCA) which can detect the energy of characteristic X-rays.

The Detector is a self contained vacuum system (cryostat) with cryogenic pumping created by cooling with liquid nitrogen. Principal elements of an EDX detector are Entrance window, Si (Li) crystal, Field Effect Transistor (FET), and Pre-amplifier (Figure 2-20 right). The entrance window allows photons to enter the detector, while maintaining the vacuum integrity of the cryostat. The critical front-end components, the crystal and FET are mounted on a cold finger within the detector cryostat. The pre-amplifier is mounted on the exterior of the cryostat. The detector normally consists of a small piece of semiconducting silicon which is held in such a position that as many as possible of the X-rays emitted from the specimen fall upon it. It must be in the same line of sight of the specimen (in SEM similar position to the secondary electron detector). When a sample is exposed to an electron or X-ray beam, photons are generated (e.g. SEM, X-ray Fluorescence (XRF)) and analyzed in the system. To collect as many X-rays as possible the silicon should be near to the specimen as is practicable. Each incoming X-ray excites a number of electrons into the conduction band of the silicon leaving an identical number of positively charged holes in the outer electron shells. The energy for each of these excitations is 3.8 eV; consequently the number of electron-hole pairs generated is proportional to the energy of the X-ray photon being detected. The number of generated holes (or electrons) is proportional to the X-ray energy. In an electron microscope, the contrast is formed by the scattering of electrons by the specimen. In order to make objects visible, the image details must show contrast differences with respect to their background or with respect to each other. Sample details which are scattered by the electrons under such angles that the objective aperture will block them, will be imaged darker with respect to their background.

The scanning electron microscope (SEM) combined with EDX can give, beside imaging very high magnified pictures of the specimen, many information about the structure and elements of the sample. SEM is used for morphology analysis to obtain information about particle shapes and sizes as well as conducting fracture studies. It is also possible to study

the interface behaviour and localize the boundaries between regions of different atomic numbers.

3 MATERIALS AND METHODS

A schematic workflow of the project with its main steps is presented in Figure 3-1. A simplified scheme of the filler regarding their origins and treatments is shown in Figure 3-2. The defatted soy flakes were provided by Bunge Inc. (Hamilton, Ontario), the soy flour was provided by Ford Motor Company and the polypropylene was provided by A. Schulmann Inc. All other material and equipment used during this project is listed in Section 3.1 and the methods are explained in Section 3.2.

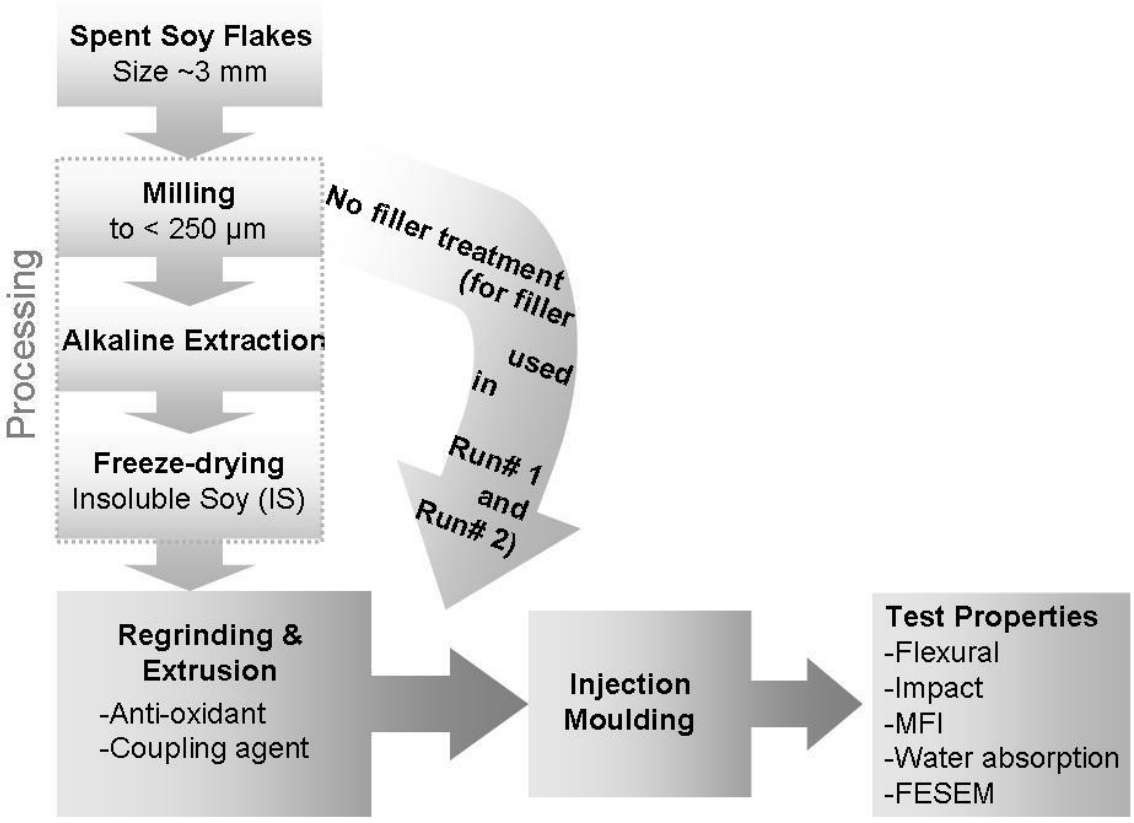

Figure 3-1 Flow chart of the preparation, production and testing of the biocomposites.

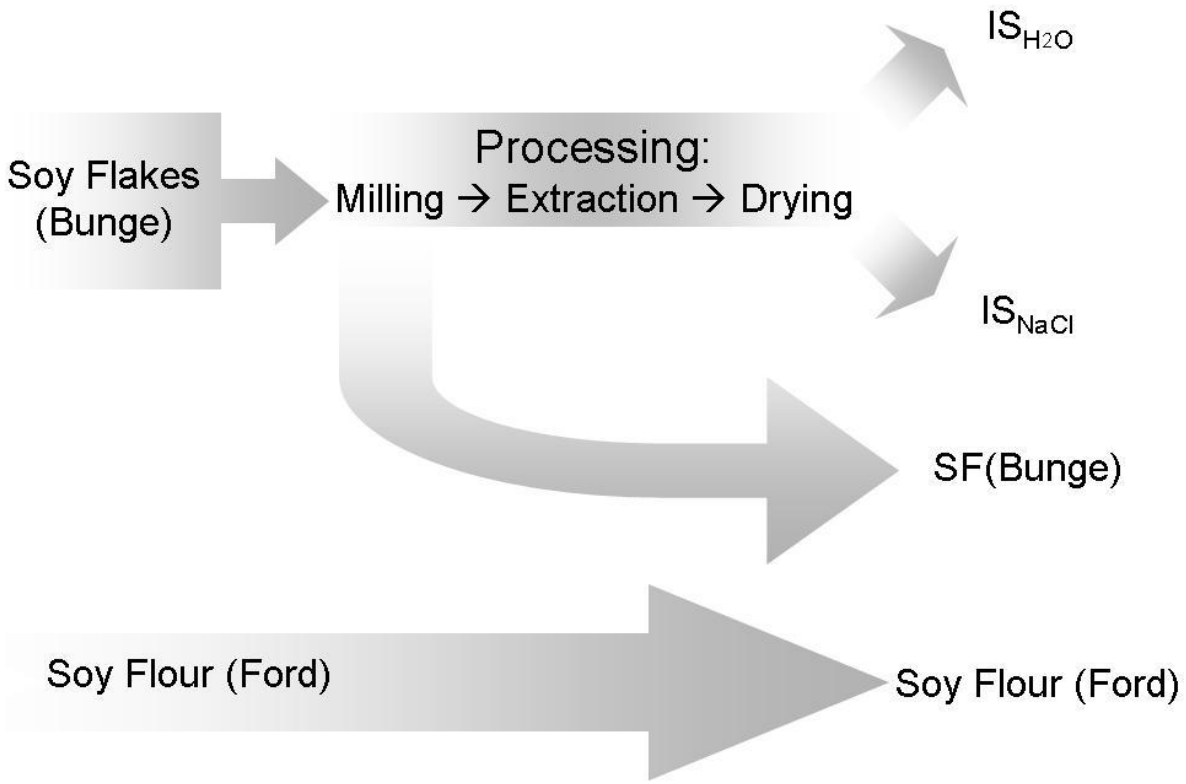

Figure 3-2 Overview about the origins and treatments of the different filler used in Run # 1 – 8. Soy flour (Ford) was used as received, SF (Bunge) was taken after the milling without any further treatment and IS_{H2O} and IS_{NaCl} are extracted in either water (H_2O) or 1M sodium chloride solution (NaCl), freeze-dried, and regrinded.

3.1 MATERIALS AND EQUIPMENT

3.1.1 CHEMICALS

Table 3-1 and Table 3-2 show all the materials and chemicals that were used in this thesis.

Table 3-1 List of filler materials with their supplier

Filler material	Supplier
Defatted soy flakes	BUNGE Inc., Hamilton, Canada
Soy flour	Supplied by Ford Motor Company (sourced from CHS Oilseed Processing, Inc. Mankato, MN, USA)

Table 3-2 List of materials and chemicals used during the project.

Material/Chemical	**Manufacturer**
Ammonium sulphate ($(NH_4)_2SO_4$)	Sigma
Cellulose (powder, fibrous, medium)	Sigma-Aldrich
Cellulose (Sigmacell type 101)	Sigma Chemical Co., USA
Cellulose (Sigmacell type 50)	Sigma Chemical Co., USA
Coomassie Brilliant Blue	Bio-Rad Laboratories, CA
EPO-FIX embedding resin and hardener	Electron Microscopy Science, USA
Irganox 1010	Ciba
Lignin, alkali (Batch# 11615BE; 370959-100G); typical M_n 5,000, typical M_w 28,000	Aldrich
Lignin, alkali, low sulphate content (Batch# 09724CE; 471003-100G); typical M_n 10,000, typical M_w 60,000	Aldrich
Maleic anhydride polypropylene P MD353D	DuPont – Fusabond®
Methylene Blue 1 % w/v aqueous	VWR
Nessler's Reagent for Ammonia - Nitrogen	VWR
Polypropylene 2407-01 Natural MI 1.5	A. Schulman Inc.
Ponceau S ($C_{22}H_{12}N_4Na_4O_{13}S_4$) MW 760.61	Bio Basic Inc.
Potassium Sulfate (K_2SO_4) MW 174.26	BDH Inc.
Selenium oxychloride ($SeOCl_2$)	Fisher Scientific
Sodium Chloride (NaCl) MW 58.44	BDH Inc.
Sodium Hydroxide, solid (NaOH) MW 40.00	Fisher scientific, International
Soy beans	Ontario, Canada
Soy protein subunits 7S and 11S	provided by M. Corredig, University of Guelph, ON, Canada
Sulfuric acid (H_2SO_4) 95-98 % MW 98.075	Fisher Scientific

3.1.2 SOFTWARE

Table 3-3 List of software used in this project.

Software	Version	Company
Ascent software	2.4.1, 1996	Labsystems Oy
Excel 2003	SP-2	Microsoft Corporation
Genesis Imaging/Mapping	3.61 18-Nov-2003	EDAX Inc.
ImageJ	1.38x	National Institutes of Health, USA
Leica Application Suite	2.6.0 R1 Build 1192	Leica Microsystems GmbH
LEO 32 (FESEM)	030201 2-Oct-2002	
MiniMat	2.4.B	Rheometric Scientific Inc.
OPUS	4.2 Build 4, 2, 37 (20030313)	Bruker Optik GmbH
Universal Analysis 2000	4.5A Build 4.5.0.5	TA Instruments – Waters LLC
Windows System	98, XP, Vista	Microsoft Corporation
Word 2003	SP-2	Microsoft Corporation

3.1.3 EQUIPMENT AND SUPPLY

Table 3-4 presents the laboratory equipment used in this project.

Table 3-4 List of laboratory equipment used in this project.

Equipment	Manufacturer
Analytical balance AB304-S	Mettler Toledo
Band saw (for bars) Racer V50 V50929	Racer machinery Co.
Centrifugal Mill ZM 200	Retsch GmbH
Digital Camera Panasonic Lumix DMC-TZ2	Matsushita Electric Industrial Co., Ltd. Osaka Japan
DSC Q2000	TA Instruments
FESEM gold coating unit Desk II with Argon (inert gas)	Denton Vacuum, USA
Field Emission Scanning Electron Microscope (FESEM) Leo 1530 with EDX/OIM PV9715/69 ME	Leo Gemini (now Carl Zeiss AG, Germany); EDAX (AMETEK, Inc.)
Freeze-Dryer Super Modulyo	Thermo Savant Fisher Scientific
FTIR Tensor 27	Bruker Optik GmbH
Grinder for MA-PP M20	IKA® Werke
Grinder KSM2 Aromatic	Braun GmbH

Continuation of Table 3-4.

Equipment	Manufacturer
Heating Equipment Type 056-PT	Hevi-Duty Heating Equipment Co.
Heating units (for Kjeldahl)	Lab Con Co.
Hotplate/Stirrer Cat. No. 11301-012	Henry Troemner LLC
Injection Moulding Apparatus RR/TSMP	Ray-Ran
MFI Dynisco Polymer Test D4001DE	Alpha Technologies
Microplate reader Multiscan Ascent Model No. 354 Serial No. 354-00735	Labsystems
Microtome EM UC6	Leica Microsystems GmbH, Germany
MiniLab Extruder Haake	Thermo Electron Corporation
MiniMat	Maple Instruments
Moisture Analyzer MB45	OHAUS
Multiskan Ascent spectrophotometer 354	Labsystems
MVP 2 Series	Harrick Scientific Products, Inc.
Oven 5890A GC (for annealing)	Hewlett Packard
pH Electrode 511080	Beckmann
pH-meter/controller Model No. 5652-00 Serial No. M92006193	Chemcadent®
Pipettors	Eppendorf Research, Germany
Plastic Impact Tester	Tinus Tolsen
Platform Shaker	Eberbach Corporation, USA
Scale Scout Pro	OHAUS
SDT 2960 Simultaneous DTA-TGA	TA Instruments
Specimen Notch Cutter XQZ-I, Travel: 24 mm	Chengde JinJian Testing Instrument Co., Ltd.
Stereo microscope MZ6	Leica Microsystems GmbH., Germany
Testing Sieve Shaker RO-TAP	W.S.Tyler Inc.
Tzero Hermetic low-mass pan and lid (DSC)	TA Instruments
U.S standard testing sieves	VWR
Ultracentrifuge Rotor A-621	Thermo Electron Corporation
Ultracentrifuge Sorvall WX Ultra Series	Thermo Electron Corporation

3.2 METHODS

3.2.1 ALKALINE EXTRACTION

In order to remove the proteins from the soy flakes, an alkaline extraction was conducted because soy proteins are known to be soluble for such conditions. The conditions selected for the alkaline extraction were typical conditions reported in the literature (L'Hocine, Boye et al. 2007; Lee, Ryu et al. 2003; Wu, Hettiarachchy et al. 1998) for soy protein removal: a temperature of 50 °C, pH 9, water or 1M NaCl solution and a solid/liquid ratio of 1 : 9 (wt/wt). The duration of the extraction was one hour with mixing using a hot plate (Henry Troemner LLC, Hotplate/Stirrer Cat. No. 11301-012). After the extraction, the solution was centrifuged in a ultracentrifuge (Sorvall WX Ultra, Rotor A-621) at 10,000 rpm for 35 min to separate the solubilized components contained in the supernatant from the unsolubilized components i.e. the pellet. After the extraction, the pellet was freeze-dried in a Super Modulyo Freeze-Dryer (Thermo Savant Fisher Scientific) for about three days without a washing step.

With the initial conditions for alkaline extraction, a fractional factorial design was developed to find the optimal conditions for the extraction and to identify the significant factors (Table 4-1).

3.2.2 KJELDAHL PROTEIN ANALYSIS

The protein concentration was determined with the Kjeldahl method according to Lang (Lang 1958) and modified for microtiter plates. A standard solution of ammonium sulphate in NANOpure® water was prepared in a concentration of 4.714 g/l and stored at 4 °C until use. The test was carried out in duplicates. Approximately 10 mg of each sample was placed into a 30 ml Kjeldahl flask as well as 1 ml of the ammonium sulphate standard. A digestion solution containing 40 g potassium sulphate, 250 ml deionised water, 250 ml sulphuric acid, and 2 ml selenium oxychloride was prepared and 3 ml of this solution was transferred into each flask. The mixture was placed on a heating unit and boiled until the solution remained clear as the standard that should not change the colour. After cooling the flask to room temperature, each sample was transferred into a 100 ml volumetric flask and diluted to 100 ml with deionised water. The diluted samples were used for the subsequent colorimetric assay. A calibration curve was prepared by using the standard in different concentrations and subjected to the same treatment as the samples. The colorimetric assay

was carried out in triplicates. From each diluted sample, standard and blank (deionised water), 50 µl were placed into a 96-well microtiter plate. Then 150 µl of deionised water was added to each well. At last, 50 µl of Nessler's reagent was added to the each well. The microtiter plate was shaken for about 30 seconds and placed in the dark for 15 min (color development). The microtiter plate was then inserted into a Multiskan Ascent spectrophotometer (Labsystems 354), shaken for approx. 15 seconds and analyzed at 420 nm. The calibration curve was plotted with the known concentration of nitrogen. The protein concentration of the samples was determined by using Equation 5-1 and the factor 6.25 characteristic of soy proteins. The formula and an example for calculation are given in Equation 5-1 and Equation 5-2 in the appendix.

3.2.3 GRINDING AND PARTICLE SIZE ANALYSIS

Figure 3-3 Centrifugal Mill, Retsch ZM 200 (RETSCH GmbH 2006).

In order to use the soy flakes as filler in a composite the size of the flakes had to be reduced. The size range of the soy flakes as received was between 0.1 mm and 5 mm. The main part with 70 % was between 1.5 mm and 3 mm (see appendix Figure 5-7). The milling of the soy flakes was done in batches at 10,000 rpm in a Retsch ZM 200 mill using a 250 µm sieve. Thus the final particle size was smaller than 250 µm. According to Retsch GmbH, over 50 % of the particles will have a size about half the size of the sieve (Retsch GmbH & Co. KG 2003).

The particle size analysis was carried out by using a technique developed in the lab (Kapustan Krüger 2007). This technique involves a light microscope (Leica Microsystems) and an image analysis software (ImageJ). The particles were first separated so that they did not touch each other. The particles were placed under the microscope and a picture was

taken from the camera connected to the microscope. For the analysis of the pictures the contrast was set to "threshold" and the particles were counted and measured according to their major and minor (length and width) direction.

3.2.4 CHARACTERIZATION OF THE FILLER MATERIAL

This section describes the tests that were used for the characterization of the thermal degradation and composition of representative filler materials.

THERMOGRAVIMETRIC ANALYSIS (TGA)

Thermogravimetric analysis was used to obtain the thermal stability of the filler material. The chamber was filled with helium or nitrogen (depending on the system) as inert gas and the chamber was heated up at a rate of 10 °C/min. The initial temperature was 40 °C and the heating phase was stopped at 600 °C for most of the materials. The weight of the sample was recorded by a computer connected to the balance.

LIGHT MICROSCOPY AND STAINING

For soybean staining as described below, the soybeans were embedded in epoxy resin and cut with a microtome (Leica Microsystems, Stereo microscope MZ6, Germany) in 5 to 10 µm thin slices. To prevent potential deformation of the samples during the staining, the thin sample slices were fixed on a transparent tape and put on an objective slide.

Staining of Cellulose

The cell wall of plants is composed mainly of cellulose, a polymer of glucose subunits linked by β(1→4) bonds. The cellulose is usually c linked with hemicellulose and lignin.

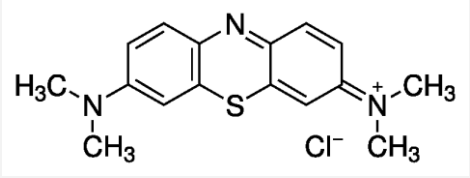

Figure 3-4 Chemical structure of methylene blue, $C_{16}H_{18}N_3ClS$ (Calvero 2006).

Methylene blue was selected for the staining of cellulose because it is an anisometric dichroitic cellulose staining dye, which means that the light rays having different polarizations are absorbed by different amounts. According to W. Herth and E. Schnepf methylene blue, as anisomeric particle, is oriented in the interfibrillar spaces of the parallel

texture and imposes its own anisotrophy (Herth, Schnepf 1980). The chemical structure of methylene blue is presented in Figure 3-4.

The methylene blue solution was prepared as a 0.1 % (v/v) aqueous solution. After the incubation time (less than one minute) the sample was washed with deionised water until the unbound methylene blue was rinsed off. Pictures were taken with a Leica microscope (Leica Microsystems, Stereo microscope MZ6, Germany).

Staining of Proteins

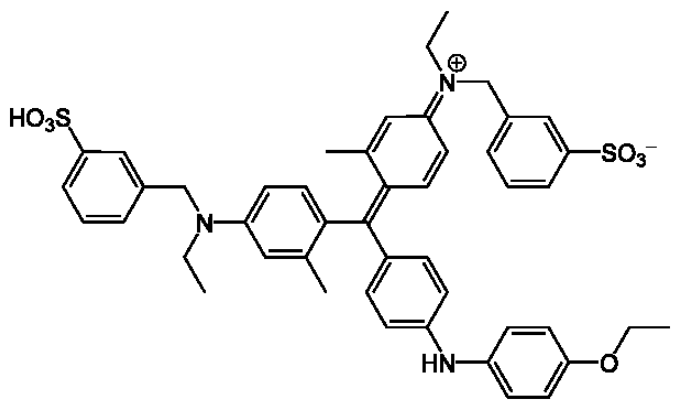

Figure 3-5 Coomassie Brilliant Blue G-250 ($C_{47}H_{50}N_3O_7S_2$+) (Yikrazuul 2008).

Two staining methods were used. The first method involved Coomassie brilliant blue because it is commonly used for protein staining in SDS Polyacrylamide gel electrophoresis (SDS-PAGE) analysis and for total protein quantification in the Bradford protein assay. Coomassie brilliant blue binds via adsorption (Van der Waals) to the amino acids arginine and histidine present on the surface of the proteins and thus shows different colour intensity depending on the amino acid compositions located at the surface of a protein.

The composition of the staining solution and the destaining solution is presented in Table 3-5. The samples were soaked over night in the staining solution with continuous agitation on a platform shaker (Eberbach Co.). The destaining of the samples was achieved by replacing the solution approximately every hour until no dye could be visually detected in the solution i.e. the solution remained clear.

Table 3-5 Solutions for the protein staining with coomassie brilliant blue.

Staining Solution	Destaining Solution
1600 ml ethanol	1600 ml ethanol
400 ml acetic acid	280 ml acetic acid
4 g coomassie brilliant blue	Volume was brought up to 4 l with water
Volume was brought up to 4 l with water	

The second method involved Ponceau S (Figure 3-6), a sodium salt which is widely used for rapid reversible detection of protein bands on nitrocellulose or PVDF membranes (Western blotting), as well as on cellulose acetate membranes. Ponceau S binds to the proteins at a low pH. The binding reaction can be reversed by washing with water.

The Ponceau S stain formulation included 0.1 % (w/v) Ponceau S in 5 % acetic acid. After an incubation time of about one minute the staining solution was removed and the pictures were taken by using a stereomicroscope (Leica Microsystems, Stereo microscope MZ6, Germany).

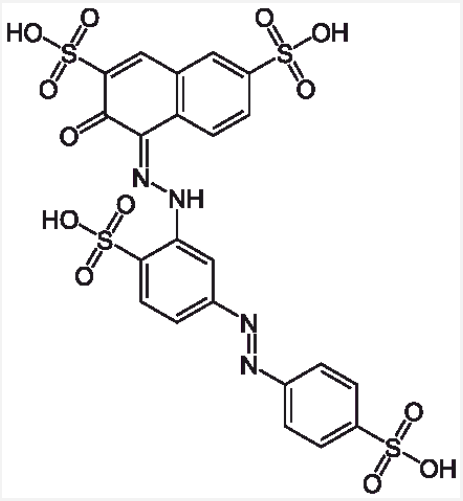

Figure 3-6 Chemical structure of Ponceau S (NEUROtiker 2008).

3.2.5 EXTRUSION

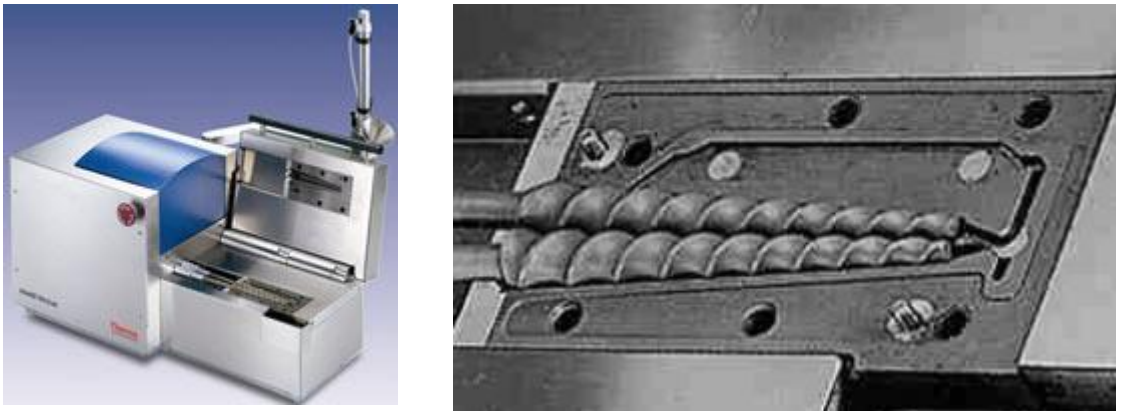

Figure 3-7 Haake MiniLab Twin-Screw extruder (Pharmaceutical Online 2009) (left); Conical Twin-Screws in MiniLab Extruder (Thermo Haake, 2002) (right).

For compounding of the polypropylene with the filler and additives a twin-screw extruder with intermeshing co-rotating screws (stainless steel 1.4122; max torque 5 Nm/screw) was used (Figure 3-7). The operating conditions were kept constant at 190 °C and 40 rpm. The feeding of the material was done continuously into the stainless steel barrel (max. volume 7 cm^3). The final compounding formulation of each run is presented in Table 3-6. Throughout this thesis, each formulation will be referred as "Run #" and the respective number. Runs with Roman numbers correspond to the formulations without filler that represent the control formulations. Runs with Arabic numbers correspond to the formulations with filler, generating the biocomposites. This nomenclature is summarized in Table 3-6 (and Table 5-2 in Appendix, page 122).

Table 3-6 Compounding formulations for extrusion.

Run	Filler type	Filler treatment	Matrix/Coupling agent	Filler [%]	Anti-oxidant
I	None	None	PP (no extrusion)	None	None
II	None	None	PP		
III	None	None	PP		0.35 % Irganox 1010
IV	None	None	3 % MA-PP		
1	SF (Bunge)	None	PP	30	0.35 % Irganox 1010
2	SF (Bunge)	None	3 % MA-PP		
3	IS	AE in H_2O	PP		
4	IS	AE in H_2O	3 % MA-PP		
5	IS	AE in NaCl	PP		
6	IS	AE in NaCl	3 % MA-PP		
7	Soy Flour (Ford)	None	PP		
8	Soy Flour (Ford)	None	3 % MA-PP		

3.2.6 INJECTION MOULDING

Figure 3-8 Injection Moulding Apparatus, detailed overview, Ray – Ran RR/TSMP (left) (Ray-Ran Polytest); pellets and injection moulded bars from Run # 4 (right).

The extruded pellets were pressed into bars with dimensions according to the ASTM test methods for plastics (ASTM International 2008d, ASTM International 2008a) and using an injection moulding apparatus from Ray-Ran (Figure 3-8). The pellets were fed into the feeding funnel and melted in the barrel at 195 °C until the material was liquid enough to get pushed through the sprue. The melted material was then pushed for about 15 seconds under high pressure into a metal mould with a temperature of 50 °C. The conditions for all samples were kept constant. The exact dimensions for the bars are presented in Table 3-7. Before the bars were tested they were put into an oven and annealed. For annealing the bars the initial temperature of 25 °C was kept for 2 minutes, the heating rate was 10 °C/min until the final temperature of 151 °C was reached and was kept for 10 minutes. The cooling rate was 10 °C/min with air until room temperature was reached.

Table 3-7 Dimensions for the bars pressed with injection moulding apparatus for ASTM property testing.

	Izod impact	Water absorption	Flexural Modulus
Length [mm]	63.5 (+/- 0.2)	63.5 (+/- 0.2)	31.8 (+/- 1)
Width [mm]	12.7 (+/- 0.2)	12.7 (+/- 0.2)	12.7 (+/- 0.2)
Depth [mm]	3.3 (+/- 0.2)	3.3 (+/- 0.2)	3.3 (+/- 0.2 mm)

3.2.7 PROPERTIES TESTING

FLEXURAL MODULUS

When stress is applied onto a specimen it will deform elastically up to a certain point and beyond this the deformation will be plastically, thus permanent. The Three–Point–Bending test according to ASTM D 790 – 07 (ASTM International 2008a) was used. A force/displacement diagram is shown in Figure 3-9 (left). Equation 3-3 was used to calculate the flexural modulus.

The rate of the crosshead motion of the device, the flexural stress, and the modulus of elasticity were determined by using following equations:

$$R = \frac{ZL^2}{6d}$$ Equation 3-1

$$\sigma_f = \frac{3PL}{2bd^2}$$ Equation 3-2

$$E = \frac{L^3 m}{4bd^3}$$ Equation 3-3

R = rate of crosshead motion [mm/min]
L = support span [mm]
Z = rate of straining [mm/mm/min]; shall be equal to 0.01
d = depth of specimen [mm]
b = width of specimen [mm]
σ_f = flexural stress [MPa]
P = load [N]
E = modulus of elasticity in bending [MPa]
m = slope of tangent Force/ΔL [N/mm]

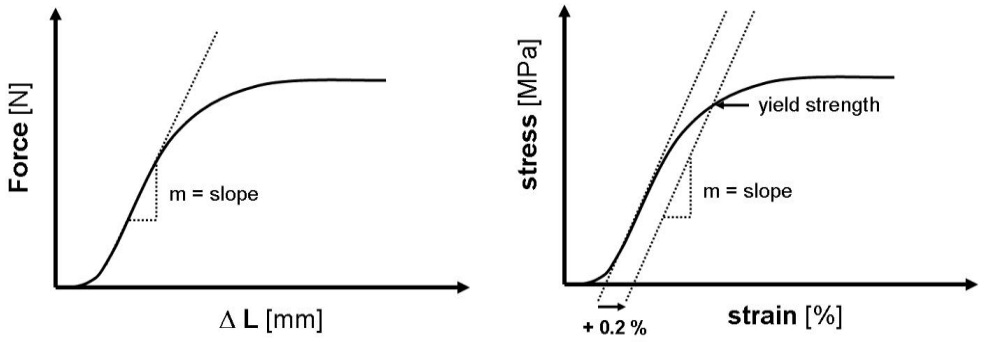

Figure 3-9 Typical force/ΔL graph for the determination of the E-modulus (left) and stress/strain graph for the determination of the yield strength (right).

IMPACT TEST

The Izod impact test is a test for determining the impact resistance of a specimen with brittle properties. In the ASTM method D 256 – 06a the dimensions of the specimen and the apparatus are defined (ASTM International 2008d). The specimens were prepared with a milled notch cutter. After notching, each specimen was placed into the test apparatus and fixed in such a position (180 ° in the clamping device) that the pendulum hit it in a 90° angle. Each sample was tested at least five times and the average as well as the standard deviation of the test was calculated and compared to each other and to the standards.

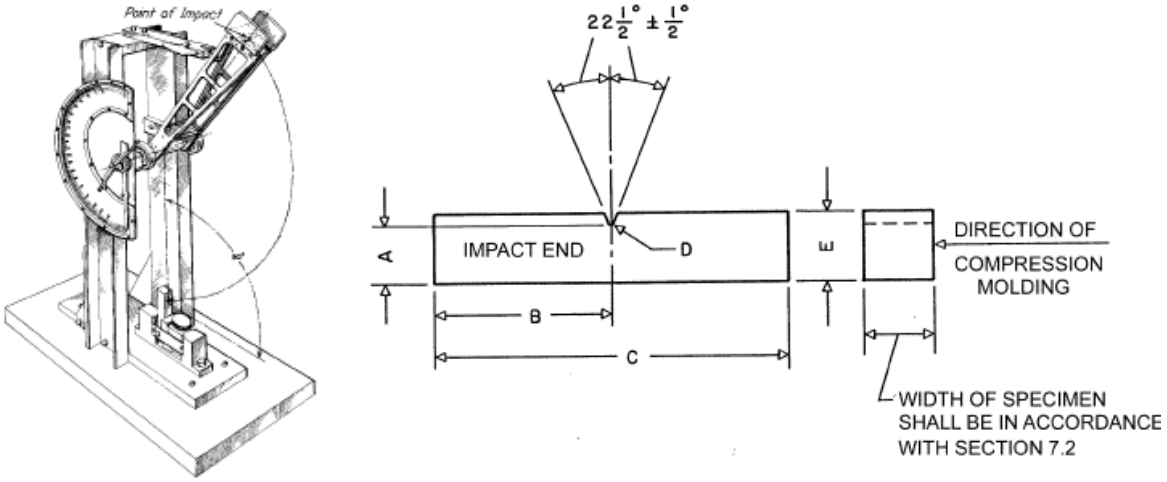

Figure 3-10 Izod impact tester (left); scheme of the specimen with position of notching (ASTM International 2008d) A = 10.16 +/- 0.05 mm; B = 31.8 +/- 1 mm; C = 63.5 +/- 2 mm; D = 0.25R +/- 0.05 mm; E = 12.7 +/- 0.2 mm (right).

Constant temperature and moisture conditions are required during the test. This test is considered as a one-point test which means that even though with all the care during preparation of the test specimen each test produces a single value for the way in which the material responds to short-term loading. Progelhof and Throne emphasize that because the dimensions of each specimen varies the energy absorbed from it will vary with it. Thus, during the impact test it is especially important to keep all conditions as constant as possible to prevent from more deviations than already introduced because of the dimensions of the specimen (Progelhof, Throne 1993).

MELT FLOW INDEX (MFI)

The mass flow rate (g/10 min extruded) of a polymer is measure using a melt flow indexer with particular orifice. This test requires specified conditions of temperature and load. Commonly used test methods are published by ISO, DIN and ASTM. Specifications for the heat chamber and piston tip diameter are given so that “the shear stress on the polymer is the same in all machines for a given load”. Some materials can require further specification depending on the type of material (Dynisco Polymer Test Systems).

The test performing the melt flow test is described by ASTM D1238 (ASTM International 2008c) and ISO 1133.

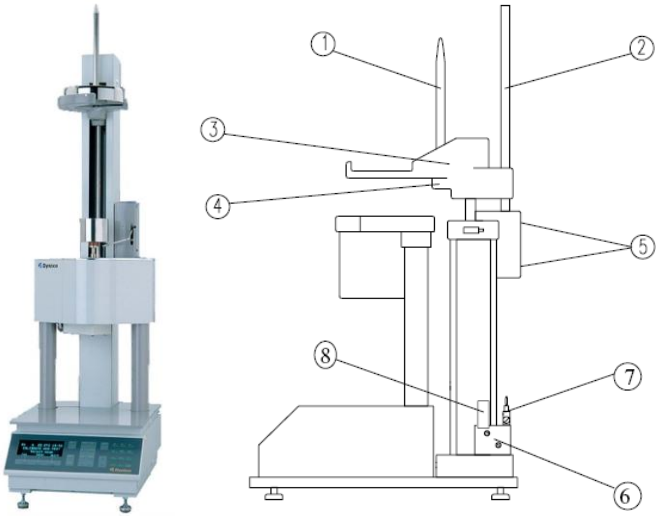

1 – safety spike

2 – guide post

3 – aluminium weight bucket

4 – set screw

5 – guide block set screws

6 – main solenoid valve

7 – switch

8 – low voltage solenoid switch

Figure 3-11 Melt flow index apparatus Dynisco (Celsum Technologies Limited 2008, Dynisco Polymer Test Systems).

There are different methods described for the melt flow test: Method A, Method B, and a combination from both, Method A/B. For the material tested in this project method A was used because the MFI of the polypropylene was 1.5 and the manual from Dynisco suggests method A for materials with a MFI below 50 g/10 min.

For method A the material is melted at 230 °C in the apparatus and a 2.13 kg weight was placed on top of the device. The extrudate is pushed out of the melt indexer and collected over a set period of time. The extrudate needed to be cut at the exact start- and endpoint of time across the orifice face. The result is reported in g/10 min.

Method B bases its measurement on the volumetric displacement instead of the weight per time. Method A/B is a combination of both and performs them on the same charge of material.

For the MFI test method A was used for all materials.

WATER ABSORPTION

The absorption of water was measured over several months according to the (ASTM International 2008e) methods. The bars were weighted and then soaked in deionised water for 6 months. The water was replaced regularly so that the development of bacteria and fungi was reduced. The weight of the bars was taken after drying them and was plotted as water uptake (wt-%) over time. Another plot was drawn, according to the method described

by Panthapulakkal and Sain (Panthapulakkal, Sain 2007), where the logarithm of time versus the logarithm of M_t/M_m was plotted. M_t is the water uptake (% wt/wt) at any time and M_m (% wt/wt) is the saturation point of the material.

By using Equation 3-6 and plotting $\log\left(\frac{M_t}{M_m}\right)$ against the logarithm of the time, the diffusion coefficient D can be estimated Equation 3-7.

$$Water\ absorption\ M_t[\%] = \frac{W_{(t)} - W_{(0)}}{W_{(0)}} * 100 \qquad \text{Equation 3-4}$$

$$kt^n = \frac{M_t}{M_m} \qquad \text{Equation 3-5}$$

$$\log\left(\frac{M_t}{M_m}\right) = \log(k) + n\log(t) \qquad \text{Equation 3-6}$$

$$\frac{M_t}{M_m} = \frac{4}{h}\left(\frac{D}{\pi}\right)^{1/2} t^{1/2} \qquad \text{Equation 3-7}$$

$W_{(t)} = weight\ of\ sample\ at\ time\ t$
$W_{(0)} = initial\ weight\ of\ sample\ (at\ time\ t = 0)$
$M_t = moisture\ content\ at\ time\ t$
$M_m = moisture\ content\ at\ equilibrium$
$k = constant; intercept\ with\ y-axis\ obtained\ from\ plot\ Equation 3-4$
$n = constant; slope\ obtained\ from\ plot\ Equation 3-4$
$D = Diffusion coefficient$
$h = height\ of\ sample$

DIFFERENTIAL SCANNING CALORIMETRY (DSC)

The calibration for the test device (DSC Q 2000) was done with the Tzero™ method. The first calibration experiment is done without any samples or pans for the baseline and the second calibration experiment involved a 96.21 mg sapphire disk (without pans) on the sample and reference positions. The temperature range was 0 °C to 400 °C.

The test specimens were put in an aluminium pan and sealed with a lid. The test was done in three steps: first heating, cooling and second heating. The first cycle was carried out at a

heating rate of 10 °C/min and a temperature range from 25 °C to 210 °C. The same conditions were used for the second heating cycle. The cooling phase was 10 °C/min until room temperature was reached. The purge gas was nitrogen. The data were plot as shown in Figure 2-19 and the crystalline fraction was determined by using Equation 3-8, Equation 3-9, and Equation 3-10.

$$H_{melting} - H_{crystallization} = H'_{crystalline\ before\ heating} \quad \text{Equation 3-8}$$

$$\frac{mass_{crystalline}}{mass_{total}} = fraction\ of\ crystallinity \quad \text{Equation 3-9}$$

$$\frac{H'_{crystalline\ before\ heating}}{H^*_{specific\ melting\ heat}} = mass_{crystalline} \quad \text{Equation 3-10}$$

$$\frac{H'_{crystalline\ before\ heating}}{H^*_{specific\ melting\ heat}} * \frac{100}{mass_{polymer}} = degree\ of\ crystallinity \quad \text{Equation 3-11}$$

3.2.8 FIELD EMISSION SCANNING ELECTRON MICROSCOPY WITH ENERGY DISPERSIVE X-RAY ANALYSIS (FESEM WITH EDX)

The gold coating was done with the gold coating unit Desk II from Denton Vacuum (USA) and as inert gas Argon was used. A Field Emission Scanning Electron Microscope (FESEM) model Gemini Leo 1530 from Carl Zeiss AG (Germany) was used. The EDX detector and the software were from EDAX (AMETEK, Inc.).

4 RESULTS AND DISCUSSION

4.1 ALKALINE EXTRACTION

The alkaline extraction was performed at different temperatures, times, pH and NaCl conditions. The protein concentration was determined before and after the extraction using the Kjeldahl method and are shown in Table 4-1. The variable X represents the protein content [wt-%] for each sample.

For a better comparison of the extraction, an ANOVA table (Table 4-2) was created and the significant effects were identified. Significant terms are marked with a star. The residual plot and the normal probability plot of the residuals (Figure 5-1 and Figure 5-2) can be found in Appendix.

Table 4-1 2^{4-1}_{VI} Fractional factorial design for the alkaline extraction of protein from soy flakes. The variable X represents the protein content [wt-%] for each sample.

	A	**B**	**C**	**D**		
Run	T [°C]	pH	NaCl	Time [h]	X [%]	SD (n = 6)
1	50	7	water	1	50.38	0.02
2	80	7	water	3	48.55	0.11
3	50	10	water	3	43.21	1.03
4	80	10	water	1	41.04	1.03
5	50	7	1 M NaCl	3	40.73	0.58
6	80	7	1 M NaCl	1	40.64	0.75
7	50	10	1 M NaCl	1	40.34	0.46
8	80	10	1 M NaCl	3	36.70	0.16

The average protein removal (wt-%) based on the 8 experiments listed in Table 4-1 is 42.7 % +/- 4.57 %. The confidence interval obtained with the t-Test ($t_{0.05;\ 7} = 2.36$) is between 38.88 and 46.52 %. The role of the experimental conditions of the 2^{4-1} is given by Equation 4-1.

$$y_i = \beta_0 - 0.967\,\beta_1 - 2.3765\,\beta_2 - 3.0968\,\beta_3 + 1.2926\,\beta_4 \qquad \text{Equation 4-1}$$

$\beta_0 = \overline{X}$; β_1 = A = BCD; β_2 = B=ACD; β_3 = C=ABD; β_4 = AD=BC;

Table 4-2 ANOVA for the 2^{4-1}_{VI} factorial design.

	Effect	SS	df	MS	F_{obs}
A = BCD	-1.934	7.48069	1	7.4807	10.63*
B = ACD	-4.7531	45.1834	1	45.183	64.23*
C = ABD	-6.1936	76.7225	1	76.723	109.06*
D = ABC	-0.7998	1.27925	1	1.2793	1.82
AB = CD	-0.9689	1.87742	1	1.8774	2.67
AC = BD	0.0669	0.00894	1	0.0089	0.01
AD = BC	2.5852	13.3666	1	13.367	19.00*
Error		2.11041	3	0.7035	
				$F_{1,3,0.05} = 10.13$	

The statistical analysis shows significant effects for temperature (A), pH (B) and NaCl (C). A significant interaction is identified between the time and the temperature (AD) or NaCl and pH (BC).

To comment on the success of the extraction, the yield of extracted protein was calculated by using Equation 4-2 and the experimental data (Table 4-1). The yield of protein extraction for water (Y_{H20}) is 61.09 % and 51.39 % for the extraction in a 1 M NaCl solution (Y_{NaCl}).

$$Extraction\,Yield = \frac{Protein\ mass_{before\ AE}(g) - Protein\ mass_{after\ AE}(g)}{Protein\ mass_{before\ AE}(g)} * 100 \qquad \text{Equation 4-2}$$

The effect of the NaCl on the filler composition, was also obtained from the ash content determined according to the standard test method (ASTM International 2008b). The ash content, shown in Table 5-1 and displayed graphically in Figure 4-1, shows a significant increase in the ash content (more than 10 %) when NaCl was present. A summary of the data is shown in the appendix (Table 5-1) with the protein and the ash content measured experimentally and the carbohydrates content determined by t difference.

4.1.1 MATERIAL BALANCE APPROACH A

Material balance approach A is based on the measurement of the protein content determined with the Kjeldahl nitrogen method and the ash content with the ASTM standard method E 1755 – 01 (ASTM International 2007). The amount of carbohydrates is the difference of proteins and ash subtracted from the total mass of the freeze-dried samples.

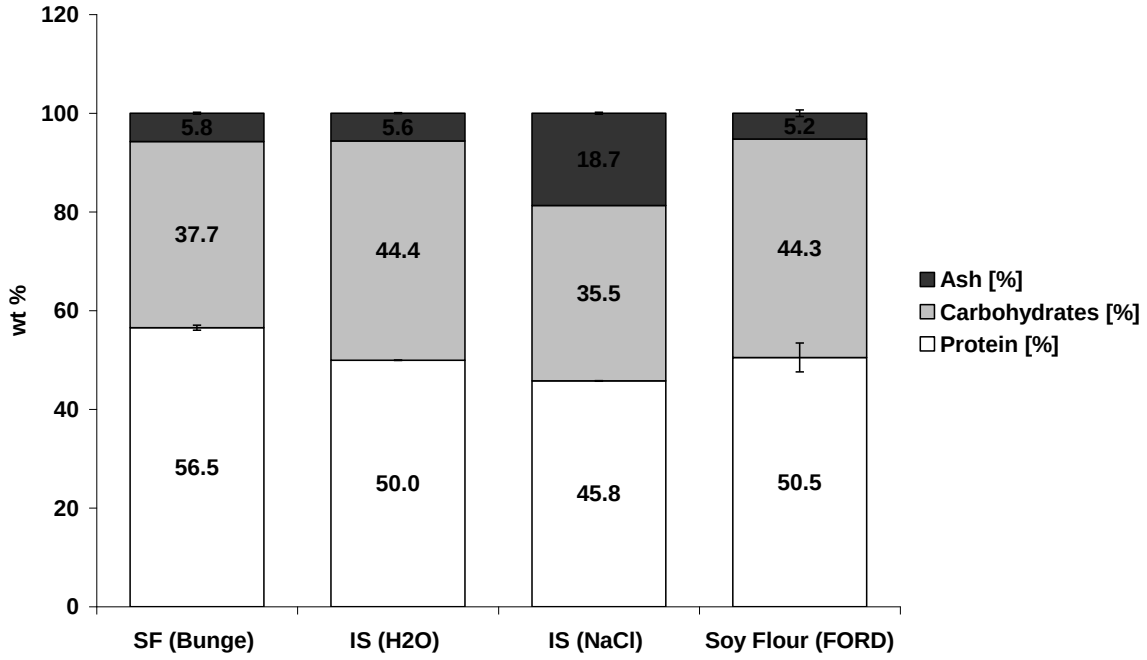

Figure 4-1 Material composition (protein, carbohydrates, and ash) for the different filler (SD: $n_{min} = 3$): SF (Bunge), IS_{H2O}, IS_{NaCl}, and Soy Flour (Ford). The carbohydrate content is the difference between the total mass and the mass of protein and ash.

The amount of ash in IS_{NaCl} is significantly higher (2.2 higher than SF (Bunge)) compared to the other filler because it includes the salt remaining from the alkaline extraction with 1 M NaCl. The protein content varies from 45.8 wt-% for IS_{NaCl} and 56.5 wt-% for SF (Bunge). The protein content of the soy flour (Ford) is nearly identical to the protein content of IS_{H2O}. The ash content and subsequently the carbohydrate content are nearly the same for the soy flour (Ford) and the IS_{H2O}.

4.1.2 MATERIAL BALANCE APPROACH B

An alternative material balance, approach B, was conducted using methods of the food industry. In this approach, the agricultural material is represented as a combination of acid detergent fiber, neutral detergent fiber, protein and lignin. This analysis was carried out by Agriculture and Agri-Food Canada, Guelph, Ontario, Canada.

ADF means acid detergent fiber and describes the amount of cellulose and lignin where the neutral detergent fiber (NDF) represents cellulose, hemicellulose and lignin which are mainly present in the cell walls.

The protein content determined by Agriculture and Agri-Food Canada shows 10 to 19 % decreased value for IS_{H2O} and IS_{NaCl}. The ADF content which represents cellulose and lignin increased of 45 % for IS_{H2O} but decreased to 57 % of ADF in SF (Bunge) before the treatment. The NDF content in IS_{H2O} shows again an increase and IS_{NaCl} a slightly decrease. By comparing the total amount of the four components it is noticeable that IS_{NaCl} has 33.5 % of unidentified parts which is labelled as loss. SF (Bunge) and soy flour (Ford) is missing 20.7 and 16.2 % of its mass and IS_{H2O} has the lowest loss with 11.1 %. It is quite likely that this loss is constituted of water soluble particles such as sugars and salts. The NaCl in IS_{NaCl} got dissolved again and could not be detected with any of the used methods.

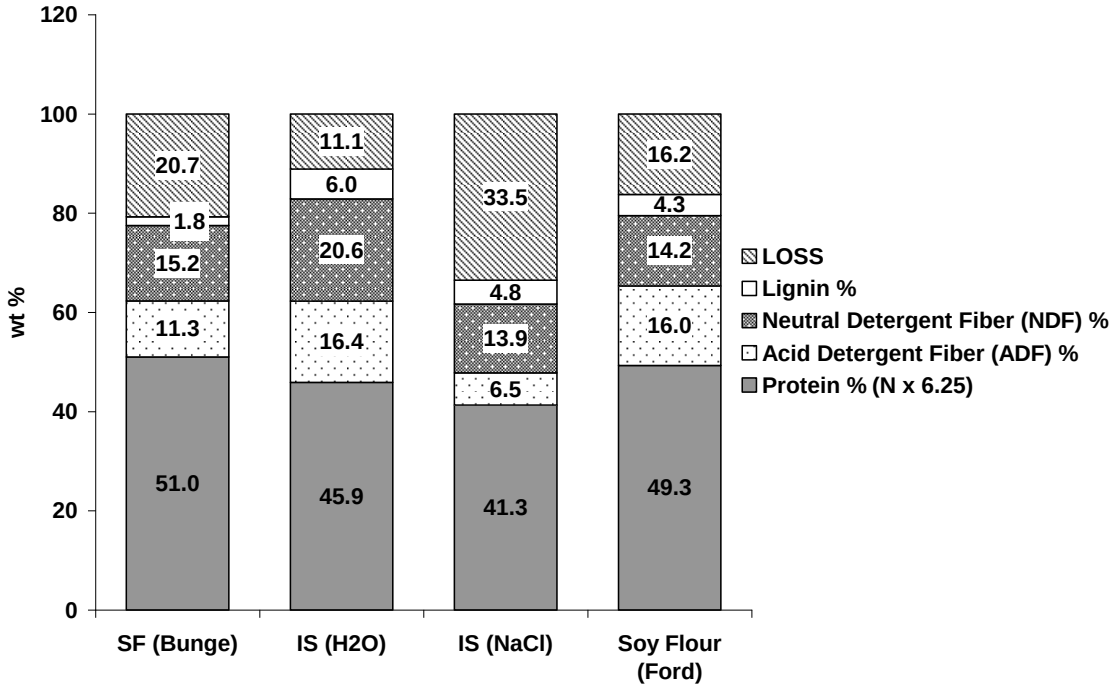

Figure 4-2 Filler composition based on the determination of ADF, NDF, protein and lignin contents according to commonly used methods in the food industry, carried out by Agri-Food Laboratories, Guelph, Ontario, Canada.

4.2 GRINDING

The grinding of the soy flakes was performed to increase the yield of the protein extraction (Russin, Arcand et al. 2007) but also to decrease the particle size for compounding. A smaller particle size can improve the dispersion and distribution of the filler and thus increase the mechanical properties of the composite material. The particle size distribution and aspect ratio distribution for the filler are presented in Figure 4-3 to Figure 4-9.

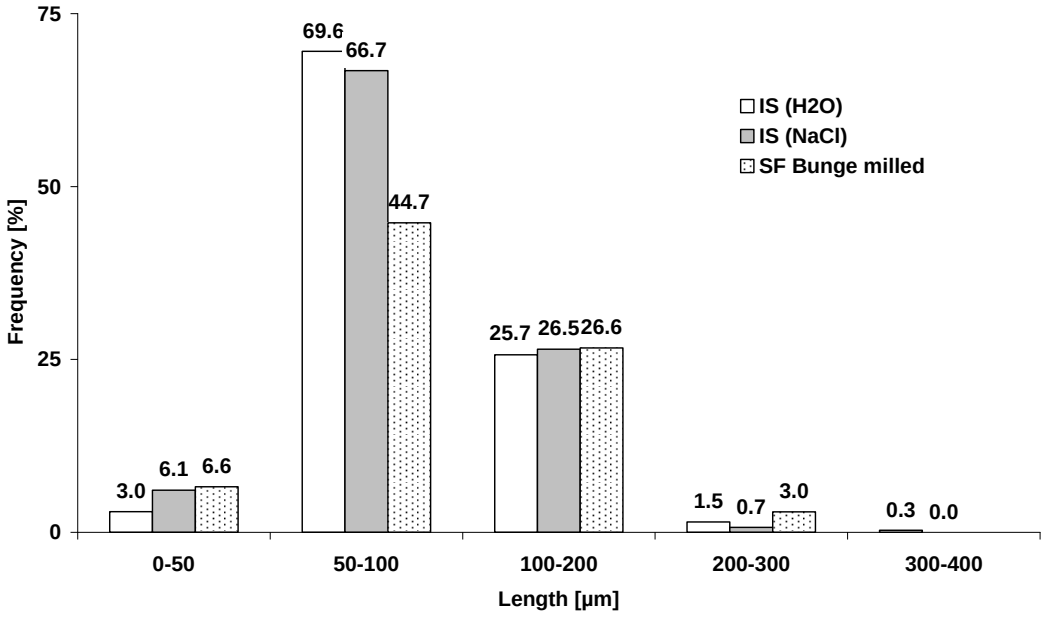

Figure 4-3 Length distribution for IS_{H2O}, IS_{NaCl}, and SF (Bunge) after milling.

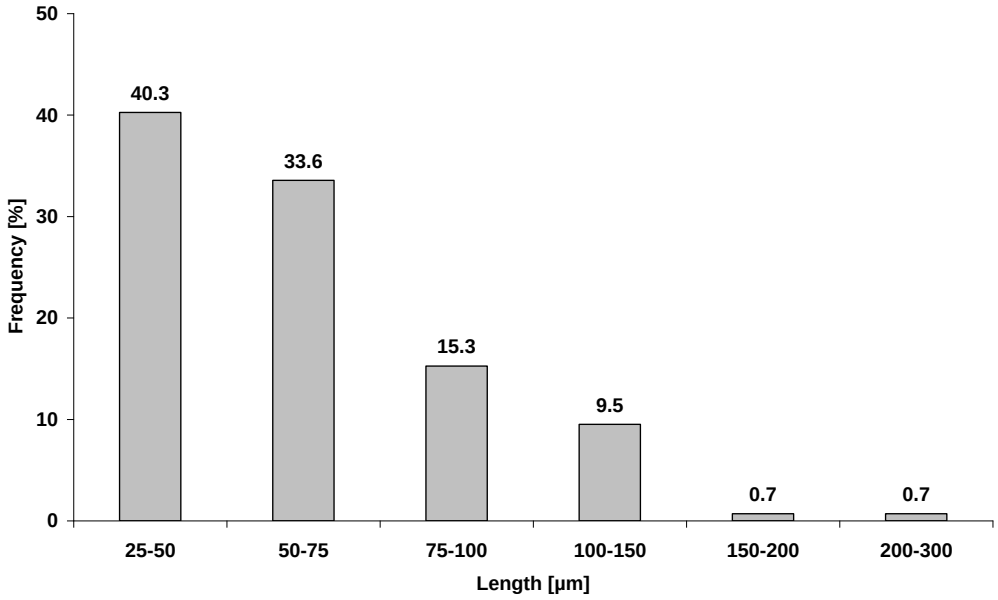

Figure 4-4 Length Distribution for Soy Flour (Ford).

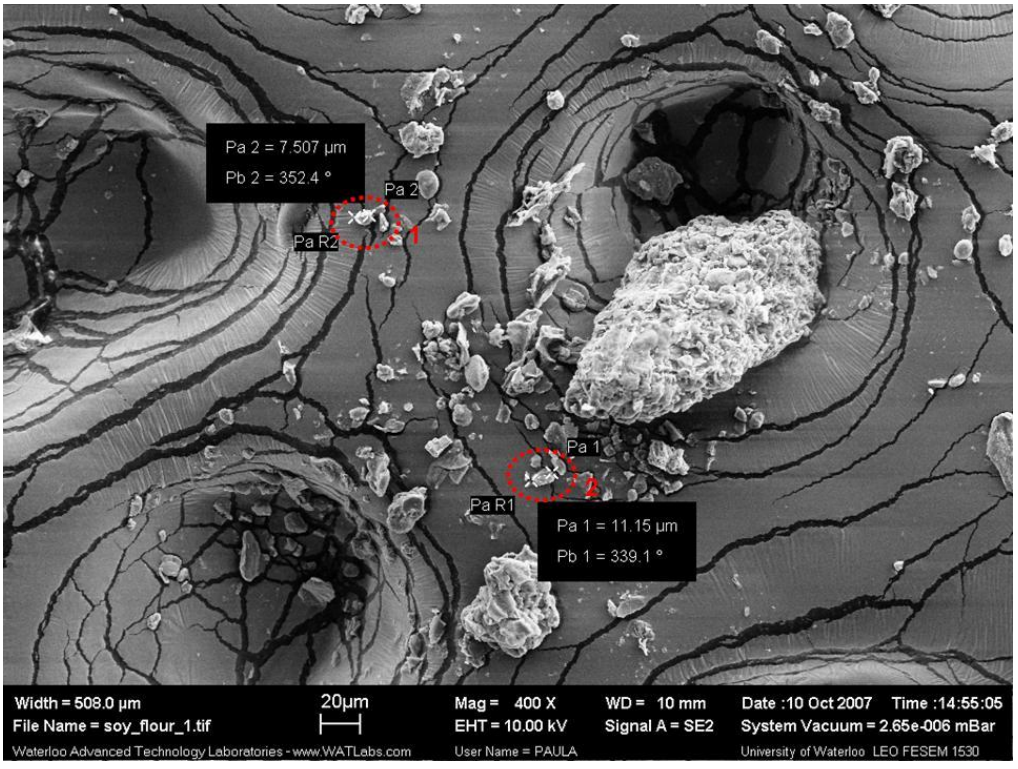

Figure 4-5 Scanning electron micrograph of the soy flour (Ford) with particle size measurements.

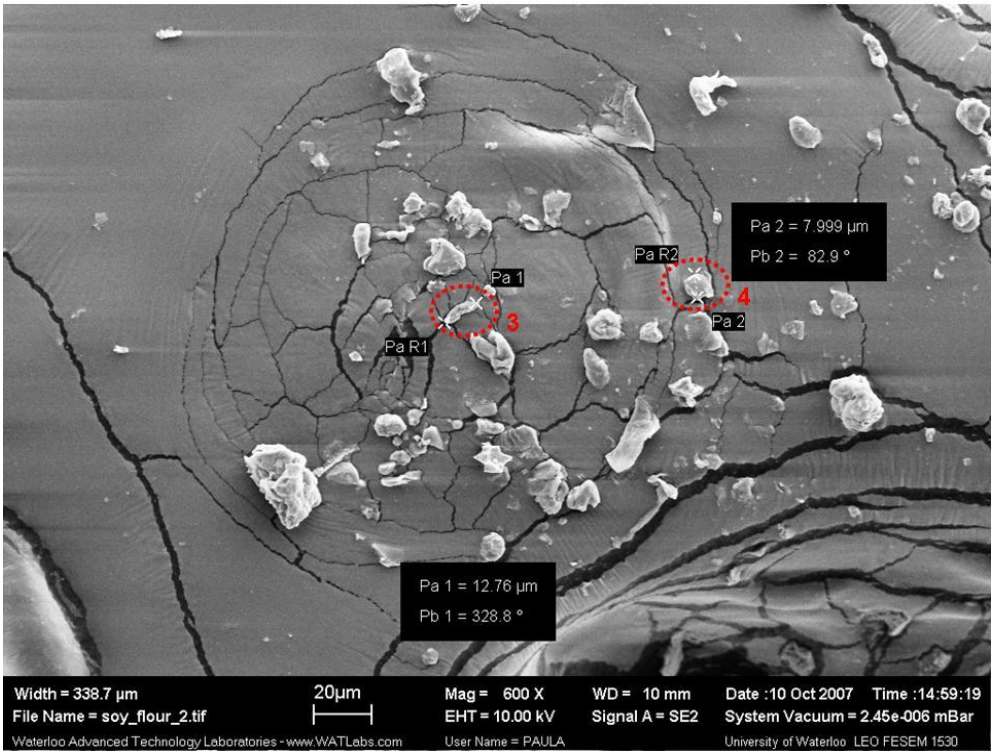

Figure 4-6 Scanning electron micrograph of the soy flour (Ford) with particle size measurements.

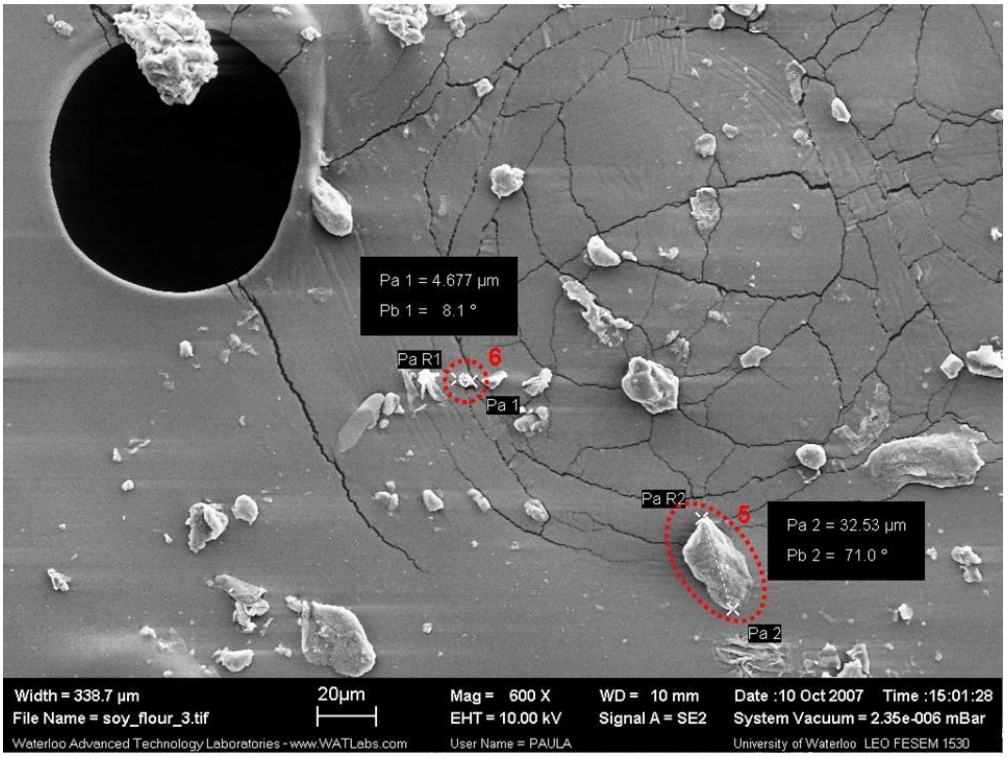

Figure 4-7 Scanning electron micrograph of the soy flour (Ford) with particle size measurements.

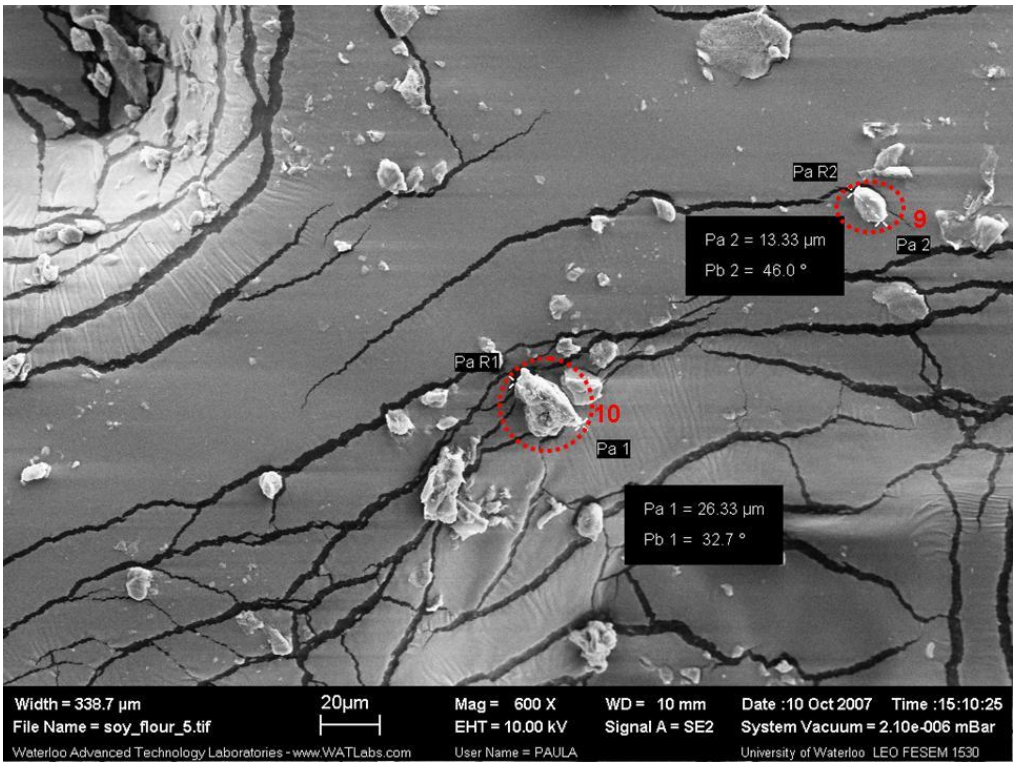

Figure 4-8 Scanning electron micrograph of the soy flour (Ford) with particle size measurements.

Table 4-3 Particle size of soy flour (Ford), measured from the FESEM images.

Particle	Size [µm]
1	7.51
2	11.15
3	12.76
4	8.00
5	32.53
6	4.68
7	13.00
8	11.87
9	13.33
10	26.33
	Average = 14.1153 µm (SD (n = 10) = 8.67)

The length distributions of the filler as well as the aspect ratio show a similar pattern. The predominant size (near 70 %) is in the range of 50 – 100 µm. The remaining predominant particle size (over 25 %) is in the 100 – 200 µm size range. A small fraction of the filler has a particle size below 50 µm. Overall, the particle size of the filler is below 200 µm for both types of extracted filler (98.3 % of IS_{H2O} and 99.3 % of IS_{NaCl}).

The analysis of the length distribution of the soy flour was done by using the scanning electron microscope and measuring the size of some particles. These measurements only provide preliminary data of a small sample that are limited in validity. The size measurements are presented in Figure 4-4, indicates that the soy flour has a small particle size. This small size is outside of the range where the technique is reliable. Based on these considerations, one can assume that the actual size of the particles is less than 50 µm. Also one has to keep in mind the presence of static charges that cause the clumping of several particles and lead to false measurements. One clump may have been counted as one large particle instead of several small particles. The presence of such clumps is confirmed by FESEM images (Figure 4-5, Figure 4-6, Figure 4-7, and Figure 4-8) where a particle that appears large is in reality a combination of small particles. This situation is supported by the wide range of particle size measured, 4.67 and 32.53 µm, and presented in Table 4-3.

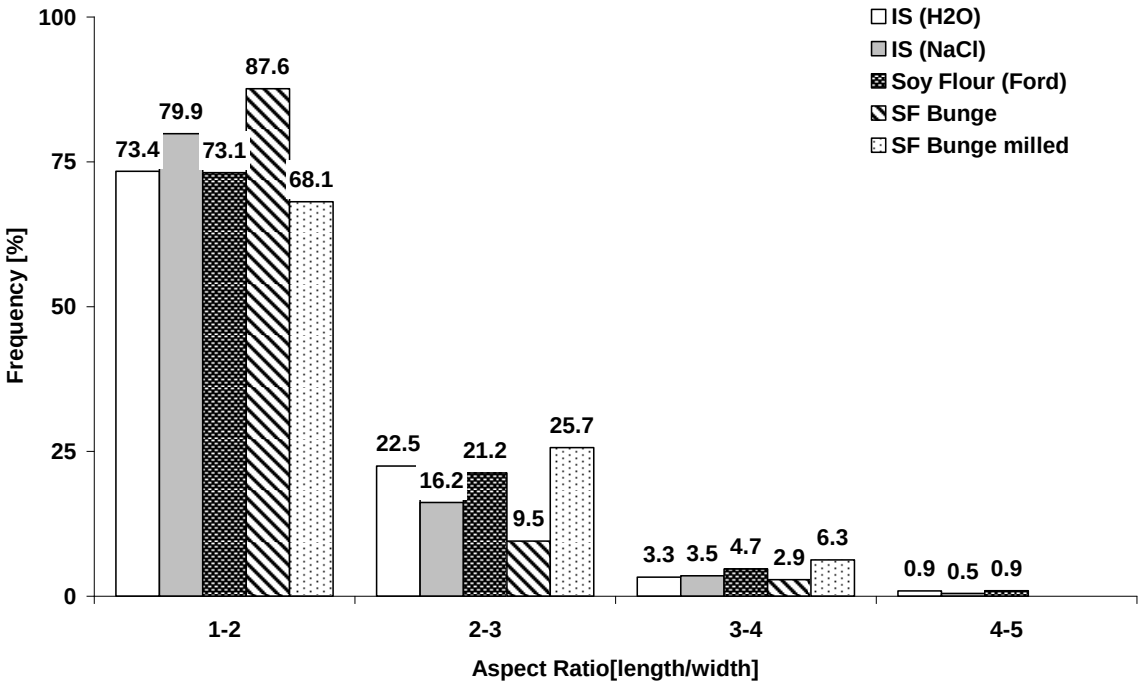

Figure 4-9 Aspect ratio distribution for IS_{H2O}, IS_{NaCl}, Soy Flour (Ford), SF (Bunge), and SF (Bunge) after milling.

The aspect ratio, the ratio of the length and width, of a particle describes its shape. A particle with an aspect ratio larger than 10 is considered to be a fiber. The aspect ratio for the IS_{H2O}, IS_{NaCl} and Soy Flour (Ford) presented in Figure 4-9, indicates that all filler materials have an aspect ratio <5 which is characteristic of a particle shape. An aspect ratio

of 1 (equal length and width) was observed for at least 73 % of the total IS_{H2O} and the total Soy Flour (Ford) and near 80 % of total IS_{NaCl}.

4.3 THERMOGRAVIMETRIC ANALYSIS (TGA)

Thermogravimetric analysis provides information on the thermal stability of a single material or a composite material. Depending on the composition and the structure of materials, the degradation due to temperature can change.

The thermal degradation of the individual components contained in soy flakes, proteins, cellulose, lignin and ash, was obtained. In Figure 4-10 the degradation profile of the cellulose, lignin and two of the major soy proteins (7S and 11S) standards are presented. Table 4-4 shows the onset of degradation, the temperature at the peak maximum and the corresponding weight loss for each peak.

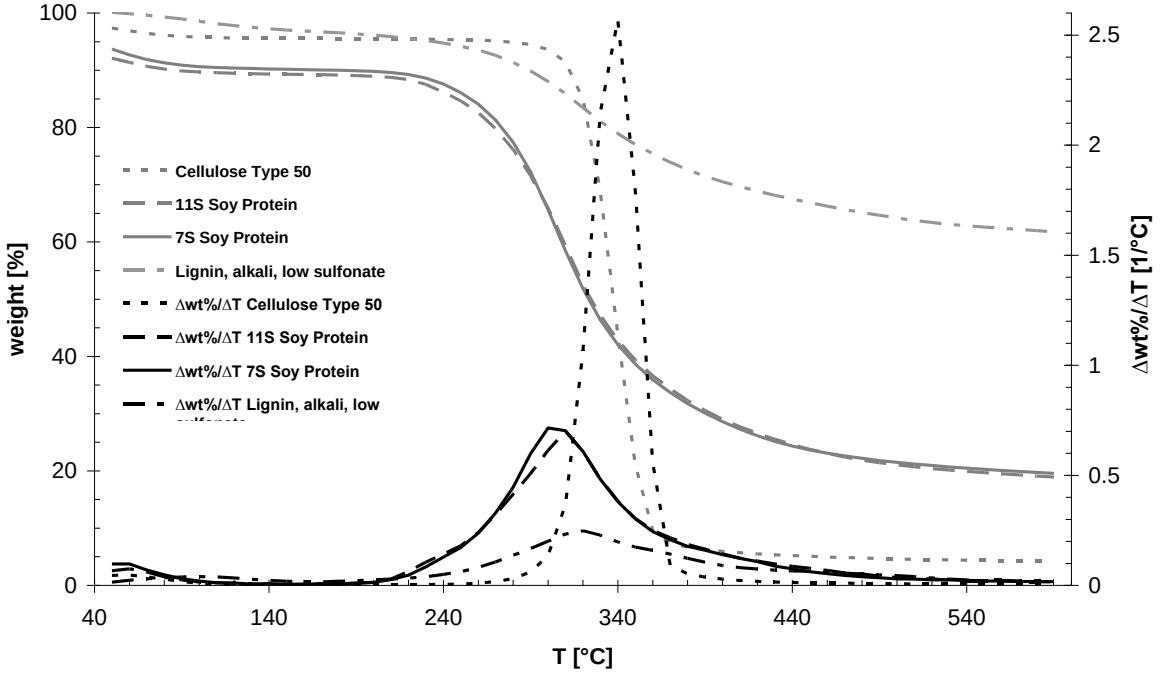

Figure 4-10 Thermal gravimetric analysis of lignin, cellulose, 7S soy protein, and 11S soy protein, TGA was carried out at a heating rate of 10 °C/min in nitrogen (Δwt%/ΔT is the derivative curve corresponding to the right-side axis; these curves are plotted in black color).

The thermal degradation of lignin (Figure 4-10) has a very broad peak over a wide temperature range. The onset of degradation is observed at 164 °C and a total weight lost at

600 °C is about 40 %. This profile reflects the complex and heterogeneous structure of lignin and the effects of the extraction protocol that may affect its chemical structure and the corresponding degradation profile. In contrast, cellulose shows a very sharp peak that starts at 268 °C and a total weight loss above 95 % at 600 °C. The 7S and 11S soy proteins have a very similar thermal degradation behaviour which is representative for soy proteins in general (Schmidt, Giacomelli et al. 2005, Nanda, Rao et al. 2007). The onset of degradation is around 200 °C and the total weight loss at 600 °C was about 80 %.

Table 4-4 Thermogravimetric analysis for standards: lignin, cellulose, 7S soy protein , and 11S soy protein (10 °C/min heating rate in nitrogen).

Sample	Onset of degradation [°C]	$Peak_1$ [°C]	Δw_1 [%]	Weight at 600 °C [%]
Lignin, alkali, low sulfonate	164	319	34.15	61.71
Cellulose	268	338	89.58	4.14
7S soy protein	194	303	68.41	19.48
11S soy protein	200	312	68.00	18.86

As the fillers considered in this study are derived from soy flakes containing lignin, cellulose and protein, their thermal degradation profile is expected to be a combination of the individual thermal degradation profiles. The thermogravimetric analysis plots for IS_{H2O} and soy flour (Figure 4-12) are nearly identical which is due to their similar composition where cellulose predominates and has an onset of thermal degradation above 250 °C and the supernatant contains mainly proteins with an onset of thermal degradation of 200 °C and other soluble components.

Figure 4-11 shows the thermal profile of soy flakes as well as the IS_{H2O} and the supernatant after the water alkaline extraction. Both peaks, the cellulose and protein peaks, are present in all samples but the intensity is different according to the sample. The supernatant has the most intense first peak which corresponds to the protein while the IS_{H2O} with the lowest protein content shows only a shoulder at the same temperature. The untreated soy flakes presents both peaks but also the supernatant (extracted protein) has the second peak. This shows that other soluble components are present with similar degradation pattern to the proteins.

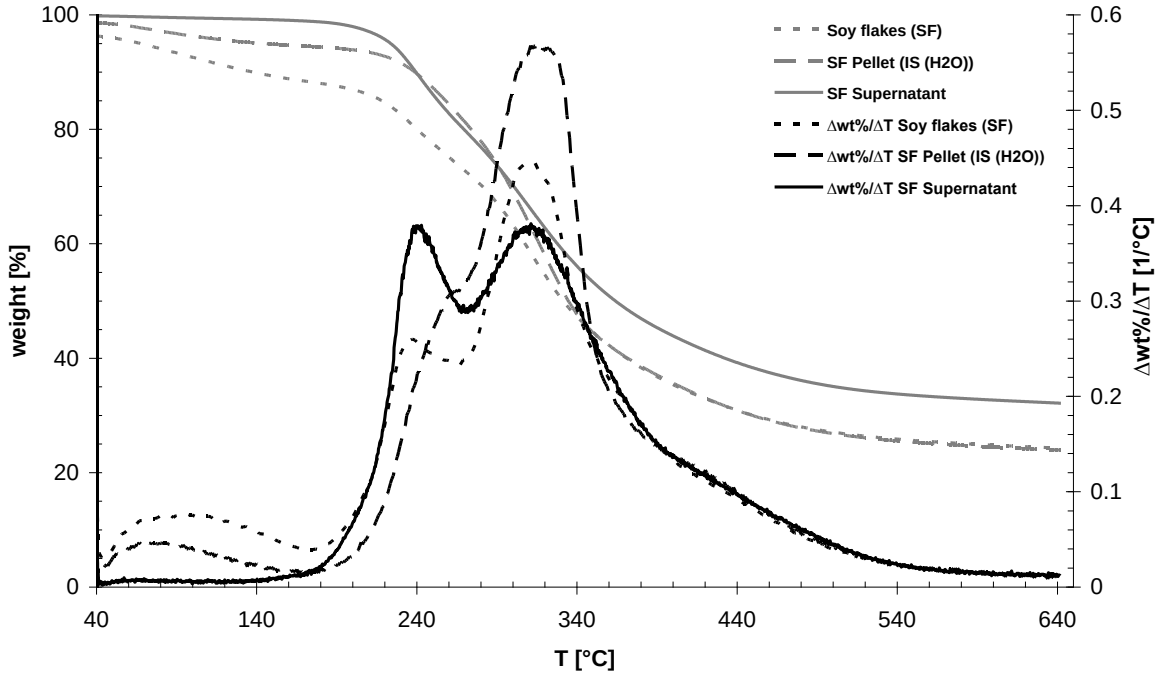

Figure 4-11 Thermogravimetric analysis of soy flakes, water insoluble pellet (IS_{H2O}), and water soluble supernatant after the alkaline extraction. TGA was carried out at a heating rate of 10 °C/min in helium (Δwt%/ΔT is the derivative curve corresponding to the right-side axis; these curves are plotted in black color).

The thermogravimetric analysis performed with nitrogen is presented in Figure 4-12. The first peak represents the thermal degradation of the proteins. The intensity of this peak for the untreated materials (soy flakes and soy flour) is higher because of the higher protein content. In contrast, the IS_{H2O} and IS_{NaCl} have a less intense peak which reflects the lower protein content due to the alkaline extraction.

The second peak is attributed to the cellulose in the material. The thermal degradation of lignin is difficult to identify because lignin has a broad thermal degradation profile which is assumed to occur over the entire temperature range and without the appearance of a significant peak. The onsets of degradation, the temperatures at the peak maxima and the weight at 600 °C are listed in Table 4-5.

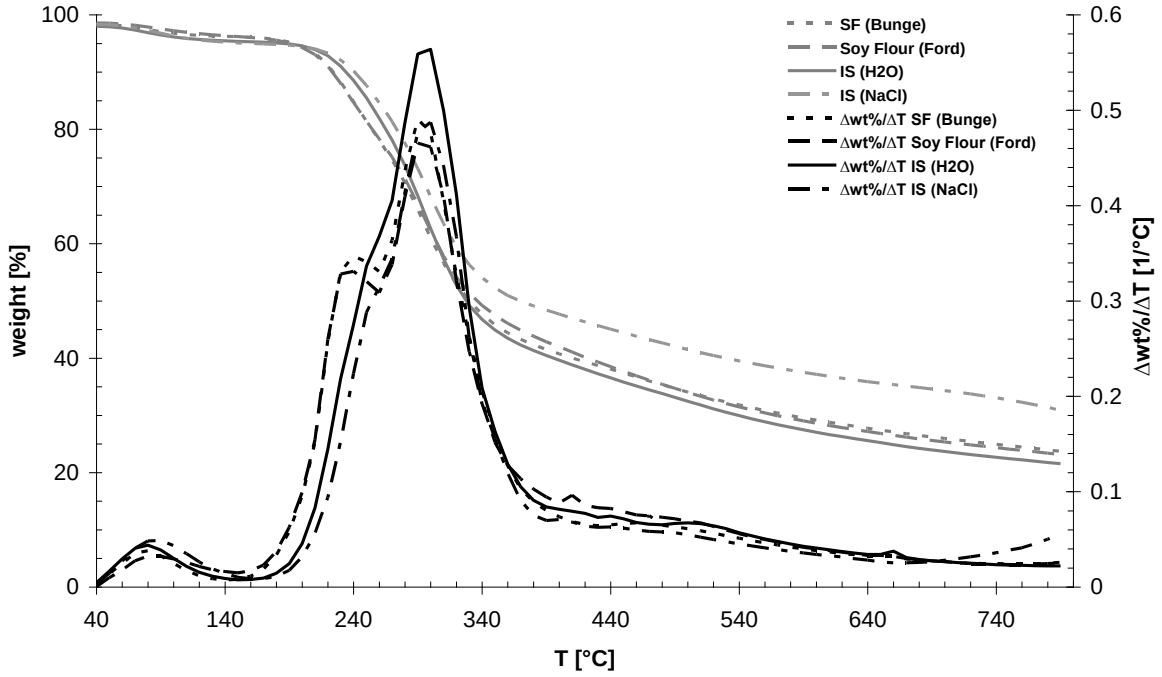

Figure 4-12 Thermogravimetric analysis of soy flour (Ford), SF (Bunge), IS_{H2O}, and IS_{NaCl}; TGA was carried out at a heating rate of 10 °C/min in a nitrogen environment (Δwt%/ΔT is the derivative curve corresponding to the right-side axis; these curves are plotted in black color).

Table 4-5 Thermogravimetric analysis features for soy flakes (Bunge), soy flour (Ford), IS_{H2O}, and IS_{NaCl}.

Sample	Onset of degradation [°C]	$Peak_1$ [°C]	Δw_1 [%]	$Peak_2$ [°C]	Δw_2 [%]	Weight at 600 °C [%]
Soy flakes (Bunge)	158	240	15.0	294.0	36.0	29.2
Soy flour (Ford)	155	234	13.5	294.0	35.5	28.6
IS_{H2O}	170	255	14.0	295.5	35.0	27.0
IS_{NaCl}	170	254	16.0	296.7	30.0	37.0

4.4 STRUCTURAL ANALYSIS BY LIGHT MICROSCOPY

Light microscopy in combination with different staining methods was used to investigate the distribution of the protein and cellulose in the filler material. Raw unprocessed soybean was used for comparison (Figure 4-13 (left)). The three major parts of a soybean are

illustrated in Figure 4-13 (right): the axis, the testa, and the cotyledons. The testa is the outside of the soybean which is subdivided in the palisade layer, the hourglass layer, the compressed parenchyma, the aleurone layer, and the compressed endosperm. A schematic image is shown in Figure 4-14.

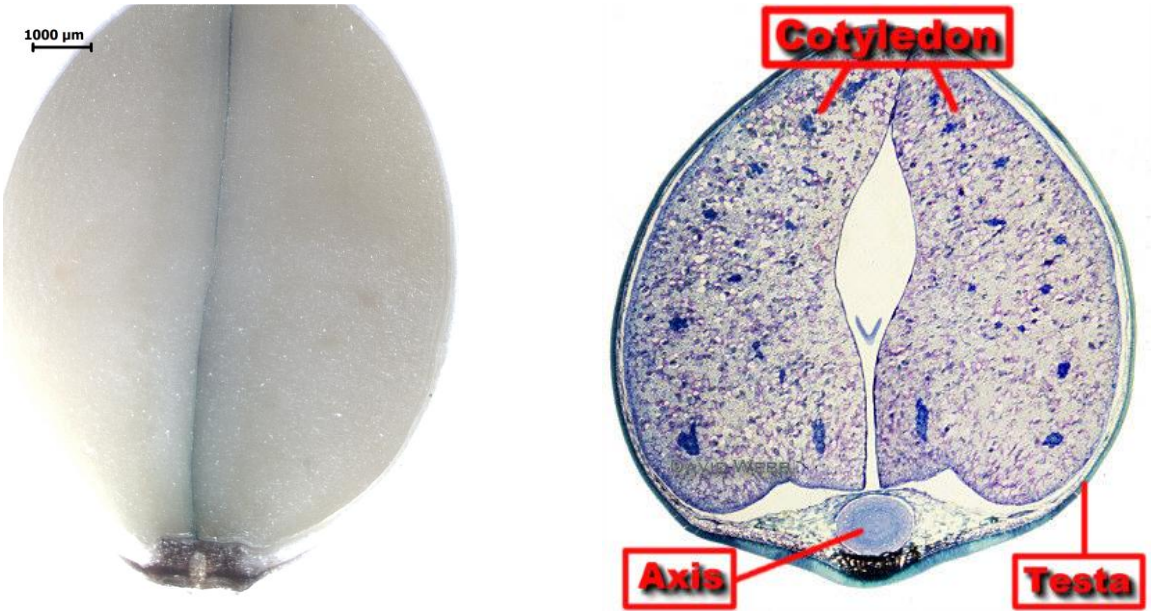

Figure 4-13 Light microscope image of a cross-section of a soybean (left) and the cross-section of a bean seed through the middle of the Embryonic Axis (right) (Webb).

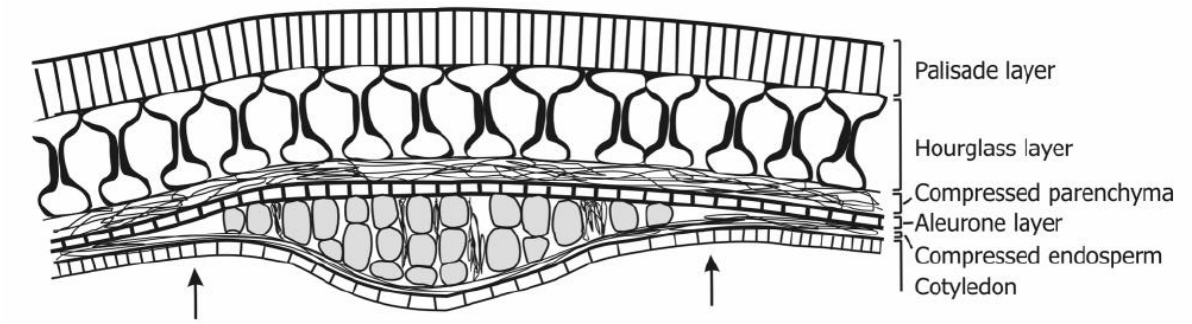

Figure 4-14 Schematic illustration of the soybean testa (Ma, Peterson et al. 2004).

A cross-section of a raw soybean was stained with methylene blue for cellulose identification and visualized with light microscopy (Figure 4-15, left). The cell wall and the palisade- and hourglass layer of the soybean are clearly visible. The protein distribution of a raw soybean was obtained by staining with Ponceau S (Figure 4-15, right).

A comparison of the cellulose and the protein distribution (Figure 4-15 and Figure 4-16) enables the identification of the palisade layer that contains mainly of cellulose. The cell walls of the soybean are also visible in the cellulose staining situation but not in the protein staining situation (Ponceau S). These observations confirm the common knowledge of plant structures and their composition.

These staining methods do not provide any quantitative analysis but gives qualitative information on the composition of the different parts of the soybean. This information will be used for the qualitative analysis of the processed soy flakes.

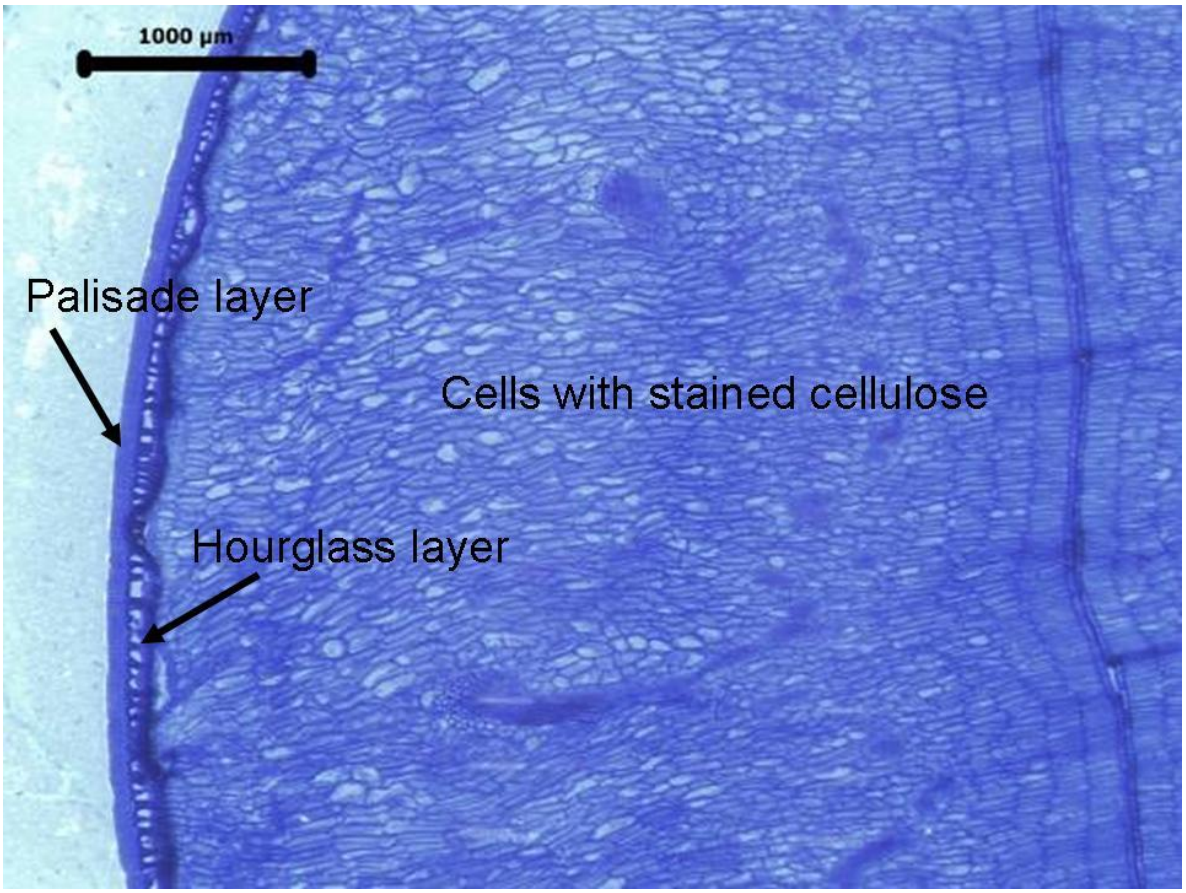

Figure 4-15 Cross-section of a soybean along the axis with methylene blue staining for cellulose visualization.

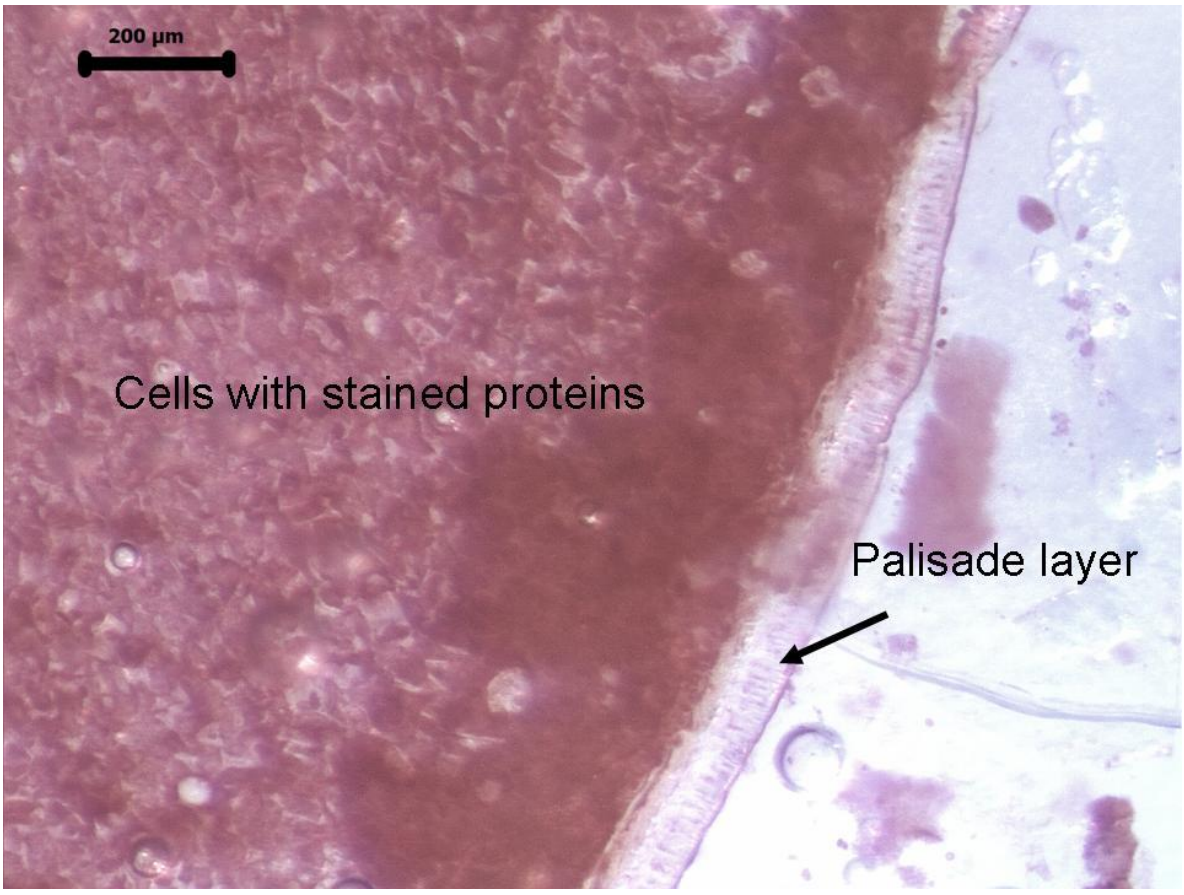

Figure 4-16 Cross-section of a soybean along the axis with Ponceau S staining for protein visualization.

Figure 4-17 and Figure 4-18 show soy flakes (after alkaline extraction) stained with Coomassie Brilliant Blue which binds via Van der Waals interactions to the amino acids histidine and arginine and thus proteins. After comparison with the images of the whole soybean we can identify again the palisade layer. The reason of the dislocation of the palisade layer is that processing of the soybean involves cracking and squeezing of the soybean to extract the oil. Some of the particles shown in Figure 4-18 are dark blue which indicates a high amount of protein but some particles are almost unstained which means that the protein content in these particles is very low. It is not possible to identify these particles as palisade layer, even though it could be an eagle eye view on a palisade layer. As shown in Figure 4-16, the only part of the soybean with a low protein content. The amount of ash in IS_{NaCl} is significantly higher (2.2 higher than SF (Bunge)) compared to the other filler because it includes the salt remaining from the alkaline extraction with 1 M NaCl. The protein content varies from 45.8 wt-% for IS_{NaCl} and 56.5 wt-% for SF (Bunge). The protein content of the soy flour (Ford) is nearly identical to the protein content of IS_{H2O}. The ash content and subsequently the carbohydrate content are nearly the same for

the soy flour (Ford) and the IS_{H2O} is the outside layer (testa). This leads to the conclusion that the unstained particles shown in Figure 4-18 must be from the testa of the soybean. The comparison of the staining of the various particles suggests relatively heterogeneous protein content in the soy flakes.

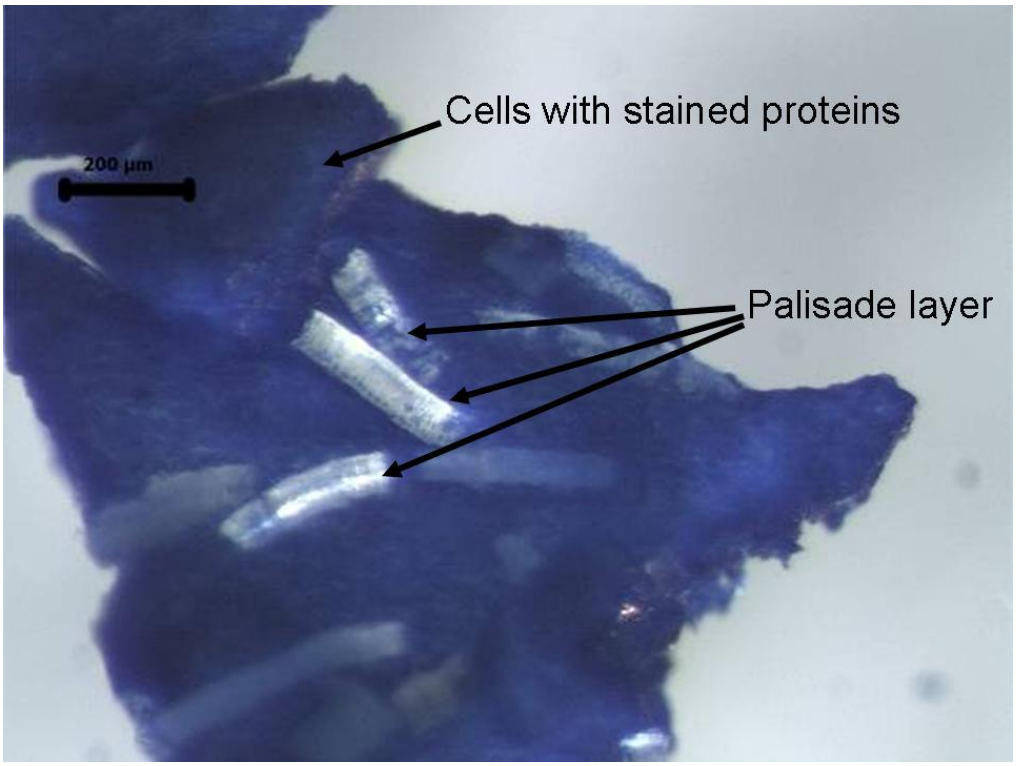

Figure 4-17 Soy Flake (Bunge) after AE and staining with coomassie brilliant blue to colour protein.

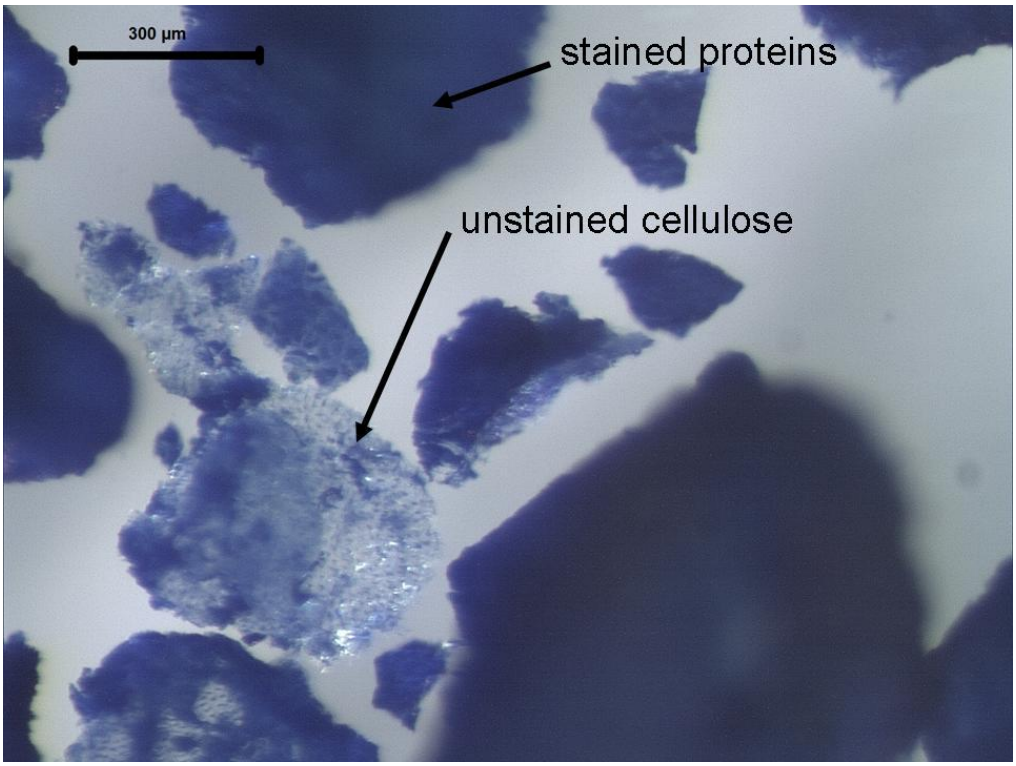

Figure 4-18 Soy Flakes (Bunge) after AE and staining with coomassie brilliant blue to colour protein.

The stained soy flake presented in Figure 4-17 was taken after the alkaline extraction of the proteins. The strong blue colour does not allow quantifying the protein left in the material but leads to the conclusion that the extraction could not remove all the protein. This is in agreement with the protein analysis as determined using the Kjeldahl method. The staining technique can show the location of the protein but does not give any information on the protein quantity. Therefore, this technique was not used for other treated soy flakes.

4.5 EXTRUSION

During the extrusion of the polypropylene and the IS, Irganox was used as anti-oxidant and maleic anhydride polypropylene was used as a coupling agent as indicated in Table 3-6. For comparison four different standards were prepared (Run # I – IV). The composition of the standard materials and the composites is shown in Table 3-6. A representative example for the extruded material is shown in Figure 4-19 with the pellets from Run # 4 (left) and a closer picture from a cross-section of an extruded pellet from Run # 1 (right). All extruded pellets had a similar appearance. The colour of the pellets changed to a brownish appearance due to the extrusion process and varied slightly depending on the type of filler used for the compounding. Bubbles appear in the pellets in all runs when a filler was present but seemed to be smaller in Run # 3 to 6 where the protein was extracted.

This change in colour could be due to the Maillard reaction that is a complex chemical process involving the amino acids or the proteins and reducing sugars and occurs during the storage or processing of foods (Morales, van Boekel 1998). The Maillard reaction can produce several products such as low molecular weight volatile compounds (Figure 4-19, right), and coloured compounds of low and high molecular weight (Morales, van Boekel 1998). Temperature, water activity, pH, moisture, and chemical composition of the organic material can increase the amount of the reaction products. The development of colour can be in the range of yellow to very dark brown. Brown pigments are contributed to aldehydes that are formed during Strecker degradation and condense with dehydration products such as themselves, sugars or furfurals (Morales, van Boekel 1998).

Geneau-Sbartai and Leyris attributed the weight loss between 100 and 220 °C during TGA of their sunflower biocomposites to two reasons: (a) to the Maillard reaction and (b) to condensation between phenolic acids and proteins (Geneau-Sbartai, Leyris et al. 2008). Another reason for the browning of the pellets could be due to the caramelization of the sugar compounds in the filler. However, Morales' and van Boekel's study on casein/sugar

solutions points out that the main reason for the browning during heating is due to the Maillard reaction of pigments bounded to the proteins (Morales, van Boekel 1998).

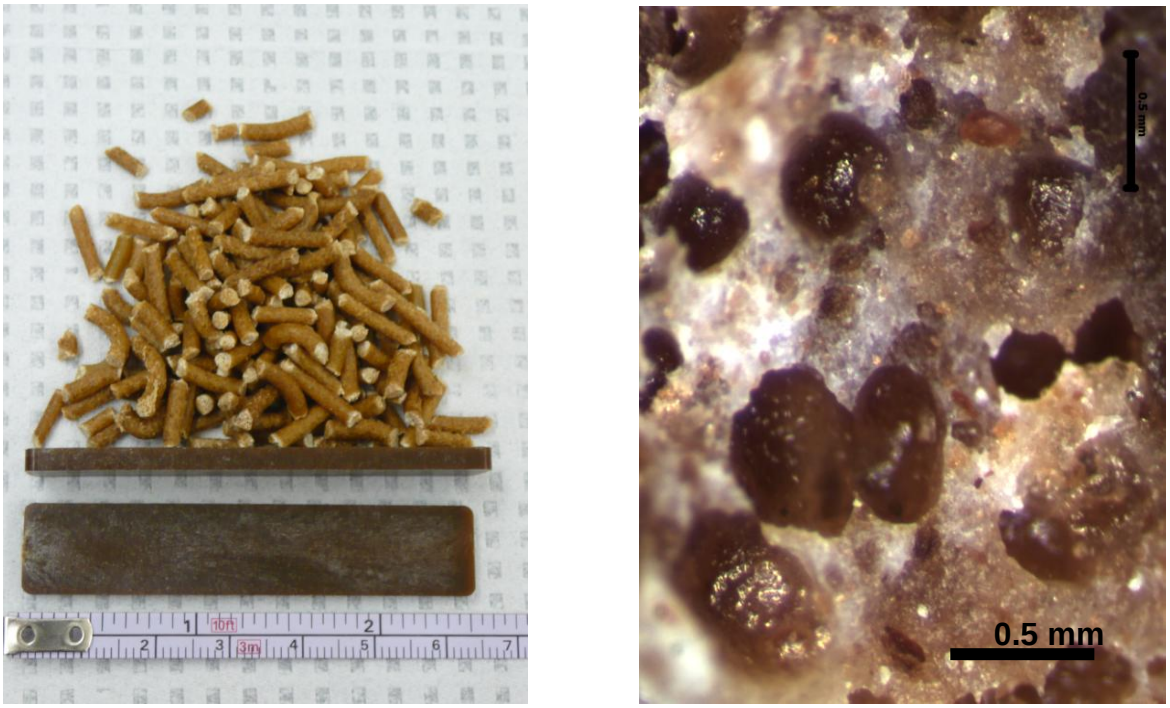

Figure 4-19 Extruded pellets and pressed bars from pp and IS_{H2O} Run # 4 (left); Cross-section of an extruded pellet (Run # 1) (right).

4.6 INJECTION MOULDING

The pellets obtained from the compounding were used to press bars with dimensions according to ASTM mechanical properties test methods for plastics (D 256 – 06a and D 790 – 03). Each bar was checked visually to identify any unevenness or inconsistent appearance which could indicate trapped air (bubbles) for instance. An identical thermal history of the bars was obtained by annealing the bars in an oven as described in section 3.2.6.

In Figure 4-20 a representative bar of each run (Table 3-6) is shown. The runs that did not undergo the alkaline extraction (Run # 1 and 2, Run # 7 and 8) seem to have a darker colour (like dark chocolate) than the runs that were subjected to the alkaline extraction (Run # 3 to 6) and appear to have a milk chocolate-like colour. The possible reason for the variation in colour might be the difference in protein content but more likely due to the different

carbohydrate content of the treated filler. Due to the alkaline extraction, the carbohydrate dissolved in the liquid (supernatant) was extracted/separated from the IS during the subsequent centrifugation.

Figure 4-20 Biocomposite bars from Run # 1 - 8 (left to right) after injection moulding.

4.7 TESTING PROPERTIES

The injection moulded and annealed bars were used for the mechanical property tests that are most commonly used in the automotive industry.

4.7.1 E-MODULUS AND YIELD STRENGTH

The ASTM D 790 – 03 method was used to evaluate the flexural properties of the bars (ASTM International 2008a). The bars were cut in half and annealed in an oven. At least five samples of each run were tested for three-point-bending. The E-modulus and yield strength were determined from the force/displacement curve (Figure 3-9). The average of the E-modulus and yield strength of every run (Table 3-6) and the four different standards are presented in Figure 4-21 and Figure 4-22.

The addition of the filler increases the elastic modulus (E-modulus) significantly to almost 200 MPa compared to the standards. The type of filler here seems to have no effect on the elastic modulus of the biocomposites. The addition of MA-PP to pure polypropylene decreases the elastic modulus and the yield strength when compared to the polypropylene standards (Run # 1 – 4). By using a coupling agent the interaction between filler and matrix can be enhanced and the stiffness of the material improved. This behaviour has been observed in other studies carried out recently in our group (Kapustan Krüger 2007).

The E-modulus increased for Run # 4 (37 %), Run # 6 (36 %), Run # 2 (35 %), and Run # 8 (33 %) when compared to the standard Run # I. The increase was more significant (up to 57 % for Run # 4 55 % for Run # 6, 54 % for Run # 2, and 52 % for Run # 8) when compared to the standard Run # IV.

The yield strength is showing no significant difference between the standards and the biocomposite materials when no coupling agent was present. The addition of maleic anhydride polypropylene increases the yield strength by up to 22 % (for Run # 2 and Run # 4) when compared to standard Run # I and by up to 37 % (Run # 2), 36 % (Run # 4), 35 % (Run # 6), and 32 % (Run # 8) when compared to the standard Run # IV.

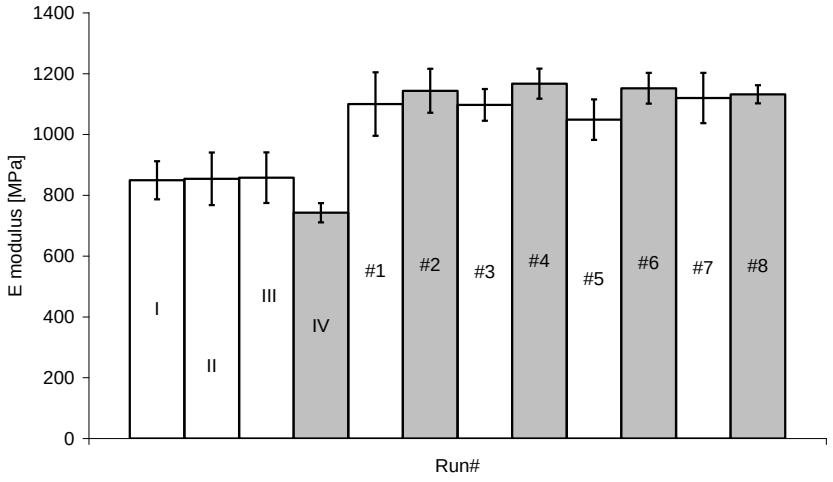

I	848 MPa
II	854 MPa
III	858 MPa
IV	743 MPa
# 1	1100 MPa
# 2	1144 MPa
# 3	1097 MPa
# 4	1167 MPa
# 5	1049 MPa
# 6	1152 MPa
# 7	1120 MPa
# 8	1132 MPa

Figure 4-21 E-modulus of Run # I – IV and 1 – 8 (error bars representing the standard deviation, n ≥ 5).

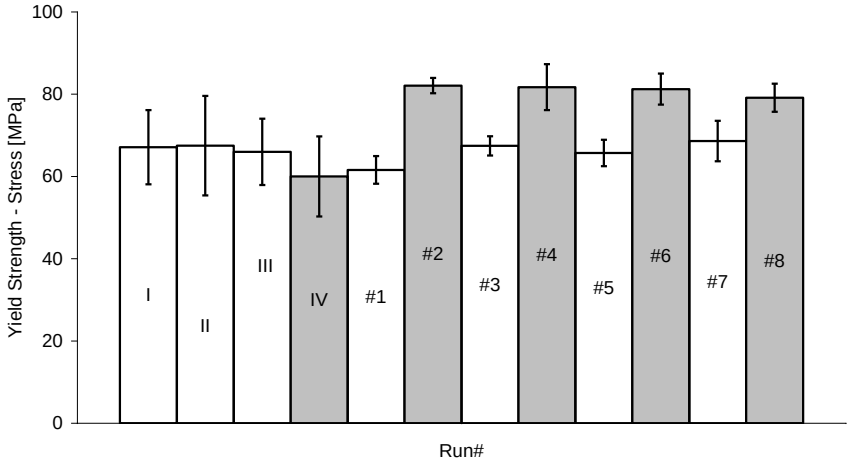

I	67 MPa
II	67 MPa
III	66 MPa
IV	60 MPa
# 1	62 MPa
# 2	82 MPa
# 3	67 MPa
# 4	82 MPa
# 5	66 MPa
# 6	81 MPa
# 7	69 MPa
# 8	79 MPa

Figure 4-22 Yield strength of Run # I – IV and 1 – 8 (error bars representing the standard deviation, n ≥ 5).

4.7.2 IZOD IMPACT

An important property of a material used in the manufacturing of cars is the performance in case of high impact. Car crash simulations can show that a very brittle and stiff material could become more dangerous in an accident, like glass that shatters by an impact and falls

apart in very sharp pieces. The energy which is needed to break a material is reported in Joule per meter. The Izod impact was performed on at least five bars of each run (Table 3-6) according to ASTM D 256 – 06a and the results are presented in Figure 4-23 and Figure 4-24.

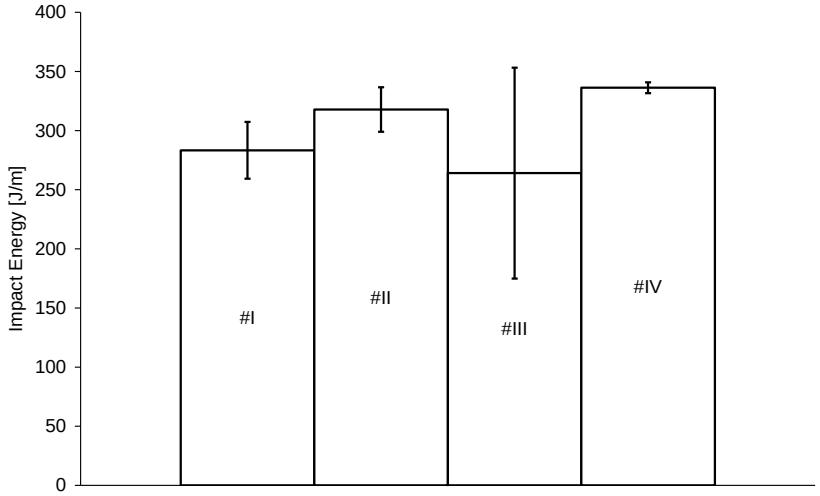

Figure 4-23 Impact Energy for standards I to IV obtained from Izod impact test.

P = partial break

H = hinge break

C = complete break

I = 283 J/m (P)

II = 318 J/m (P)

III = 264 J/m (P)

IV = 336 J/m (P)

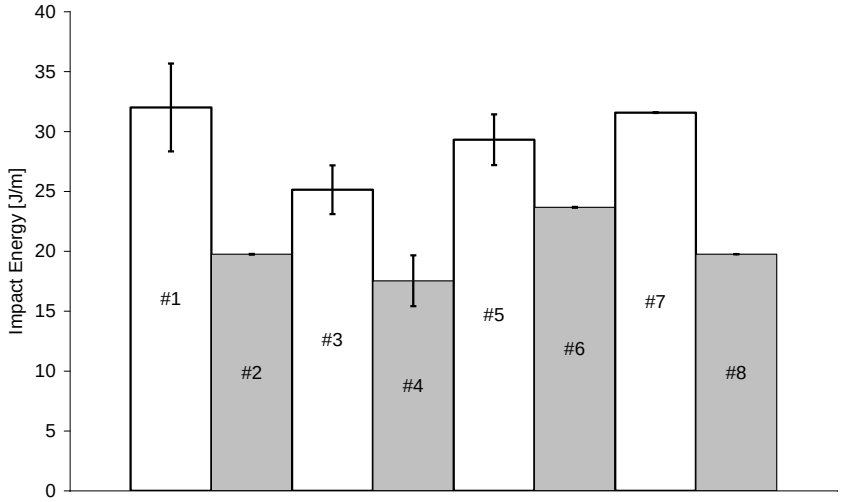

Figure 4-24 Impact energy for Run # 1 to 8 obtained from Izod impact test ASTM D 256 – 06a.

1 = 32 J/m (H)

2 = 20 J/m (C)

3 = 25 J/m (H)

4 = 18 J/m (C)

5 = 29 J/m (H)

6 = 24 J/m (H)

7 = 32 J/m (H)

8 = 20 J/m (H/C)

The polypropylene standards have an impact energy between 264 and 336 J/m but did not fully break during the test. By introducing a filler the impact energy decreases dramatically to a hundred times smaller than for the polypropylene standards. Also, the use of coupling

agent decreases the impact energy significantly. Biocomposites without a coupling agent showed an impact energy between 25 and 32 J/m where the biocomposites with MA-PP have an impact energy between 18 and 24 J/m. It is generally expected that addition of coupling agents would contribute to improvement of impact strength. However, this is not what was observed here. A plausible explanation could be the incompatibility of maleic anhydride with the chemical groups on the surface of the fillers used here. Other reports in the literature have also observed the behaviour shown here, that is, an increase in modulus with a decrease in stiffness. The reasons for such behaviour report in the literature are: (a) slippage on the matrix-filler interface (John, Anandjiwala 2009) and (b) mechanism of crack propagation (Toro, Quijada et al. 2007). Other reports have observed the same behaviour but were not able to identify the cause (Dixit, Kortschot et al. 2006).

Both, the use of filler and the use of coupling agent, makes the composite stiffer and thus more brittle. Most composites with coupling agent did have a complete break whereas the biocomposite without coupling agent had a hinge break and the polypropylene standards did partially break. Run # 6 which had no coupling agent still did not have a complete break.

4.7.3 MELT FLOW INDEX (MFI)

The melt flow of the polypropylene standards and the biocomposites is presented in Figure 4-25. For all samples (Table 3-6) the melt flow is between 2.45 and 3 g/10 min. The t-Test ($t_{0.05;\ 7} = 2.36$) with a confidence interval between 2.37 and 2.77 g/10 min shows a significant difference for Run # 5, Run # 6, and Run # 8 (Table 4-6). The decrease of the melt flow may be due to the presence of NaCl since NaCl is the only difference between Run # 3 and 5 and Run # 4 and 6. The decrease of the melt flow for Run # 8 could be due to the very small particle size of the filler combined with the presence of the coupling agent.

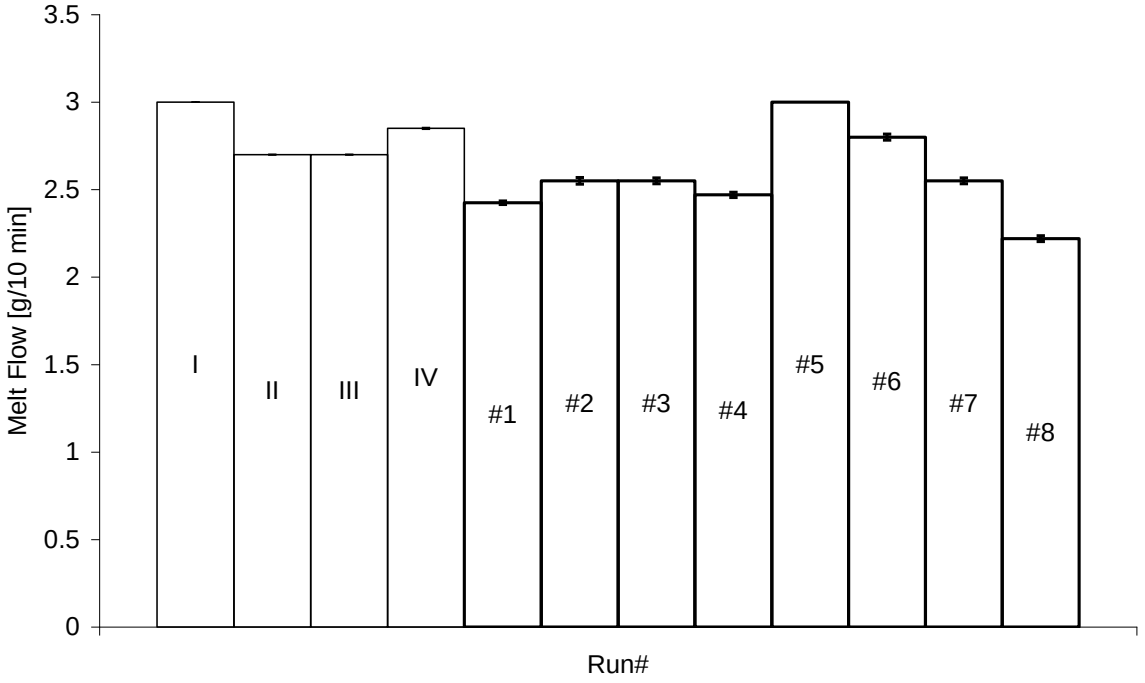

Figure 4-25 Melt Flow Index (MFI) for standards and biocomposites (error bars representing the standard deviation, n ≥ 3).

Table 4-6 MFI and t-values for polypropylene standards Run # I - IV and samples Run # 1 - 8.

Sample	MFI [g/10 min]	t(2.36)
# I	3.0	
# II	2.7	
# III	2.7	
# IV	2.9	
# 1	2.4	1.73939421
# 2	2.6	0.24635197
# 3	2.6	0.24635197
# 4	2.5	1.20189900
# 5	**3.0**	**5.12860009**
# 6	**2.8**	**2.73973251**
# 7	2.6	0.24635197
# 8	**2.2**	**4.18798348**

4.7.4 CRYSTALLINITY AND MELTING POINT

During the DSC, the material is heated above its melting temperature and cooled down to room temperature. This is done in a closed environment and a set heat and cooling rate. The energy released during melting (endothermic reaction) and the energy needed due to crystallization (exothermic reaction) of the material are obtained. Depending on the composition and the structure of the material the melting temperature as well as the degree of crystallinity can change. The crystallization temperature (peak temperature) and the degree of crystallinity (from second heating) for the standards and the biocomposites (Table 3-6) are presented in Figure 4-26.

Table 4-7 Degree of crystallinity and t-values for $t_{0.05,\ 7} = 2.36$.

Run	Degree of Crystallinity [%]	t (2.36)
1	39.64	0.94352289
2	41.54	0.12933024
3	37.59	1.82531998
4	41.34	0.21457063
5	**35.06**	**2.91580904**
6	**56.35**	**6.24018407**
7	44.98	1.35208887
8	38.20	1.56372017

$36.34 <$ Confidence interval ($t_{0.05,\ 7} = 2.36$) < 47.34

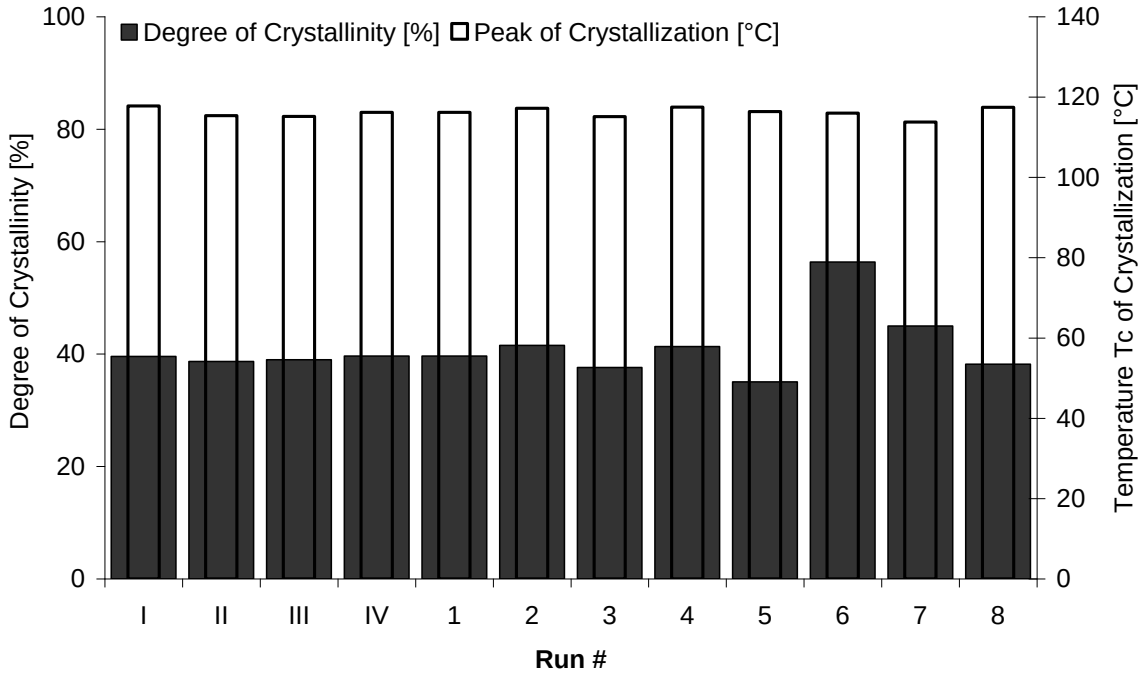

Figure 4-26 Degree of crystallinity and temperature of crystallization of the standards and biocomposites (Run # 1-8) obtained by differential scanning calorimetry (DSC).

Table 4-8 Degree of crystallinity (Equation 3-11) and temperature of crystallization of the standards and biocomposites (Run # 1-8) obtained by differential scanning calorimetry (DSC).

	Melting			Crystallization			
Run #	**Onset [°C]**	**Peak [°C]**	**ΔH_m [J/g]**	**Onset [°C]**	**Peak [°C]**	**ΔH_c [J/g]**	**Degree of Crystallinity [%]**
I	156.57	164.36	72.75	121.56	117.80	82.70	39.57
II	155.06	162.81	76.00	119.32	115.36	80.83	38.67
III	154.16	162.88	76.54	118.53	115.16	81.46	38.98
IV	153.62	164.40	79.17	120.69	116.20	82.82	39.63
1	153.51	163.48	52.75	120.57	116.17	58.00	39.64
2	154.71	162.95	52.98	121.39	117.19	60.77	41.54
3	154.06	164.15	49.55	119.77	115.12	55.00	37.59
4	154.60	164.53	52.79	122.29	117.48	60.48	41.34
5	154.75	162.12	47.65	120.27	116.37	51.29	35.06
6	152.88	163.76	76.66	120.80	116.00	82.44	56.35
7	154.11	163.74	61.42	117.17	113.80	65.81	44.98
8	154.32	162.35	51.25	122.27	117.45	55.89	38.20

The melting and crystallization temperatures (Table 4-8) are very similar to the ones published by Ng (Ng 2008). The only condition that differentiates itself from the others is Run # 5 and Run # 6 with the highest degree of crystallinity (Table 4-7). Both contain NaCl which might be able to have caused the increase in crystallinity.

An addition of salt, such as NaCl, to proteins can increase the ionic strength which increases the thermal stability. This effect is described by L'Hocine, Boye, and Jouve in their studies about the protein molecular structure of glycinin due to the neutralization of the charged amino acid groups by the counterions that neutralize the negative charged of the protein above their pI (at 6.1) and thus increase the hydrophobic interactions. Ionic strength and pH induced changed in glycinin will change the secondary and tertiary structure and thus affect the thermal stability (L'Hocine, Boye et al. 2007). Although this possible change in the protein structure present in the soy flakes (filler used here) due to the NaCl is not expected to change the way polypropylene crystallizes, one may consider this effect to play a role in the crystallization mechanism if the NaCl or the filler surface could work as a nucleating agent during the crystallization of polypropylene.

4.7.5 WATER ABSORPTION

The water absorption for the biocomposites and the standards was carried out by using the ASTM method D 570 – 98 (ASTM International 2008e). The moulded bars (Table 3-6) were immersed in water. The mass of the bars was recorded before immersion and periodically over time period of 6 months. The water uptake over time was calculated with Equation 3-4 and is presented in Figure 4-28. A visual comparison between the bars before and after water absorption (161 days) is presented in Figure 4-27.

Figure 4-27 Bars from Run # 1 – 8 before (left) and after (right) 161 days immersion in water.

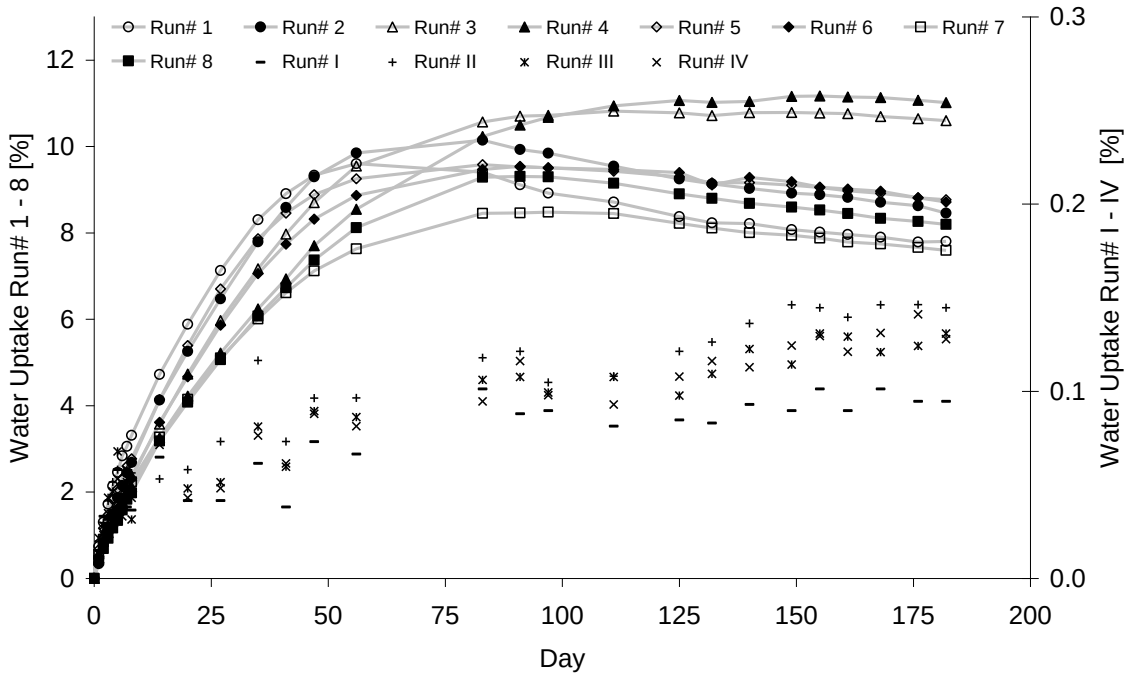

Figure 4-28 Water absorption for the standards and Run # 1 – 8 according to ASTM D 570 – 98.

During the first month the composite materials absorbed the water at a relatively constant rate. After 30 days, the rate of water uptake started to decrease. After about two months, the water uptake remained relatively constant or decreased. For example, the mass of the materials from Run # 1 and 2 started to decrease after 56 days. During the following weeks, the mass of all samples started to decrease except for Run # 3 and 4. This can be associated with the decomposition of the composite material or caused by the treatment of the filler material. For example, the filler in Run # 3 and 4 was subjected to an alkaline treatment causing a large portion of the soluble components to be removed. For the filler subjected to an extraction with NaCl (IS_{NaCl}), no such behaviour was seen because of the residual salt contained in the filler that was likely able to dissolve and diffuse into the water during the water absorption test. The maximal water uptake (Mm) of all bars is between 8.44 and 11.17 % when the weight loss is ignored. These results indicate that the addition of a coupling agent can decrease the water absorption. This can be seen clearly by comparing Run # 3 and Run # 4. For all the untreated filler and the soy flour (Ford) the immersion in water resulted in significant weight loss that could dramatically weaken the material. Therefore, a pre-treatment of the filler where protein and other soluble components are removed is essential.

The kinetics of the initial water absorption was analyzed by assuming first order kinetics (Equation 3-6). According to Pathapulakkal and Sain, when n is approximately 0.5, the water absorption indicates a Fickian diffusion mechanism. The estimates for n reported in Table 4-9 are very low, between 0.0165 and 0.0305, which designates non Fickian diffusion mechanism. The diffusion coefficient (D) was calculated using Equation 3-7 and the slope of the linear portion of the curve presented in Figure 4-29. The diffusion coefficient gives a measure of the rate of water absorption, the associated increase of mass and the resulting stability and performance of the material. The diffusion coefficient of the standards Run # I – IV and the samples Run # 1 – 8 is presented in Table 4-9. A significant difference is observed for the diffusion coefficient of Run # 1, Run # 3, and Run # 4. The highest diffusion coefficient was estimated for Run # 1 and can be due to the non-treated filler and the absence of coupling agent. The lowest diffusion coefficient was estimated for Run # 4 which can be explained by the reduced amount of soluble material that could leach out when exposed to water and the presence of a coupling agent.

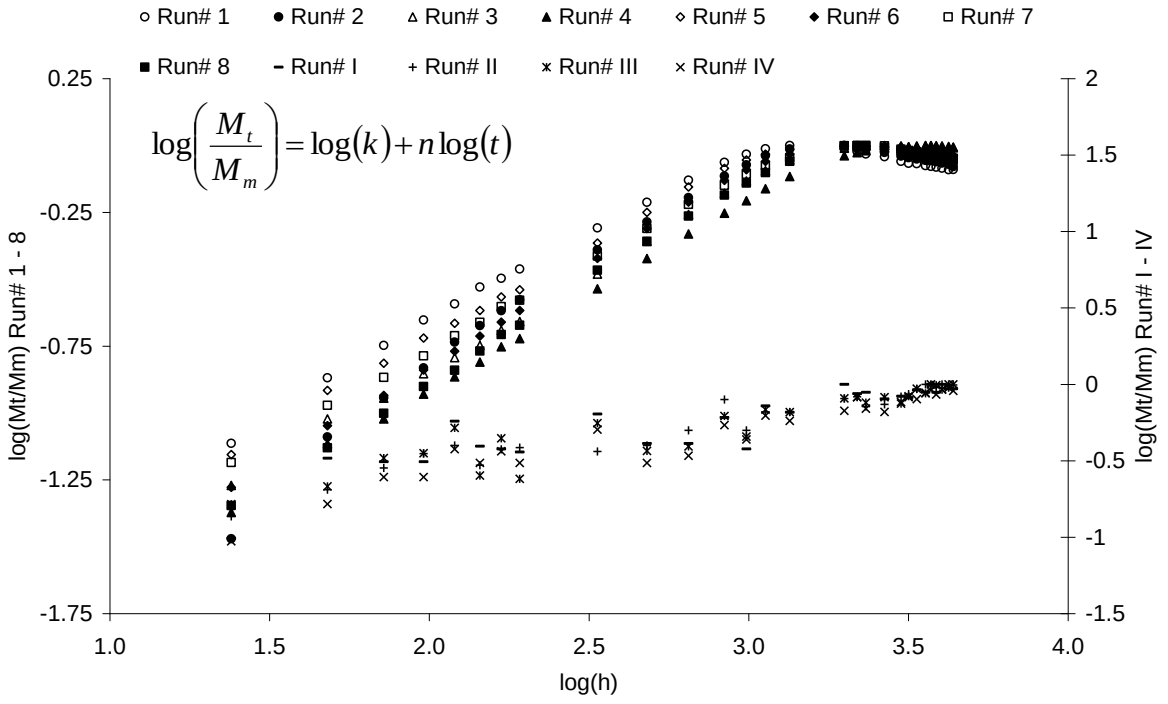

Figure 4-29 Mass of the bars as a function of time during the water absorption (log(Mt/Mm) vs. log(t)). The diffusion coefficient of the water absorption is calculated by using the slope of the initial linear curve.

Table 4-9 Water absorption kinetics: Factors k (obtained from the intercept with the y-axis) and n (obtained from the slope of the linear part of Figure 4-29); maximal water absorption and diffusion coefficient.

Run	k	n	max. water uptake (Mm)	D x 10^8 [cm^2/s]
I	0.0810	0.0280	0.10	0.3847
II	0.0594	0.0269	0.15	0.3546
III	0.0866	0.0182	0.13	0.1624
IV	0.0463	0.0280	0.14	0.3843
1	0.0111	0.0305	9.60	**0.4560**
2	0.0034	0.0262	10.15	0.3364
3	0.0057	0.0184	10.82	**0.1660**
4	0.0045	0.0165	11.17	**0.1339**
5	0.0086	0.0247	9.58	0.2994
6	0.0050	0.0212	9.54	0.2201
7	0.0080	0.0227	8.48	0.2534
8	0.0040	0.0191	9.31	0.1799

4.8 FESEM WITH EDX

To investigate the interface between the matrix and the filler, FESEM was performed and EDX was used to identify the chemical composition of certain surfaces.

The interaction between the filler and the matrix affects the mechanical properties of the composite material. Thus a better interface can increase the mechanical properties and result in better overall performance. Some particles are also able to function as a crystallization nucleus and will lead to the formation of a polymer chain. This can result in an fully integrated particle in the crystalline phase of the polymer matrix.

In Figure 4-30, Figure 4-32, Figure 4-34, and Figure 4-36 the cross-section of the biocomposites without MA-PP are presented. A gap between the filler and the matrix is clearly visible demonstrating a poor interface. In contrast, when maleic anhydride is present (Figure 4-31, Figure 4-33, Figure 4-35, and Figure 4-37) a better interaction is observed where the gap between the filler and the matrix is negligible. In Figure 4-37, the size of the filler was below 35 µm and a coupling agent was used, the surface of the cross-section shows no filler which leads to the conclusion that the filler are fully embedded into the matrix and thus a very good interface can be assumed. For further information about the inclusion of the filler in the crystal structure, one could use microscopy with polarized light.

In Figure 4-34 and Figure 4-35and it is possible to see the salt crystals which remain from the alkaline extraction in the NaCl solution. The salt crystals do not appear to be embedded in the matrix. Some of them are still attached to the filler particles. The poor interface can be explained by the charge of the salt crystals that may interfere with the charge of the polymer matrix and result in repulsion.

For all biocomposites, except the ones with the soy flour (Ford), it was possible to identify the palisade layer from the testa of the soybeans. It seemed that the palisade layer was separated from the rest of the particle and interacted as a single particle with the matrix. Because of its shape, the palisade layer has a very consistent width but varies in length. Some parts of the palisade layer were still quite long with an aspect ratio above five which is more representative of a fiber type (Figure 4-35).

a)

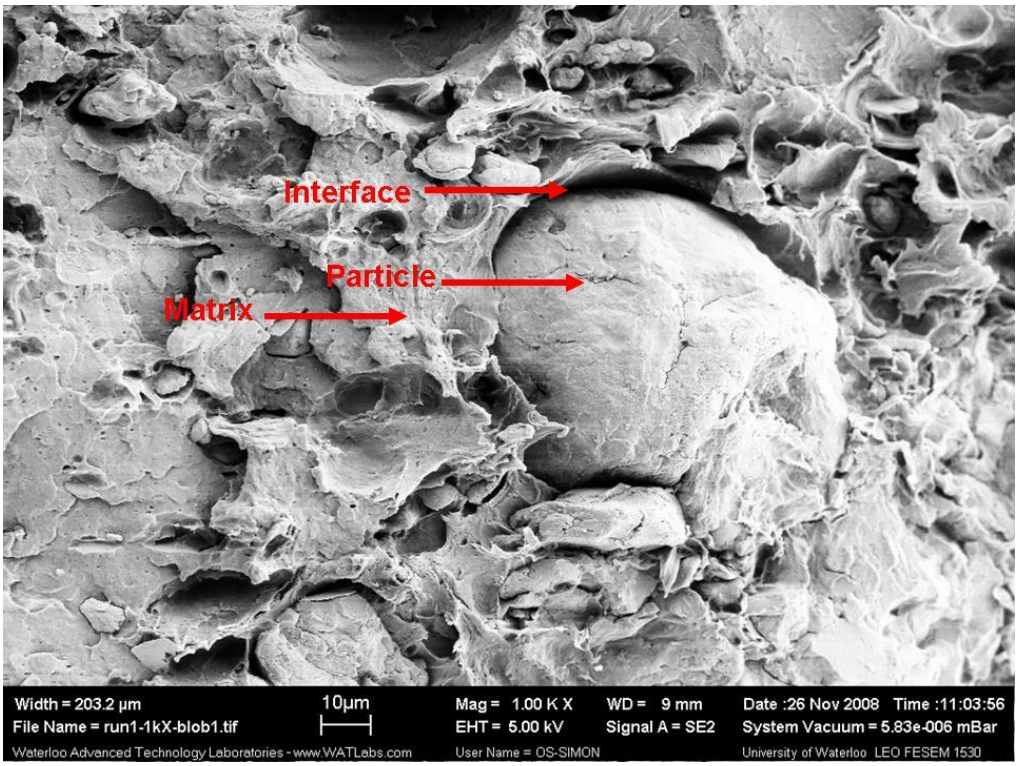

b)

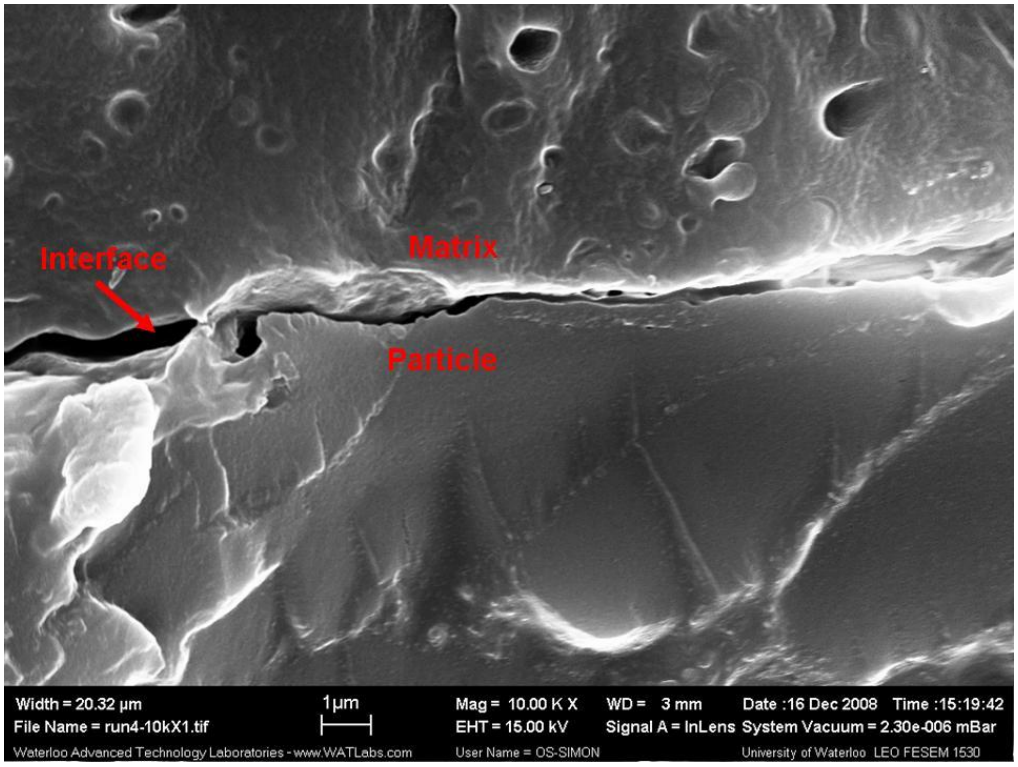

Figure 4-30 Scanning electron micrograph of a cross-section from Run # 1: a) 1,000 x magnified, 5 kV b) 10,000 x magnified, 15 kV.

a)

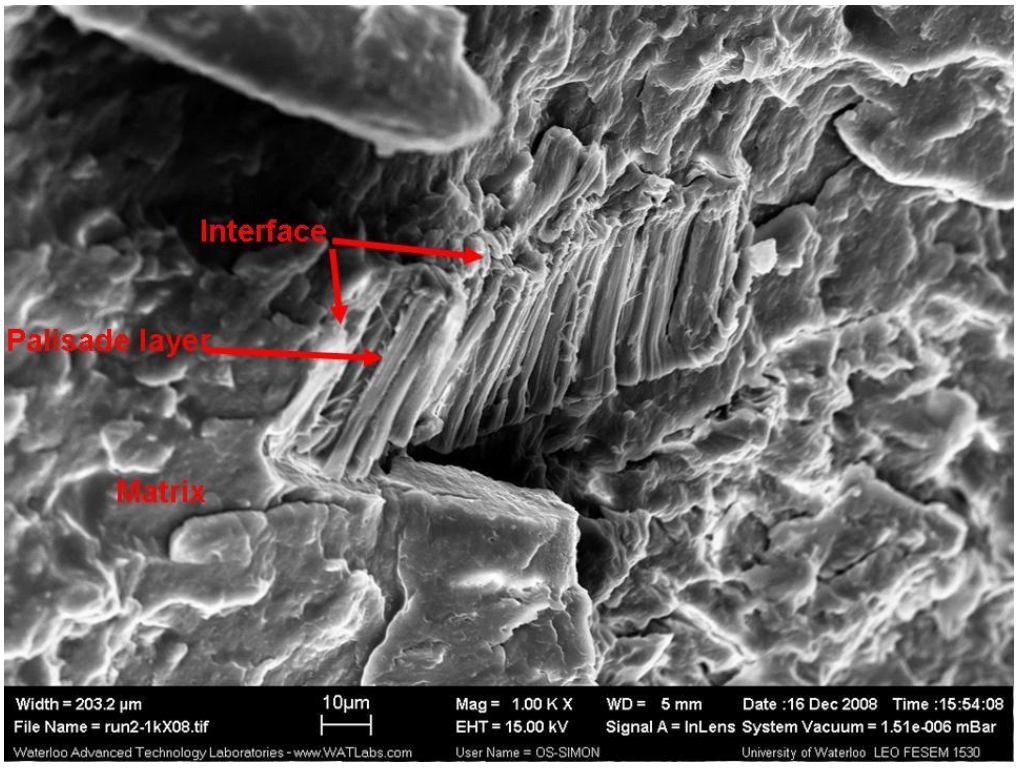

b)

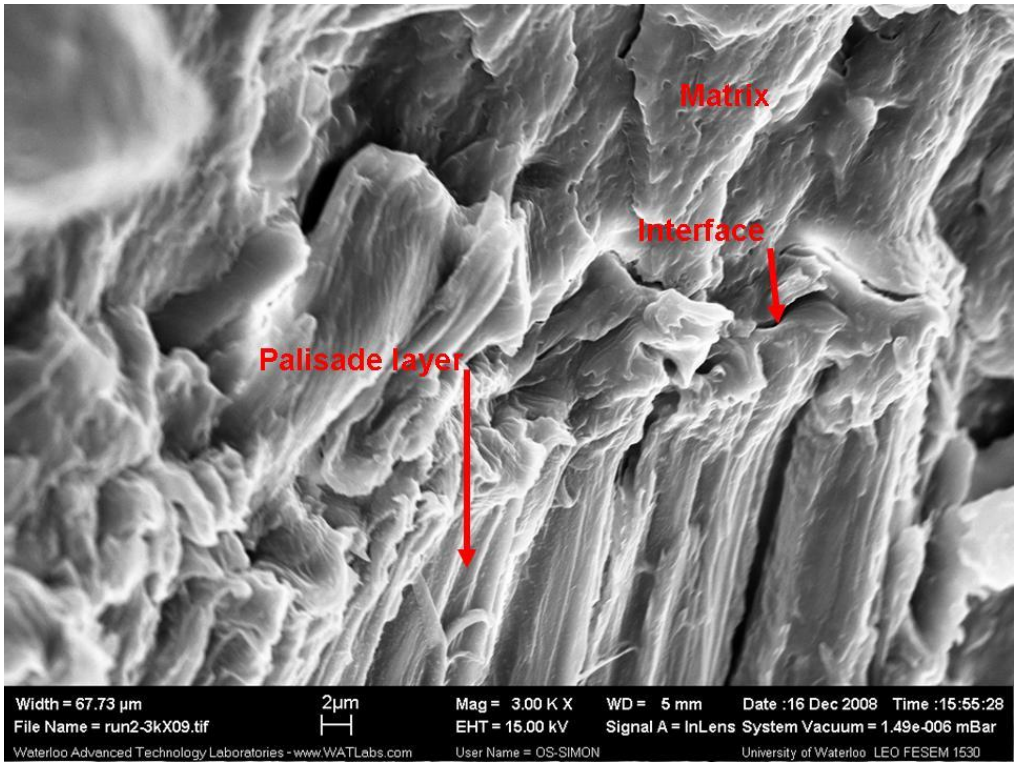

Figure 4-31 Scanning electron micrograph of a cross-section from Run # 2: a) 1,000 x magnified, 15 kV b) 3,000 x magnified, 15 kV.

a)

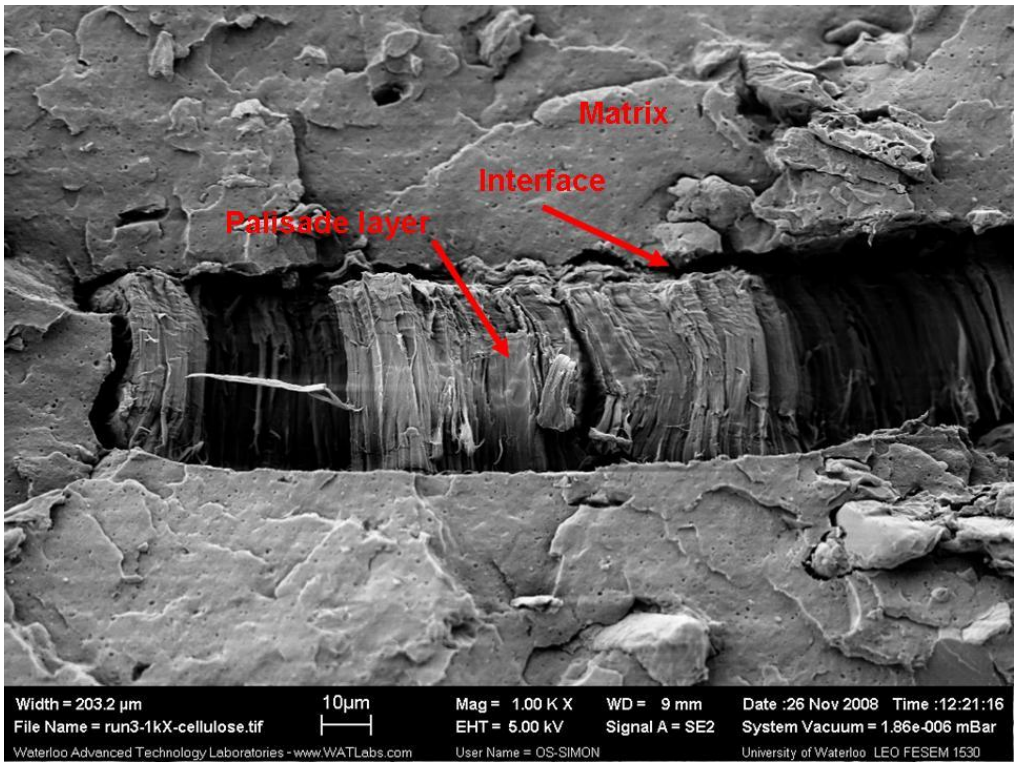

b)

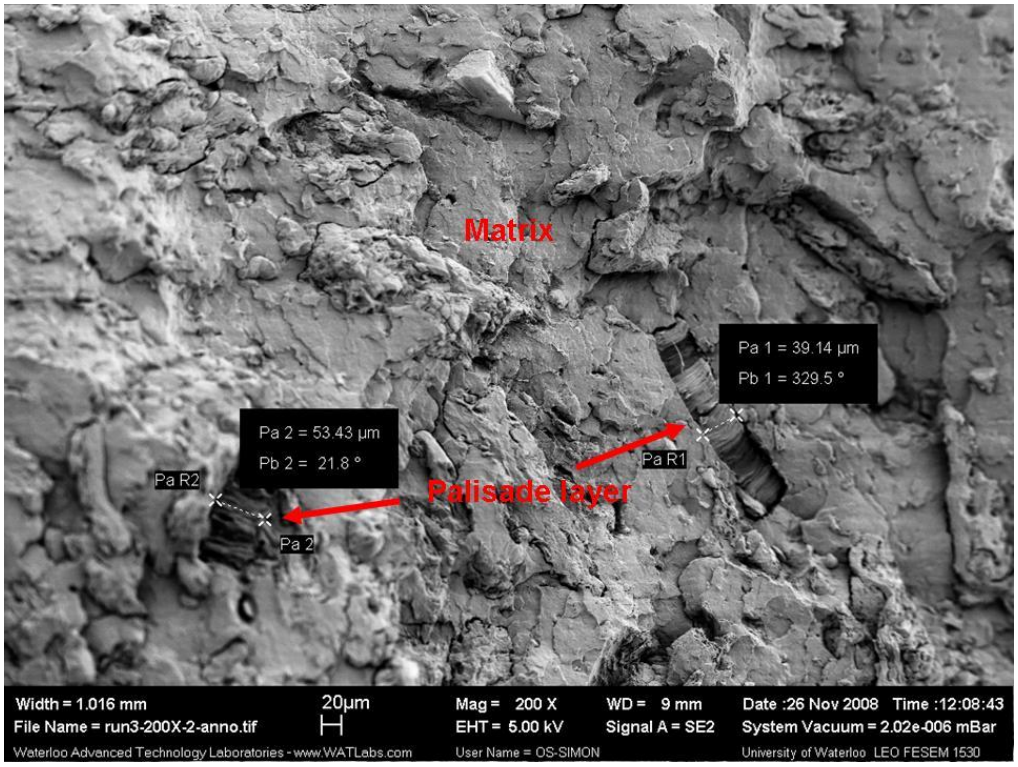

Figure 4-32 Scanning electron micrograph of a cross-section from Run # 3: a) 1,000 x magnified, 5 kV b) 200 x magnified, 5 kV. Element mapping of this image is presented in Figure 4-38.

a)

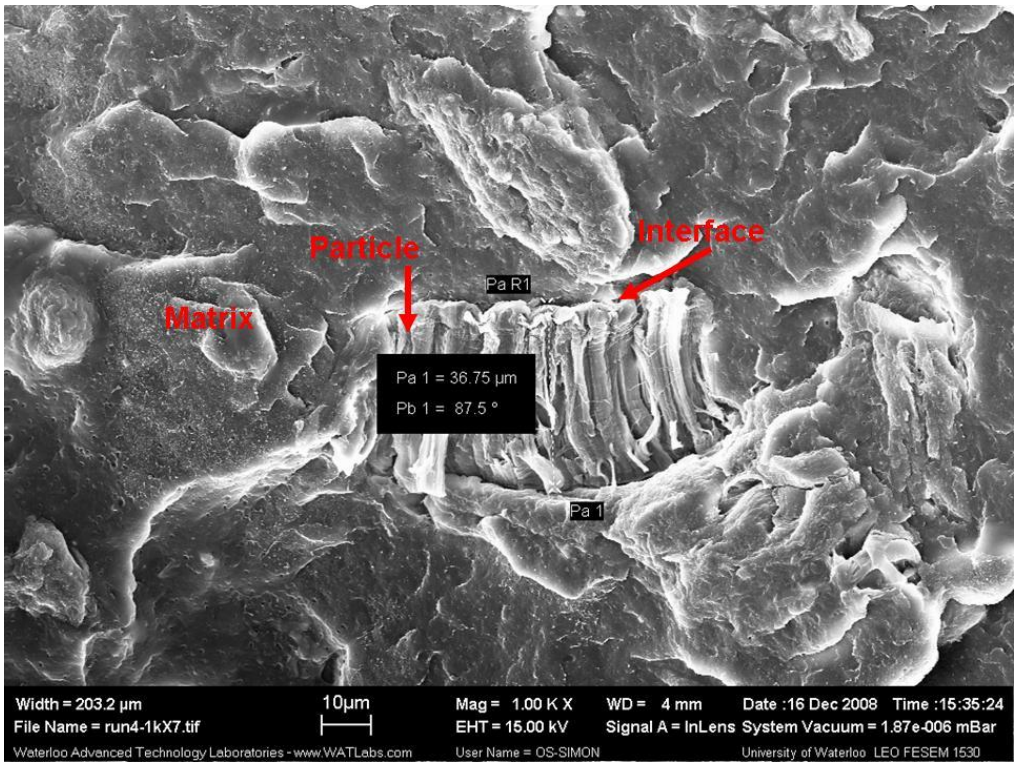

b)

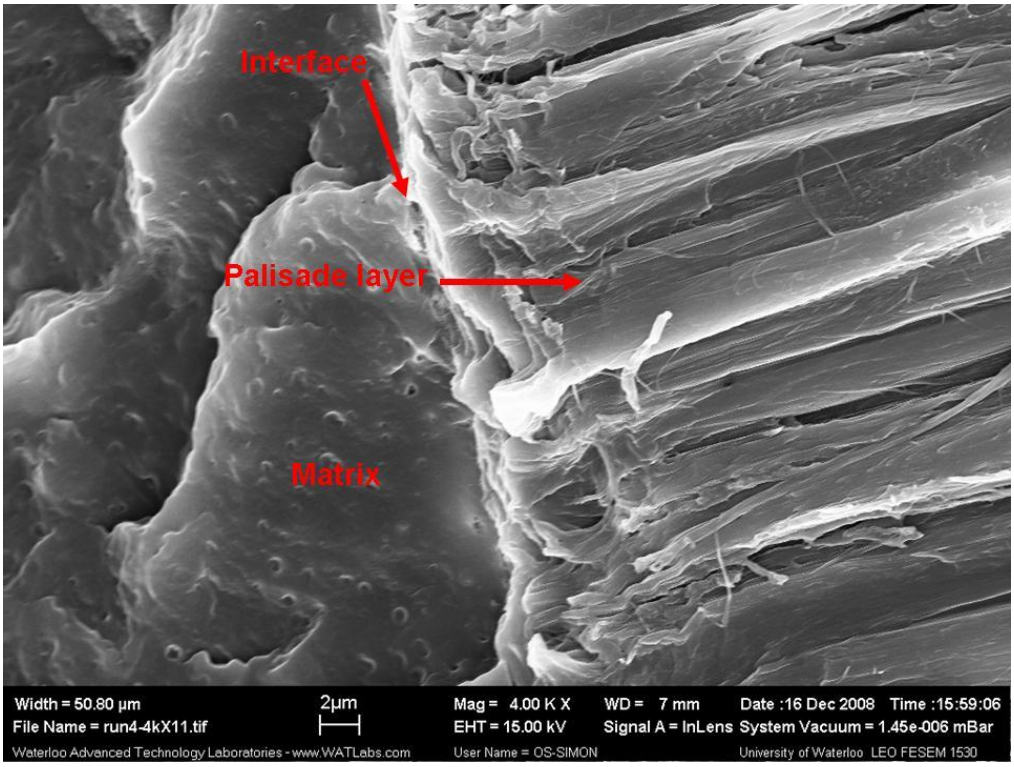

Figure 4-33 Scanning electron micrograph of a cross-section from Run # 4: a) 1,000 x magnified, 15 kV b) 4,000 x magnified, 15 kV.

a)

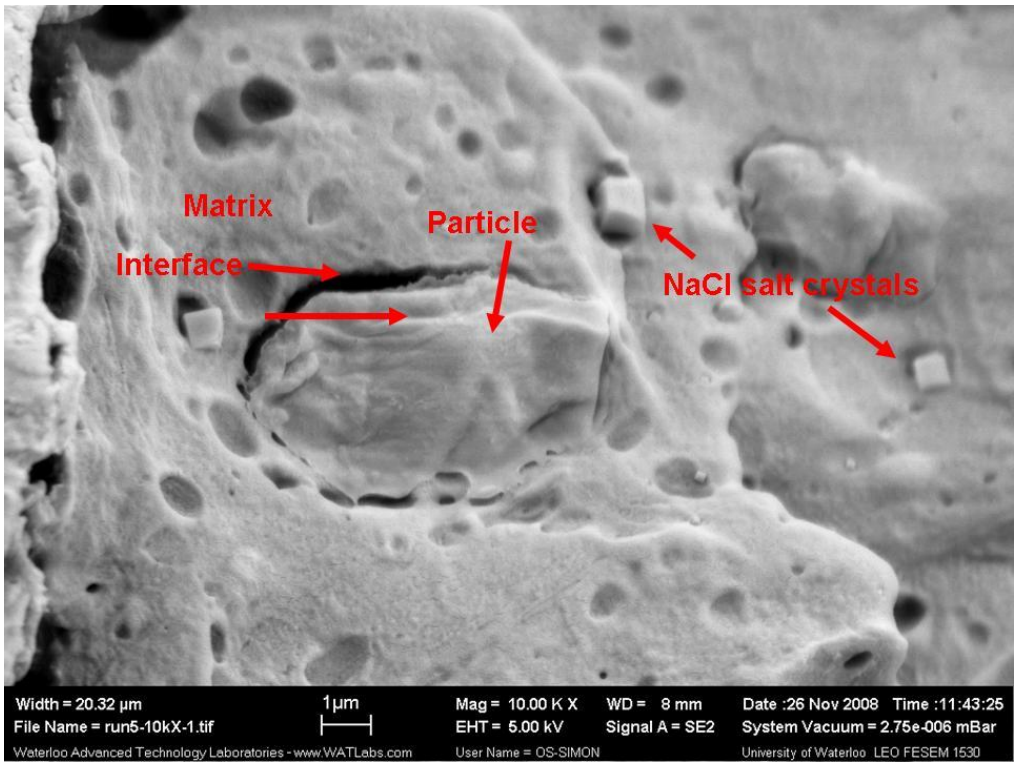

b)

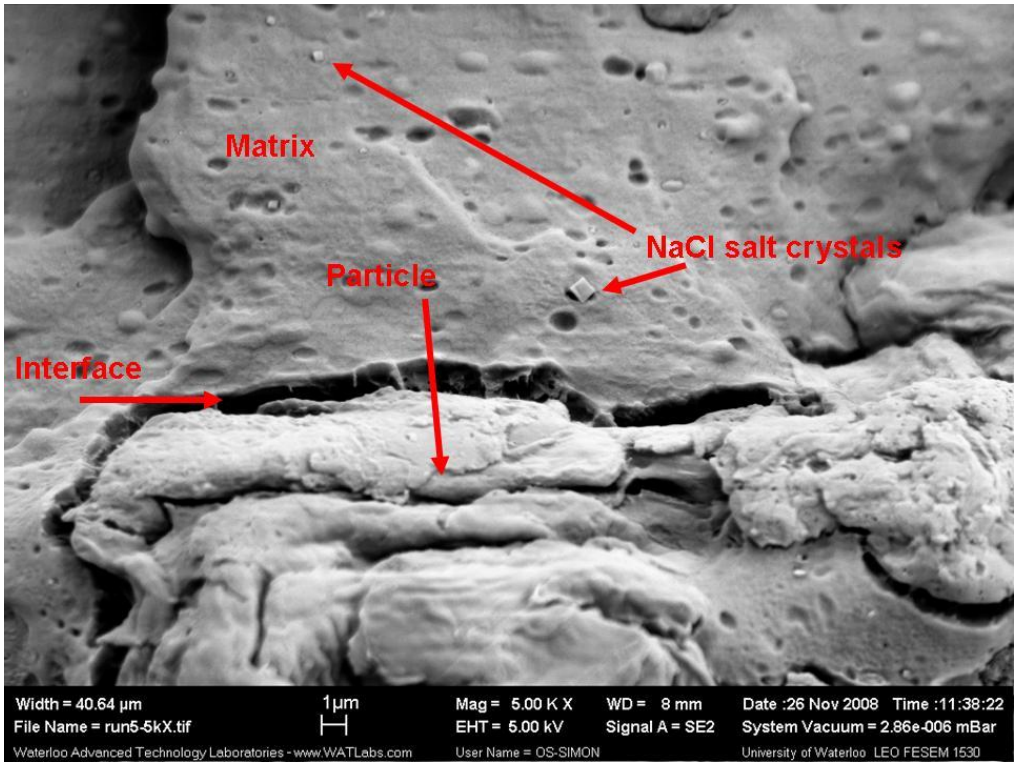

Figure 4-34 Scanning electron micrograph of a cross-section from Run # 5: a) 10,000 x magnified, 5 kV b) 50,000 x magnified, 5 kV.

a)

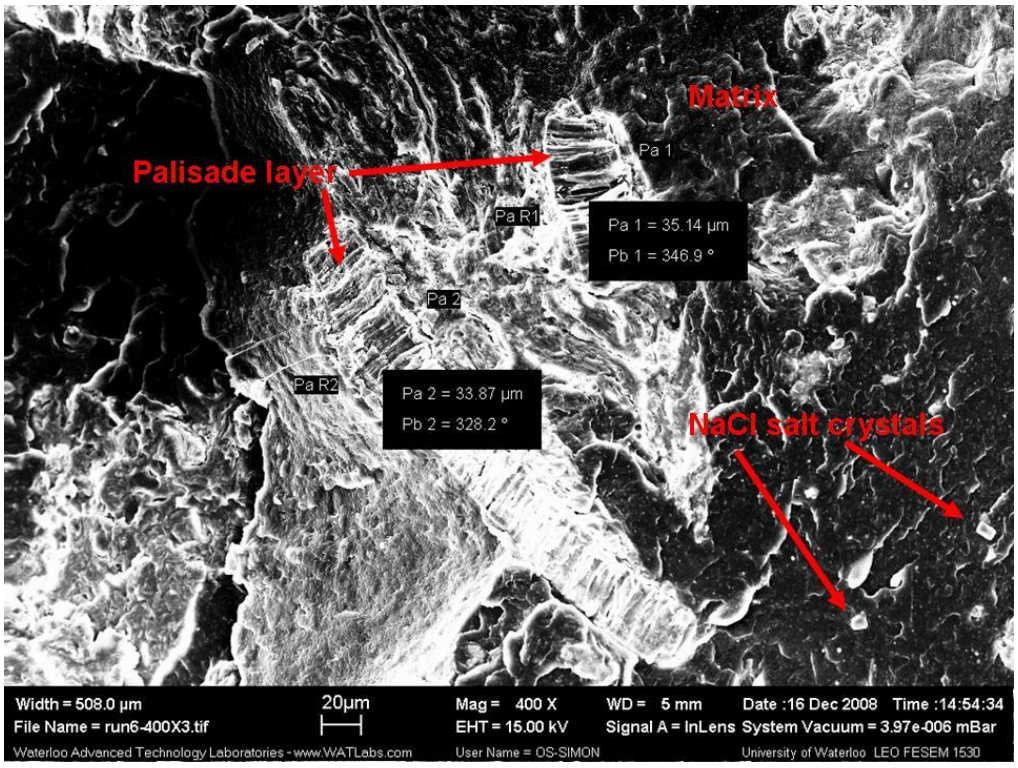

b)

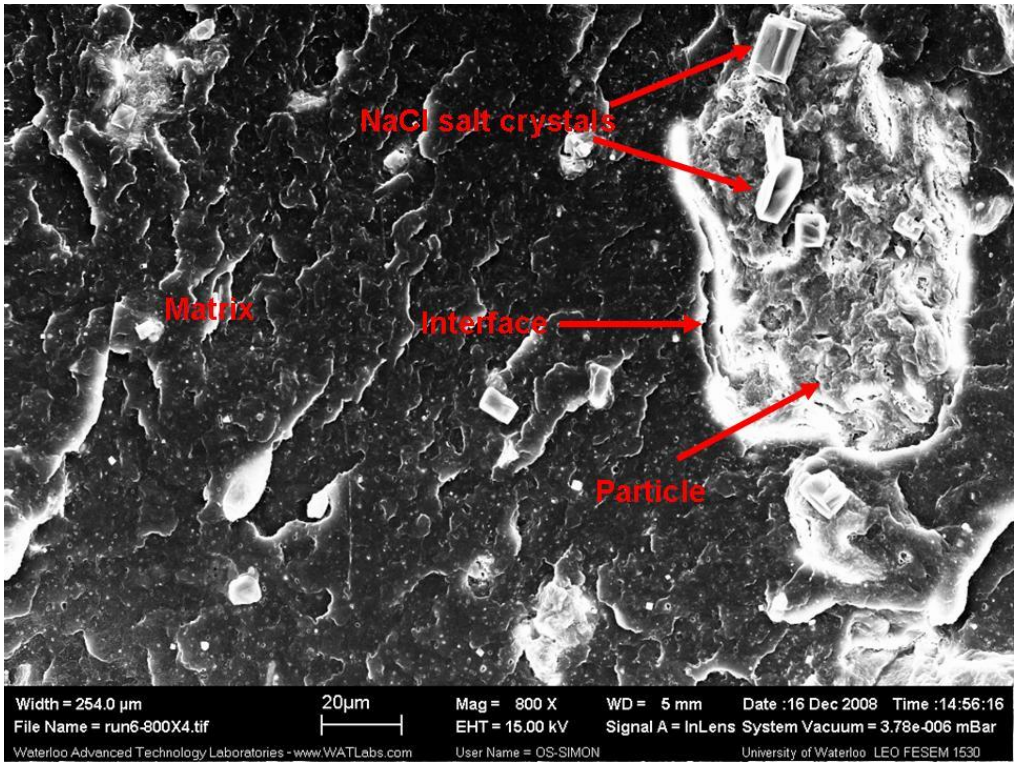

Figure 4-35 Scanning electron micrograph of a cross-section from Run # 6: a) 400 x magnified, 15 kV b) 800 x magnified, 15 kV.

a)

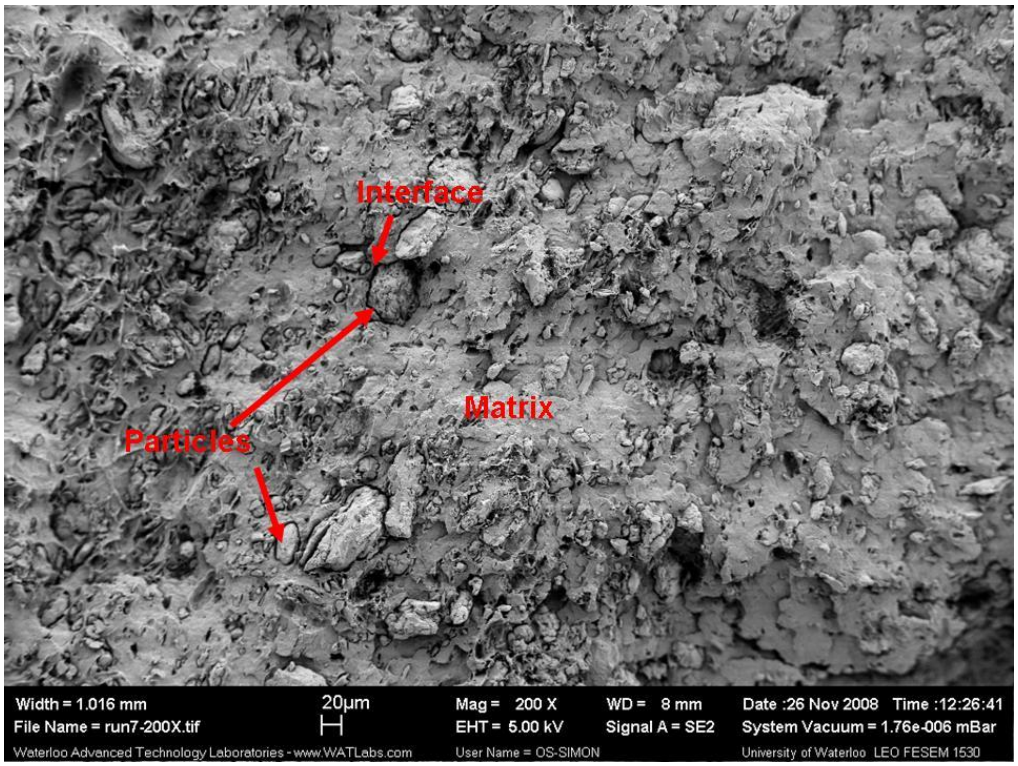

b)

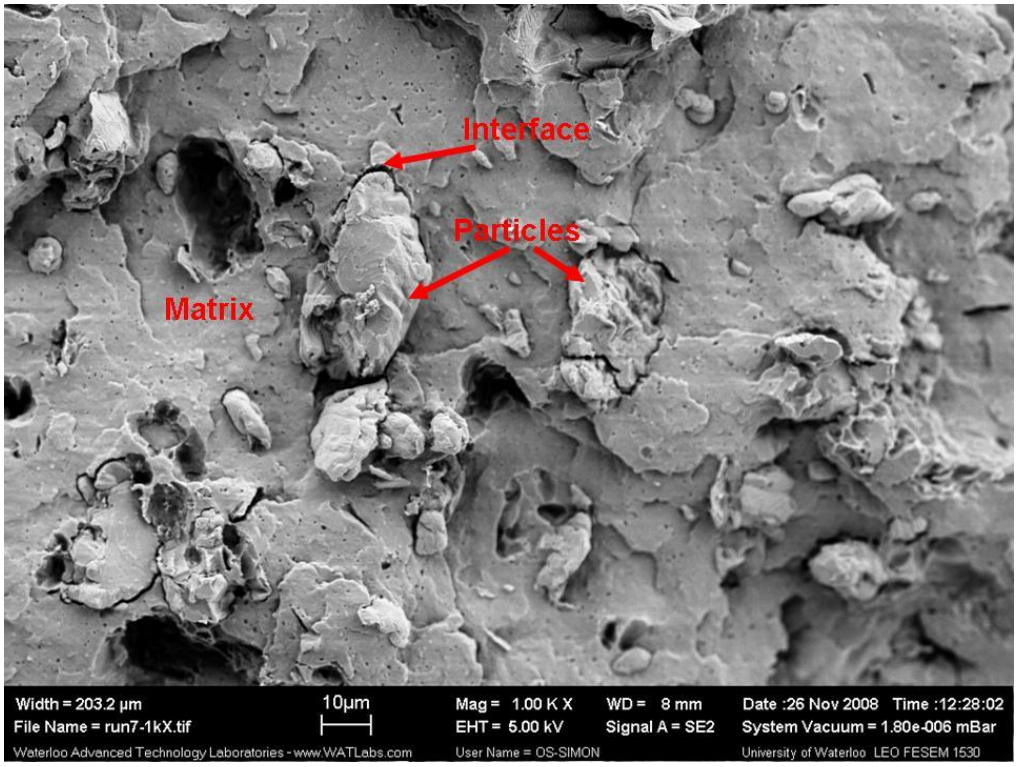

Figure 4-36 Scanning electron micrograph of a cross-section from Run # 7: a) 200 x magnified, 5 kV b) 1,000 x magnified, 5 kV.

a)

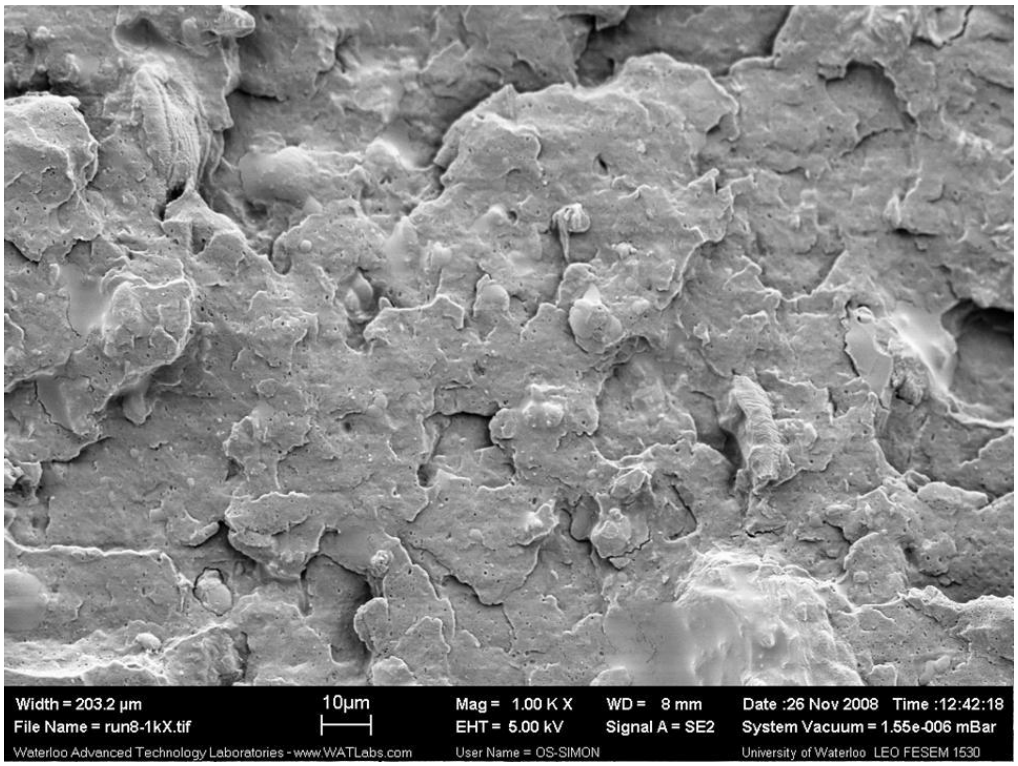

b)

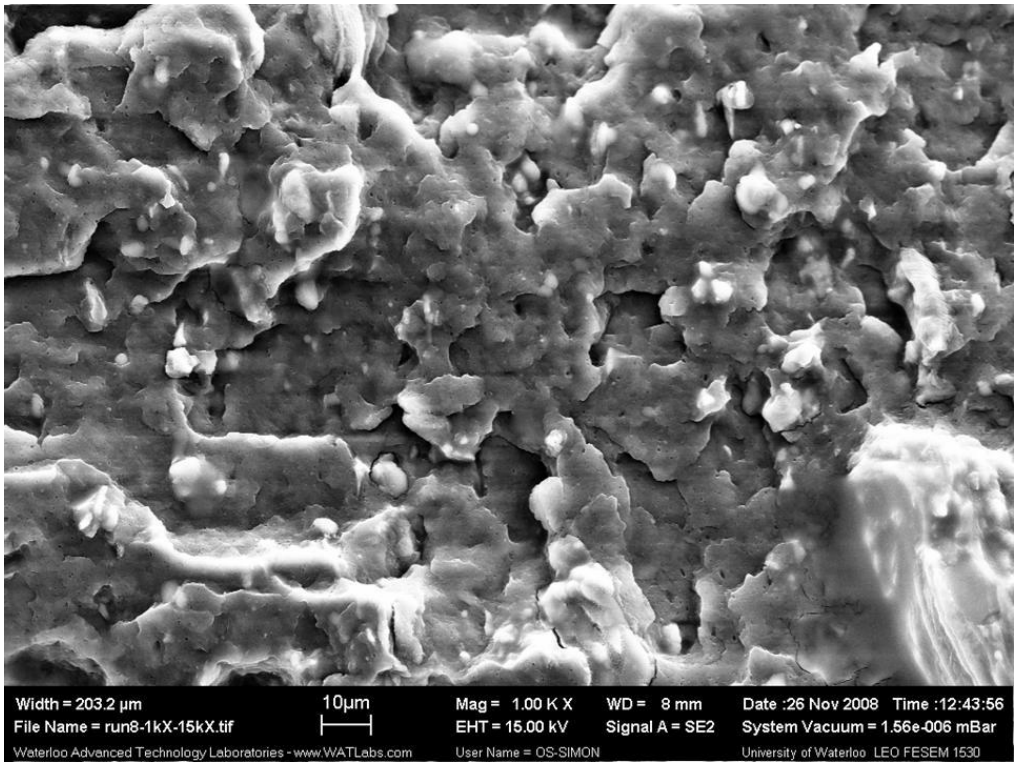

Figure 4-37 Scanning electron micrograph of a cross-section from Run # 8: a) 1,000 x magnified, 5 kV b) 1,000 x magnified, 15 kV.

Figure 4-38 shows an example of a chemical mapping for oxygen, nitrogen, and carbon obtained with the EDX detector. The mapping was carried out over a short time period, ten minutes, but shows already some regions with higher oxygen and carbon content. The nitrogen mapping is quite uniform and does not reveal regions with significant different nitrogen content.

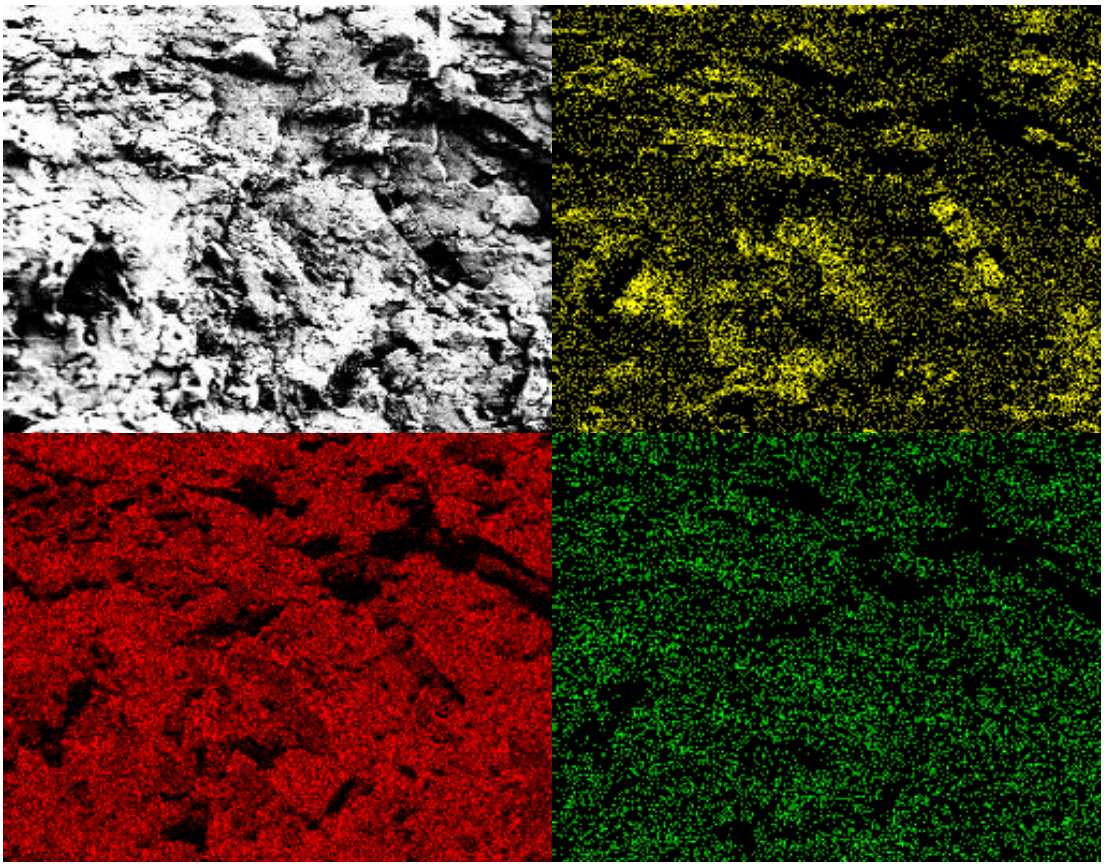

Figure 4-38 Example for chemical mapping for Run # 3; yellow = oxygen, red = carbon, green = nitrogen over 10 minutes.

For a better analysis, the chemical mapping should be performed over a longer period of time but generally the EDX is a valuable technique providing elemental composition information in direct relation to the SEM image. The qualitative analysis is extremely rapid and can give a quick "first look" on the specimen and thus simplify the analysis on a sample but a quantitative analysis requires a longer time for a valuable analysis.

The surface of the injection moulded bars appears quite smoothly with the naked eye but the analysis by FESEM reveals small pores (Figure 4-39).

a)

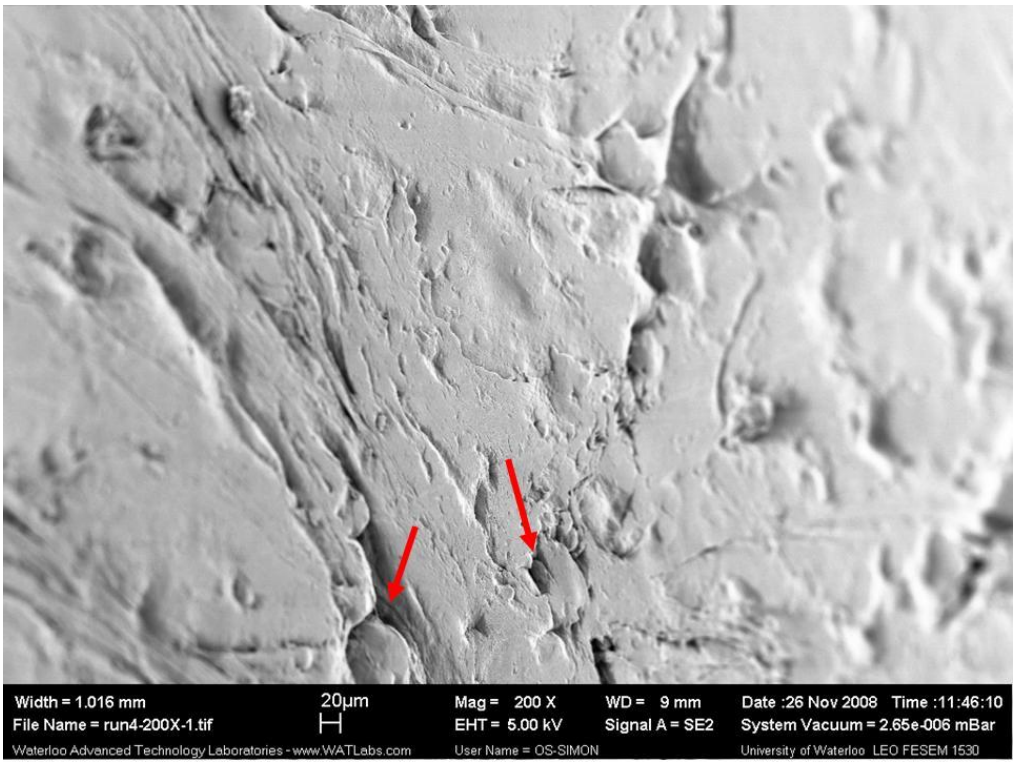

b)

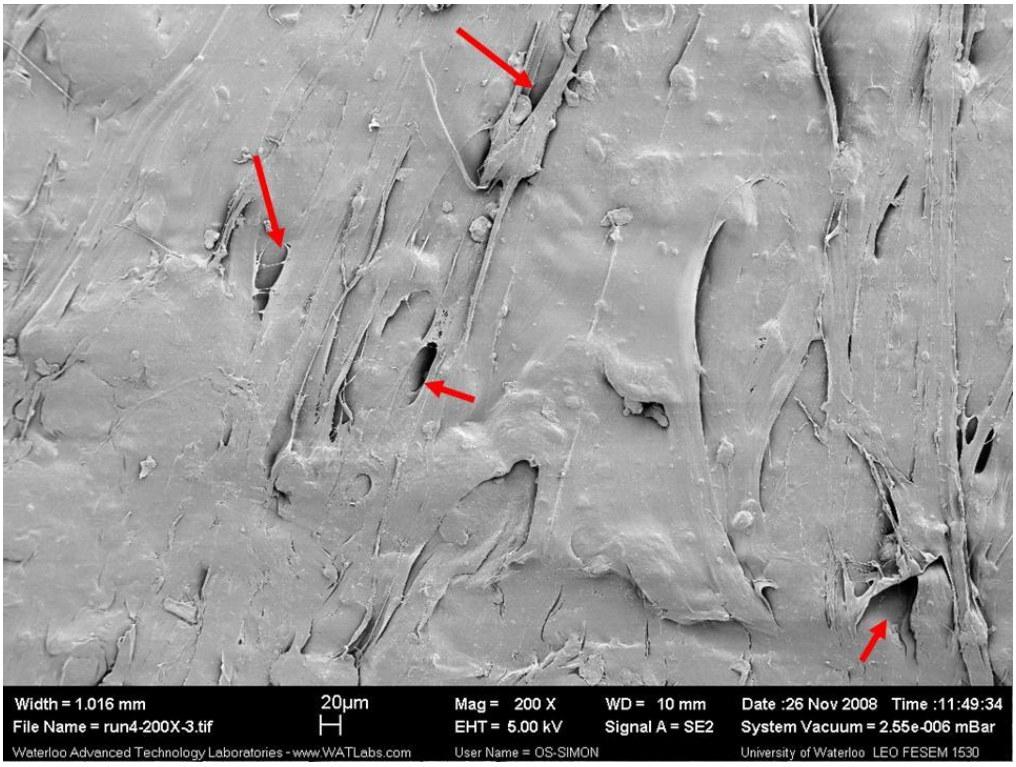

Figure 4-39 Electron micrograph of the surface from Run # 4 with arrows that show some of the pores observed on the surface: a) 200 x magnified, 5 kV b) 200 x magnified, 5 kV.

5 CONCLUSIONS AND RECOMMENDATIONS

The use of soy flakes as filler in a polypropylene matrix was investigated in this study for the preparation of biocomposites to be used in automotive applications. The filler was used after milling to a size below 250 µm and subjected to two pre-treatment methods: (1) one hour in a 50 °C pH 9 water solution in a 1 : 9 solid-liquid ratio; (2) one hour in a 50 °C pH 9 1M NaCl solution in a 1 : 9 solid-liquid ratio. A control filler, without pre-treatment was considered. The soy flakes were also compared to an industrial soy based filler provided by Ford (soy flour (Ford)).

The mechanical properties of the biocomposites are promising where an increase of the E-modulus was observed when compared to pure polypropylene. The addition of MA-PP as coupling agent increased the yield strength of the biocomposites. When pure polypropylene and the biocomposites were compared no difference could be seen for their yield strength.

The thermal behaviour deduced from differential scanning calorimetry, revealed a similar behaviour for the biocomposites and the pure polypropylene. Only the samples treated in the presence of NaCl and without a coupling agent, appear to have a slightly higher degree of crystallinity. The melt flow index was slightly increased for the biocomposites containing soy flakes pre-treated with NaCl and decreased for biocomposites containing the soy flour.

The water absorption behaviour of the biocomposites was quite similar at the beginning with a slightly lower absorption for the materials with coupling agent. After three months, all samples except the ones treated with water showed a weight loss that can be due to the leaching of the water soluble components in the untreated filler and the NaCl treated filler. The NaCl treatment resulted in the increase of the weight of the treated flakes by more than 10 %.

In conclusion, soy flakes represent an attractive filler for its use in a polypropylene matrix when an aqueous alkaline pre-treatment is performed. The aqueous alkaline extraction also leads to the recovery of the proteins that can be used in food products while the remaining insoluble material is used for the biocomposites, avoiding the competition with the use of soy for food products.

Based on the results presented in this study, future work on soy flakes reinforced polypropylene should focus on:

1- The optimization of the compounding formulation, filler and coupling agent.

2- The minimization of odour and volatile release.

3- The effect of the particle size of the filler for improved interphase adhesion between the filler and the polymer matrix.

4- The minimization of water absorption and material degradation by additional treatment.

5- The effect of significant heat and shear stress in the context of scale-up operations.

6- The life cycle assessment (LCA) of the biocomposite.

7- The assessment of the biocomposite friction and wear performance.

REFERENCES

Choosing an antioxidant: some of the basics. 2005. *Plastics, Additives and Compounding*, **7**(1), pp. 32-33.

ADVANCED ANALYSIS TECHNOLOGIES, 2005-last update, EDS operation [Homepage of Advanced Analysis Technologies], [Online]. Available: http://advancedanalysistech.com/eds.html [April/20, 2009].

ARBELAIZ, A., FERNÁNDEZ, B., RAMOS, J.A., RETEGI, A., LLANO-PONTE, R. and MONDRAGON, I., 2005. Mechanical properties of short flax fibre bundle/polypropylene composites: Influence of matrix/fibre modification, fibre content, water uptake and recycling. *Composites Science and Technology*, **65**(10), pp. 1582-1592.

ARCHER DANIELS MIDLAND COMPANY, 2004 - 2005. Protein Ingredients 2004 - 2005.

ASTM INTERNATIONAL, 2008a. ASTM D 790 - 03 Standard Test Methods for Flexural Properties of Unreinforced and Reinforced Plastics and Electrical Insulating Materials.

ASTM INTERNATIONAL, 2008b. ASTM D 1102 - 84 Standard Test Method for Ash in Wood.

ASTM INTERNATIONAL, 2008c. ASTM D 1238 - 04c Standard Test Method for Melt Flow Rates of Thermoplastics by Extrusion Plastometer.

ASTM INTERNATIONAL, 2008d. ASTM D 256 - 06a Standard Test Methods for Determining the Izod Pendulum Impact Resistance of Plastics.

ASTM INTERNATIONAL, 2008e. ASTM D 570 - 98 Standard Test Method for Water Absorption of Plastics.

ASTM INTERNATIONAL, 2008f. ASTM D 7075 - 04 Standard Practice for Evaluating and Reporting Environmental Performance of Biobased Products.

ASTM INTERNATIONAL, 2008g. ASTM D 790 - 07 Standard Test Method for Flexural Properties of Unreinforced and Reinforced Plastics and Electrical Insulating Materials.

ASTM INTERNATIONAL, 2007. ASTM E 1755 Standard Test Method for Ash in Biomass.

BATAILLE, P., RICARD, L. and SAPIEHA, S., 1989. Effects of Cellulose Fibers in Polypropylene Composites. *Polymer Composites*, **10**(2), pp. 103-108.

BLEDZKI, A.K.(., FARUK, O.(. and SPERBER, V.E.(., 2006. Cars from bio-fibres. *Macromolecular Materials and Engineering*, **291**(5), pp. 449-457.

BROUWER, W.D., 2000-last update, natural fibre composites in structural components: alternative applications for sisal? [Homepage of FAO], [Online]. Available: http://www.fao.org/docrep/004/Y1873E/y1873e0a.htm [3/27, 2009].

CALLISTER, W.D.J., 1996. Materials Science and Engineering: An Introduction. 4 edn. Wiley.

CALVERO, 2006-last update, Methylene_blue.svg [Homepage of http://en.wikipedia.org], [Online]. Available: http://en.wikipedia.org/wiki/File:Methylene_blue.svg [April/17, 2009].

CELSUM TECHNOLOGIES LIMITED, 2008-last update, LMI%204000%20Melt%20Flow%20Indexer_96dpi_300pix.jpg [Homepage of Celsum Technologies Limited], [Online]. Available: http://www.celsum.com/Graphics/LMI%204000%20Melt%20Flow%20Indexer_96dpi_300pix.jpg [April/17, 2009].

DAS, S.N., ROUTRAY, M. and NAYAK, P.L., 2008. Spectral, thermal, and mechanical properties of furfural and formaldehyde cross-linked soy protein concentrate: A comparative study. *Polymer-Plastics Technology and Engineering*, **47**(6), pp. 576-582.

DIXIT, N., KORTSCHOT, M.T., SAIN, M. and GULATI, D., 2006. Effect of interactions between interface modifiers and viscosity modifiers on the performance and processibility of the rice hulls-HDPE composites. *Journal of Reinforced Plastics and Composites*, **25**(16), pp. 1691-1699.

DYNISCO POLYMER TEST SYSTEMS, LMI 4000 Series Melt Indexer Manual Version 3.1.

EHRENSTEIN, G.W., RIEDEL, G. and TRAWIEL, P., eds, *Thermal Analysis of Plastics - Theory and Practice.* Hanser/Gardner Publications, Inc.

ESPERT, A., VILAPLANA, F. and KARLSSON, S., 2004. Comparison of water absorption in natural cellulosic fibres from wood and one-year crops in polypropylene composites and its influence on their mechanical properties. *Composites Part A: Applied Science and Manufacturing*, **35**(11), pp. 1267-1276.

FOOD AND AGRICULTURE ORGANIZATION OF THE UNITED NATIONS, 2009-last update, y1873e0u.jpg [Homepage of Food and Agriculture Organization of the United Nations], [Online]. Available: http://www.fao.org/docrep/004/Y1873E/y1873e0u.jpg [April/17, 2009].

FOWLER, P.A., HUGHES, J.M. and ELIAS, R.M., 2006. Biocomposites: technology, environmental credentials and market forces. *Journal of the science of food and agriculture,* **86**(12), pp. 1781-1789.

GARCIA, M., GARMENDIA, I. and GARCIA, J., 2008. Influence of natural fiber type in eco-composites. *Journal of Applied Polymer Science,* **107**(5), pp. 2994-3004.

GENEAU-SBARTAI, C., LEYRIS, J., SILVESTRE, F. and RIGAL, L., 2008. Sunflower Cake as a Natural Composite: Composition and Plastic Properties. *Journal of Agricultural and Food Chemistry,* **56**(23), pp. 11198-11208.

HERTH, W. and SCHNEPF, E., 1980. The Fluorochrome, Calcofluor White, Binds Oriented to Structural Polysaccharide Fibrils. *Protoplasma,* **105**(1-2), pp. 129-133.

HOLBERY, J. and HOUSTON, D., 2006. Natural-Fiber-Reinforced Polymer Composites in Automotive Applications. *JOM,* **58**(11), pp. 80-86.

JOHN, M.J. and ANANDJIWALA, R.D., 2009. Chemical modification of flax reinforced polypropylene composites. *Composites Part A-Applied Science and Manufacturing,* **40**(4), pp. 442-448.

JONG, L., 2007. Effect of soy spent flakes and carbon black co-filler in rubber composites. *Composites Part A-Applied Science and Manufacturing,* **38**(2), pp. 252-264.

KAPUSTAN KRÜGER, P., 2007. *Wheat Straw-Polypropylene Composites*, University of Waterloo.

KARUS, M. and KAUP, M., 2002. Natural Fibres in the European Automotive Industry. *Journal of Industrial Hemp,* **7**(1), pp. 119-131.

KENNISLINK, 2009-last update, 121175_962_1098360669291-soja_klein.jpg [Homepage of Kennislink], [Online]. Available: http://www.kennislink.nl/upload/121175_962_1098360669291-soja_klein.jpg [April/17, 2009].

KIMURA, K., YOSHIKAWA, T., TAGUCHI, Y., ISHIDA, Y., OHTANI, H. and TSUGE, S., 2000. Direct determination of a polymeric hindered amine light stabilizer in

polypropylene by thermal desorption-gas chromatography assisted by in-line chemical reaction. *Analyst,* **125**(3), pp. 465-468.

KUMAR, R., CHOUDHARY, V., MISHRA, S., VARMA, I.K. and MATTIASON, B., 2002. Adhesives and plastics based on soy protein products. *Industrial Crops and Products,* **16**(3), pp. 155-172.

L'HOCINE, L., BOYE, J.I. and JOUVE, S., 2007. Ionic strength and pH-induced changes in the immunoreactivity of purified soybean glycinin and its relation to protein molecular structure. *Journal of Agricultural and Food Chemistry*, **55**(14), pp. 5819-5826.

LANG, C.A., 1958. Simple Microdetermination of Kjeldahl Nitrogen in Biological Materials. *Analytical Chemistry,* **30**(10), pp. 1692-1694.

LEE, K.H., RYU, H.S. and RHEE, K.C., 2003. Protein solubility characteristics of commercial soy protein products. *Journal of the American Oil Chemists Society*, **80**(1), pp. 85-90.

LIU, W.J., MISRA, M., ASKELAND, P., DRZAL, L.T. and MOHANTY, A.K., 2005. 'Green' composites from soy based plastic and pineapple leaf fiber: fabrication and properties evaluation. *Polymer,* **46**(8), pp. 2710-2721.

MA, F.S., PETERSON, C.A. and GIJZEN, M., 2004. Reassessment of the pits and antipits in soybean seeds. *Canadian Journal of Botany-Revue Canadienne De Botanique,* **82**(5), pp. 654-662.

MARCOVICH, N.E., REBOREDO, M.M. and ARANGUREN, M.I., 1998. Dependence of the mechanical properties of woodflour-polymer composites on the moisture content. *Journal of Applied Polymer Science,* **68**(13), pp. 2069-2076.

MCCRUM, N.G., BUCKLEY, C.P. and BUCKNALL, C.B., 1990. Principles of Polymer Engineering. Oxford: Oxford University Press.

MOHANTY, A.K., MISRA, M. and DRZAL, L.T., 2002. Sustainable bio-composites from renewable resources: Opportunities and challenges in the green materials world. *Journal of Polymers and the Environment,* **10**(1-2), pp. 19-26.

MOHANTY, A.K., MISRA, M. and HINRICHSEN, G., 2000. Biofibres, biodegradable polymers and biocomposites: An overview. *Macromolecular Materials and Engineering,* **276**(3-4), pp. 1-24.

MORALES, F.J. and VAN BOEKEL, M.A.J.S., 1998. A study on advanced Maillard reaction in heated casein/sugar solutions: Colour formation. *International Dairy Journal*, **8**(10-11), pp. 907-915.

NANDA, P.K., RAO, K.K. and NAYAK, P.L., 2007. Biodegradable polymers. XI. Spectral, thermal, morphological, and biodegradability properties of environment-friendly green plastics of soy protein modified with thiosemicarbazide. *Journal of Applied Polymer Science*, **103**(5), pp. 3134-3142.

NATIONAL SOYBEAN RESEARCH LABORATORY, , processing diagram [Homepage of National Soybean Research Laboratory], [Online]. Available: http://www.nsrl.uiuc.edu/aboutsoy/images/processing_diagram.gif [April/16, 2009].

NETRAVALI, A.N. and CHABBA, S., 2003. Composites get greener. *Materials Today*, **6**(4), pp. 22-29.

NEUROTIKER, 2008-last update, Ponceau_S.svg [Homepage of http://en.wikipedia.org], [Online]. Available: http://en.wikipedia.org/wiki/File:Ponceau_S.svg [April/17, 2009].

NEW MEXICO TECH, 2007-last update, materials & metallurgical department, new mexico tech. Available: http://www.nmt.edu.proxy.lib.uwaterloo.ca/2006].

NG, Z.S., 2008. *Bulk Orientation of Agricultural Filler-Polypropylene Composites*, University of Waterloo.

NGUYEN, M., Great Expectations of Food Proteins: Can Soy Proteins measure up? "Unlocking the Value of Soy Protein in Consumer Foods" Symposium October 18th, 2007, Ontario, Canada.

NISHINO, T., MATSUDA, I. and HIRAO, K., 2004. All-cellulose composite. *Macromolecules*, **37**(20), pp. 7683-7687.

PAETAU, I., CHEN, C.Z. and JANE, J.L., 1994. Biodegradable Plastic made from Soybean Products .1. Effect of Preparation and Processing on Mechanical-Properties and Water-Absorption. *Industrial & Engineering Chemistry Research*, **33**(7), pp. 1821-1827.

PANTHAPULAKKAL, S. and SAIN, M., 2007. Studies on the water absorption properties of short hemp-glass fiber hybrid polypropylene composites. *Journal of Composite Materials*, **41**(15), pp. 1871-1883.

PHARMACEUTICAL ONLINE, 2009-last update, minilab.jpg [Homepage of VertMarkets, Inc.], [Online]. Available: http://www.pharmaceuticalonline.com/article.mvc/9-18-08-NL-Manufacturing-Tablet-Coatings-0001 [April/20, 2009].

PROGELHOF, R.C. and THRONE, J.L., 1993. Polymer Engineering Principles Properties, Processes, and Tests for Design. Hanser/Gardner Publications, Inc.

QIU, W.L., ZHANG, F.R., ENDO, T. and HIROTSU, T., 2005. Effect of maleated polypropylene on the performance of polypropylene/cellulose composite. *Polymer Composites,* **26**(4), pp. 448-453.

RANA, A.K., MANDAL, A., MITRA, B.C., JACOBSON, R., ROWELL, R. and BANERJEE, A.N., 1998. Short jute fiber-reinforced polypropylene composites: Effect of compatibilizer. *Journal of Applied Polymer Science,* **69**(2), pp. 329-338.

RAY-RAN POLYTEST, , injection_moulding_scr.pdf [Homepage of Ray-Ran Polytest], [Online]. Available: http://www.ray-ran.com/ [April/17, 2009].

REHM, B.H.A. and STEINBÜCHEL, A., 1999. Biochemical and genetic analysis of PHA synthases and other proteins required for PHA synthesis, *International Journal of Biological Macromolecules,* JUN-JUL 1999, pp3-19.

RETSCH GMBH, 2006-last update, 9249f0561e.jpg [Homepage of RETSCH GmbH], [Online]. Available: http://www.retsch-us.com/us/products/milling/rotor-mills/zm-200/ [April/17, 2009].

RETSCH GMBH & CO. KG, 2003. Technical Data Sheet for Ultra-Cetrifugal Mill ZM 200, Subject to technical modification 99.823.0001/E-05-2003.

ROSNER, R.B., 2001-last update, conductive materials for ESD applications: an overview [Homepage of Compliance Engineering], [Online]. Available: http://www.ce-mag.com/archive/01/Spring/TOC.html [April/17, 2009].

RUSSIN, T.A., ARCAND, Y. and BOYE, J.I., 2007. Particle size effect on soy protein isolate extraction. *Journal of Food Processing and Preservation,* **31**(3), pp. 308-319.

RYHÄNEN, J., 1999. *Biocompatibility evaluation of nickel-titanium shape memory metal alloy,* Oulu University Library.

SAHEB, D.N. and JOG, J.P., 1999. Natural fiber polymer composites: A review. *Advances in Polymer Technology,* **18**(4), pp. 351-363.

SCHMIDT, V., GIACOMELLI, C. and SOLDI, V., 2005. Thermal stability of films formed by soy protein isolate-sodium dodecyl sulfate. *Polymer Degradation and Stability,* **87**(1), pp. 25-31.

SOY 20/20, 8/2008. Soybean Meal – A Canadian Market Review.

STEINBÜCHEL, A., 2002. Biopolymers. Wiley-VCH.

SUE, H.J., WANG, S. and JANE, J.L., 1997. Morphology and mechanical behaviour of engineering soy plastics. *Polymer,* **38**(20), pp. 5035-5040.

SWAIN, S.N., RAO, K.K. and NAYAK, P.L., 2005. Biodegradable polymers Part II. Thermal degradation of biodegradable plastics cross-linked from form aldehyde-soy protein concentrate. *Journal of Thermal Analysis and Calorimetry,* **79**(1), pp. 33-38.

THERMO HAAKE, 2002. Instruction Manual MiniLab Rheomex CTW5; Part No. 003-5806; 3-1-067-2.

TKACZYK, A.H., OTAIGBE, J.U. and HO, K.L.G., 2001. Bioabsorbable soy protein plastic composites: Effect of polyphosphate fillers on biodegradability. *Journal of Polymers and the Environment,* **9**(1), pp. 19-23.

TON-THAT, T.M. and JUNGNICKEL, B.J., 1999. Water diffusion into transcrystalline layers on polypropylene. *Journal of Applied Polymer Science,* **74**(13), pp. 3275-3285.

TORO, P., QUIJADA, R., ARIAS, J.L. and YAZDANI-PEDRAM, M., 2007. Mechanical and morphological studies of poly(propylene)-filled eggshell composites. *Macromolecular Materials and Engineering,* **292**(9), pp. 1027-1034.

VAZ, C.A., MANO, J.F., FOSSEN, M., VAN TUIL, R.F., DE GRAAF, L.A., REIS, R.L. and CUNHA, A.A., 2002. Mechanical, dynamic-mechanical, and thermal properties of soy protein-based thermoplastics with potential biomedical applications. *Journal of Macromolecular Science-Physics,* **B41**(1), pp. 33-46.

WANG, B. and SAIN, M., 2007. Dispersion of soybean stock-based nanofiber in a plastic matrix. *Polymer International,* **56**(4), pp. 538-546.

WANG, Y., CAO, X. and ZHANG, L., 2006. Effects of cellulose whiskers on properties of soy protein thermoplastics. *Macromolecular Bioscience*, **6**(7), pp. 524-531.

WEBB, D.T., , BeanSeedXSEpi400Lab.jpg [Homepage of University of Hawaii at Manoa], [Online]. Available: http://www.botany.hawaii.edu/faculty/webb/BOT410/Angiosperm/Seeds/Seed-4.htm [April/17, 2009].

UNITED STATES DEPARTMENT OF AGRICULTURE., 2008 [Homepage of USDA], [Online]. Available: http://www.usda.gov/wps/portal/usdahome [May/10, 2009].

WOLF, W.J., 1970. Soybean proteins: Their Functional, Chemical, and Physical Properties. **18**(6),.

WU, W.U., HETTIARACHCHY, N.S. and QI, M., 1998. Hydrophobicity, solubility, and emulsifying properties of soy protein peptides prepared by papain modification and ultrafiltration. *Journal of the American Oil Chemists Society*, **75**(7), pp. 845-850.

YIKRAZUUL, 2008-last update, Coomassie_Brilliant_Blue_G-250.svg [Homepage of http://en.wikipedia.org], [Online]. Available: http://en.wikipedia.org/wiki/File:Coomassie_Brilliant_Blue_G-250.svg [April/17, 2009].

ZHANG, L., CHEN, P., HUANG, J., YANG, G. and ZHENG, L.S., 2003. Ways of strengthening biodegradable soy-dreg plastics. *Journal of Applied Polymer Science*, **88**(2), pp. 422-427.

APPENDIX

ALKALINE EXTRACTION

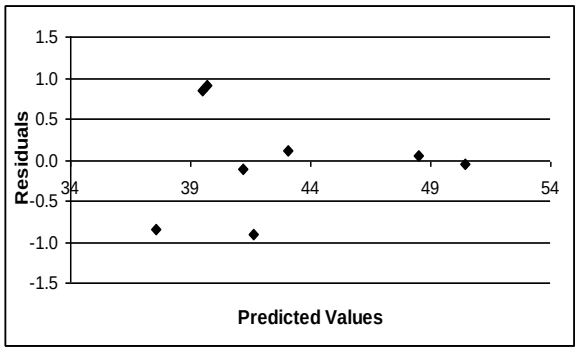

Figure 5-1 Residual plot of all results.

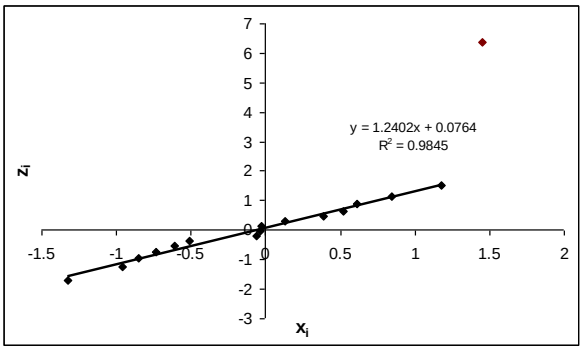

Figure 5-2 Normal probability plot of the residuals (outlier is not included in trend line).

Table 5-1 Summary of the filler compositions. The amount of carbohydrate was determined by taking the difference of the total weight and the protein and ash content.

Filler	total weight [g]	total [%]	Protein [%]	SD (n = 6) [%]	Protein [g]	Carbohydrates [%]	Carbohydrates [g]	Ash [%]	SD (n = 3) [%]	Ash [g]
SF (Bunge)	150	100	56.54	0.50	84.81	37.71	56.57	5.75	0.21	8.63
IS_{H2O}	66.07	100	49.95	0.04	33.00	44.43	29.36	5.62	0.10	3.71
IS_{NaCl}	90.11	100	45.76	0.06	41.23	35.52	32.01	18.72	0.20	16.87
Soy Flour (Ford)	150	100	50.51	2.92	75.77	44.28	66.42	5.21	0.68	7.82

KJELDAHL PROTEIN ANALYSIS

Equation 5-1 shows the formula used to calculate the protein concentration of the samples. Assuming a sample of 10 mg was tested with the Kjeldahl protein analysis explained in section 3.2.2. The solution for the calorimetric measurement shall be diluted with a factor of 2 and the average of the three measured absorbance values shall be 0.3. A typical calibration curve is shown in Figure 5-3 and is used for the calculation of this example given in Equation 5-2 with the result of 28.62 % protein in the sample.

$$protein\,(wt\text{–}\%) = \frac{Abs_{sample}}{B} * d_1 * d_2 * d_3 * 6.25 * \frac{1}{mass_{sample}} * 100 \qquad \text{Equation 5-1}$$

$d_1 = dilution\ in\ volumetric\ flask = 100$

$d_2 = dilution\ for\ measurement$

$d_3 = dilution\ in\ microtiterplate\,(50\mu l\ sample\ instead\ of\ 1ml\ \ for\ test\ tube) = 5$

$$\frac{0.3}{0.6551} * 100 * 2 * 5 * 6.25 * \frac{1}{10000\ \ \mu g} * 1000 = 28.62\ \%\ protein \qquad \text{Equation 5-2}$$

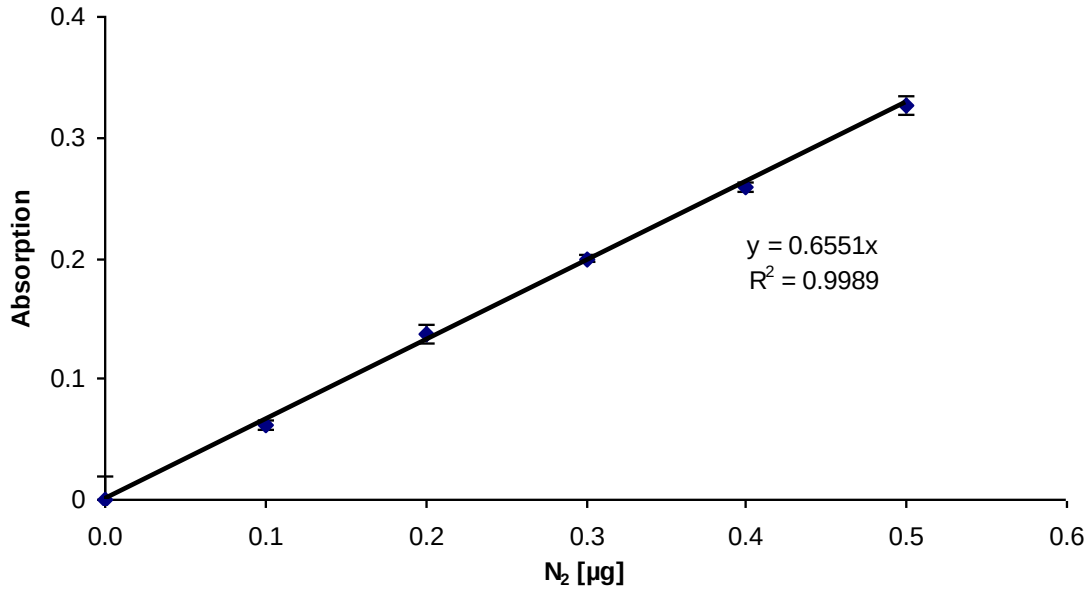

Figure 5-3 Calibration curve obtained from Kjeldahl protein analysis. The used standard was 4.714 g/l ammonium sulphate that was treated in the same way as the samples according to the method explained in section 3.2.2.

PARTICLE SIZE ANALYSIS

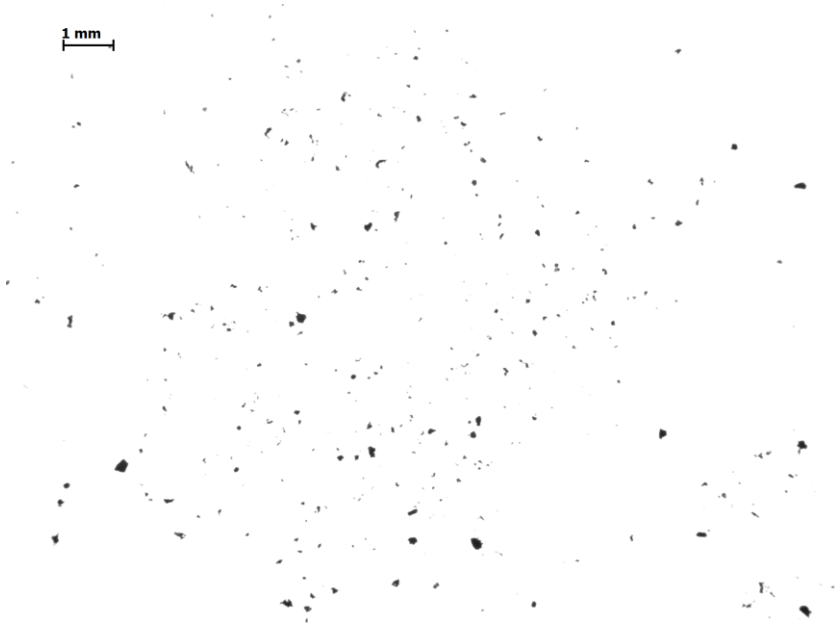

Figure 5-4 Representative image of particle size analysis of IS_{H2O}.

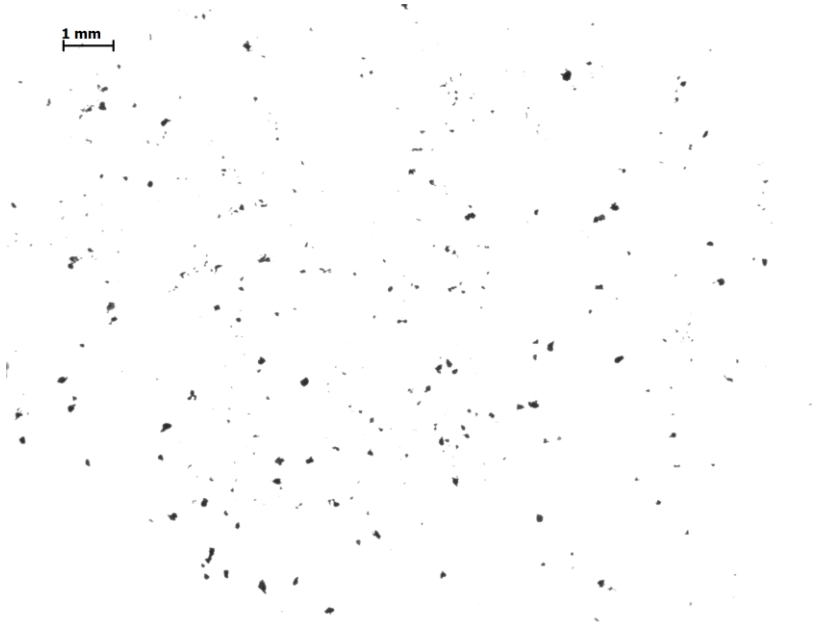

Figure 5-5 Representative image of particle size analysis of IS_{NaCl}.

Figure 5-6 Representative image of particle size analysis of soy flour (Ford).

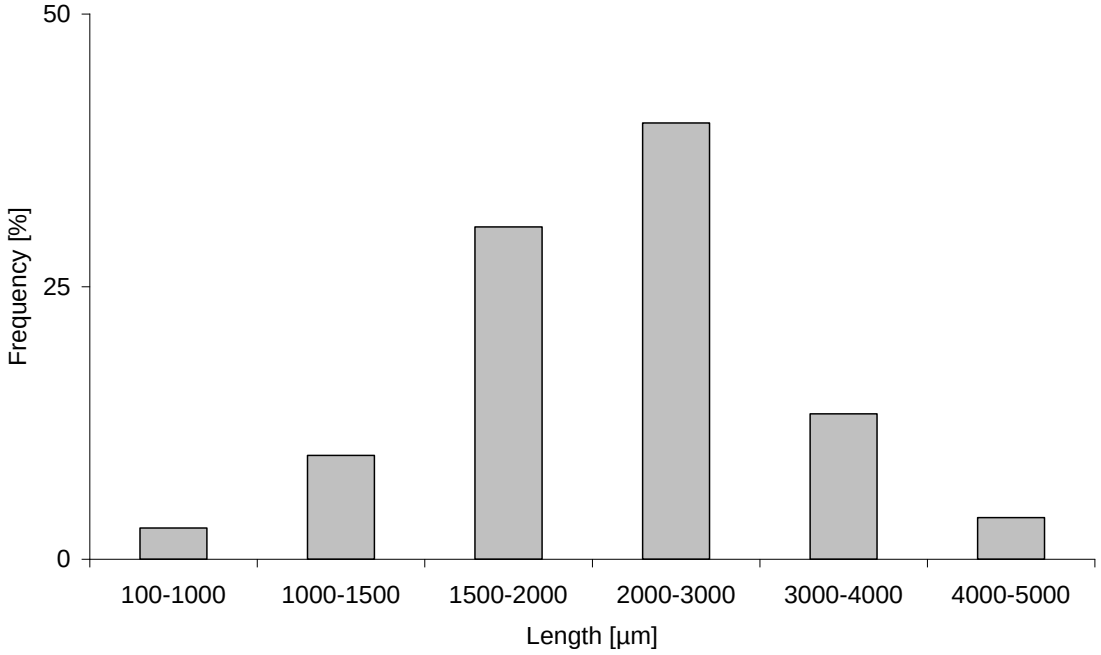

Figure 5-7 Particle size distribution of the soy flakes (as received) provided by Bunge Inc.

DIFFERENTIAL SCANNING CALORIMETRY (DSC)

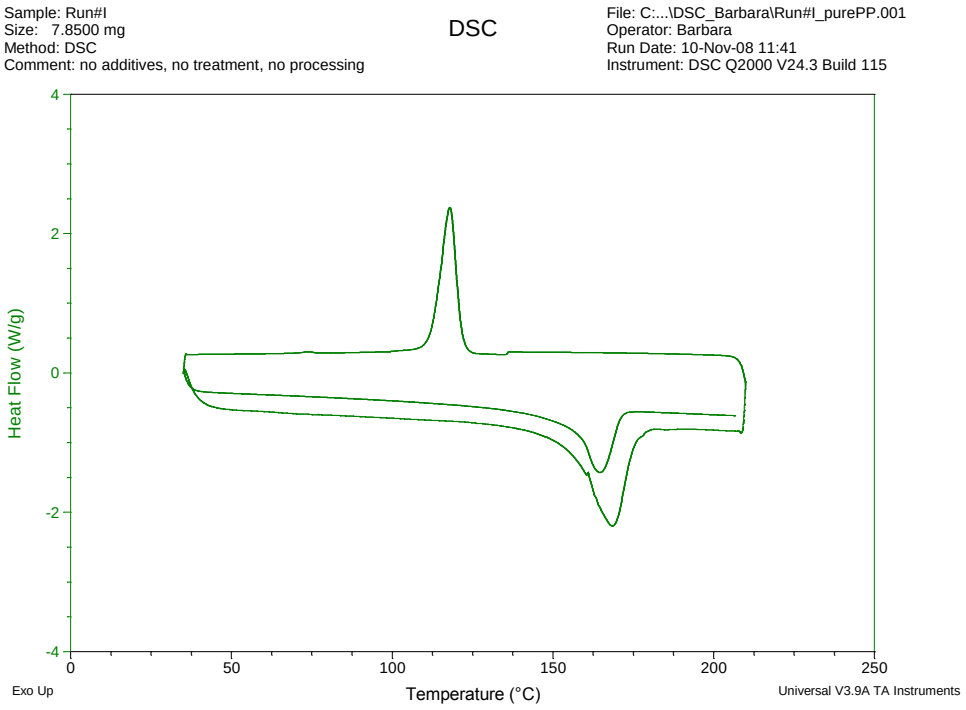

Figure 5-8 DSC curve Run # I.

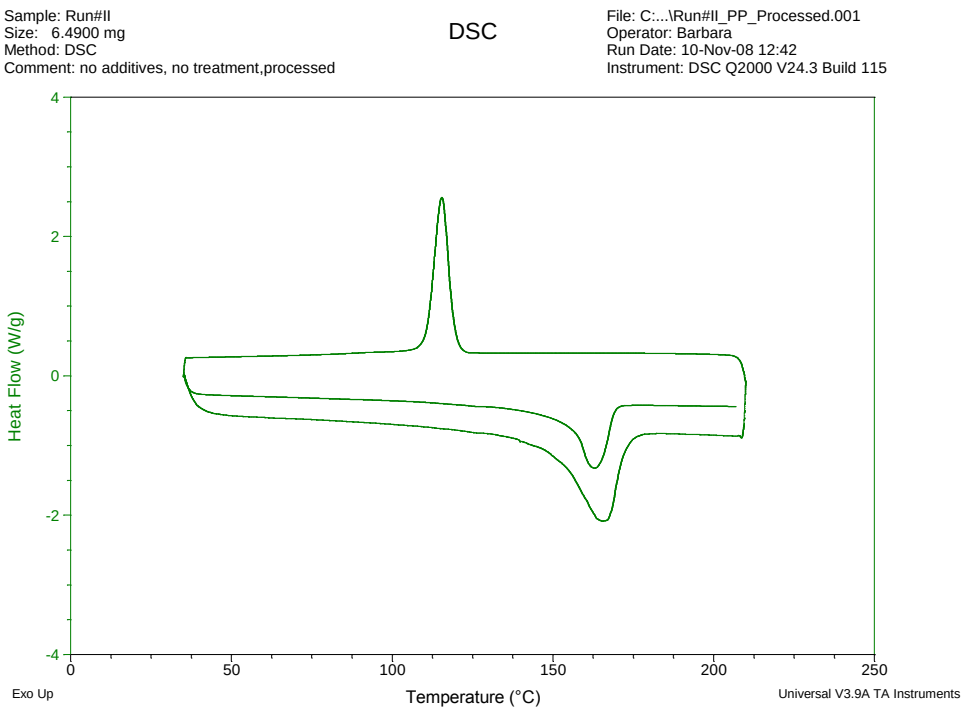

Figure 5-9 DSC curve Run # II

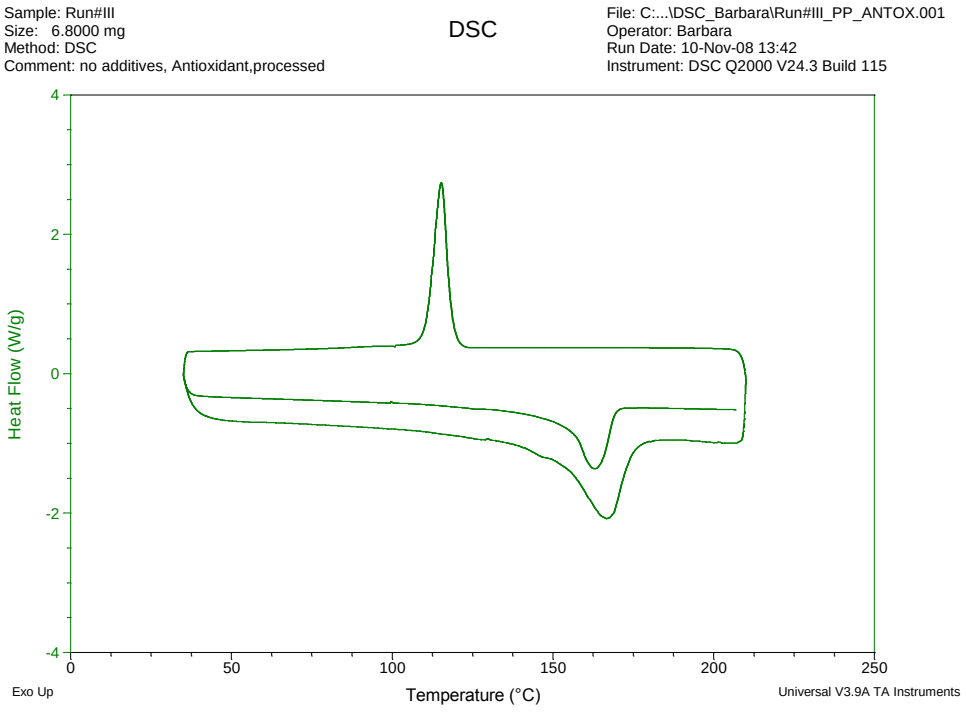

Figure 5-10 DSC curve Run # III

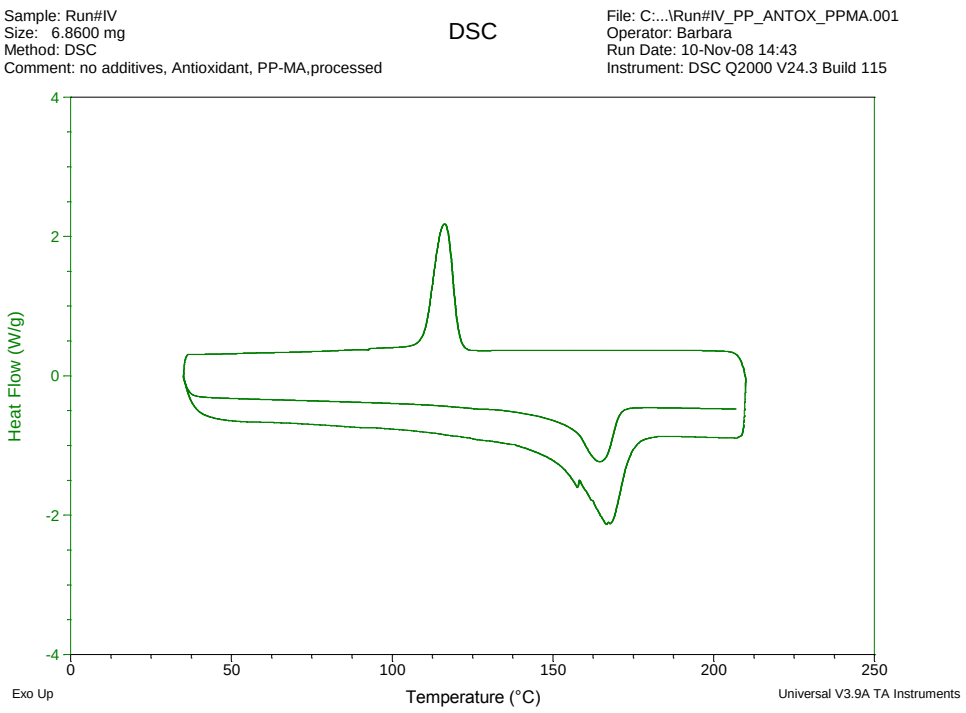

Figure 5-11 DSC curve Run # IV.

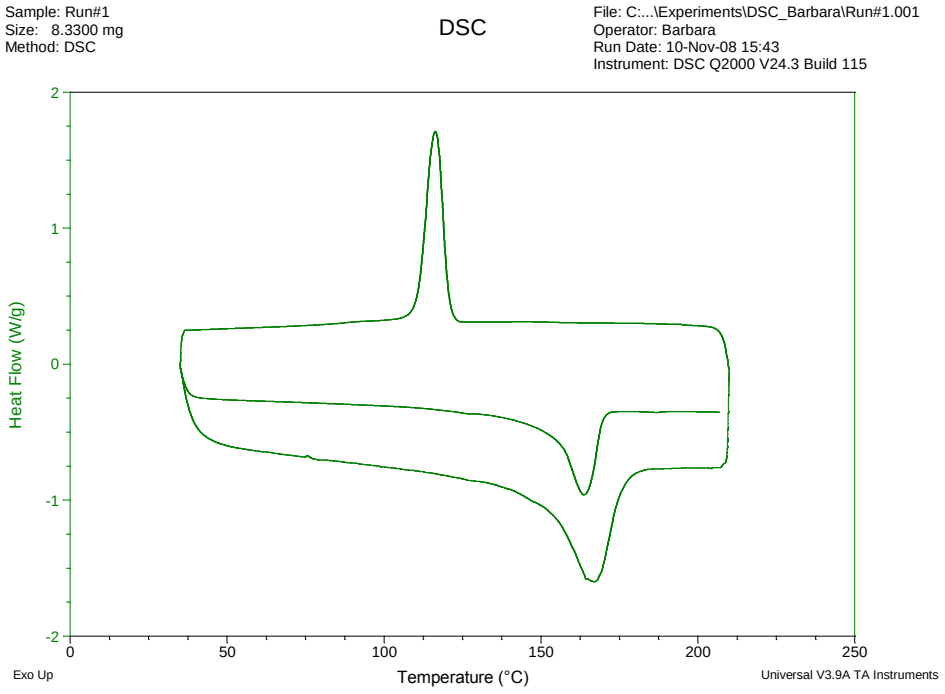

Figure 5-12 DSC curve Run # 1.

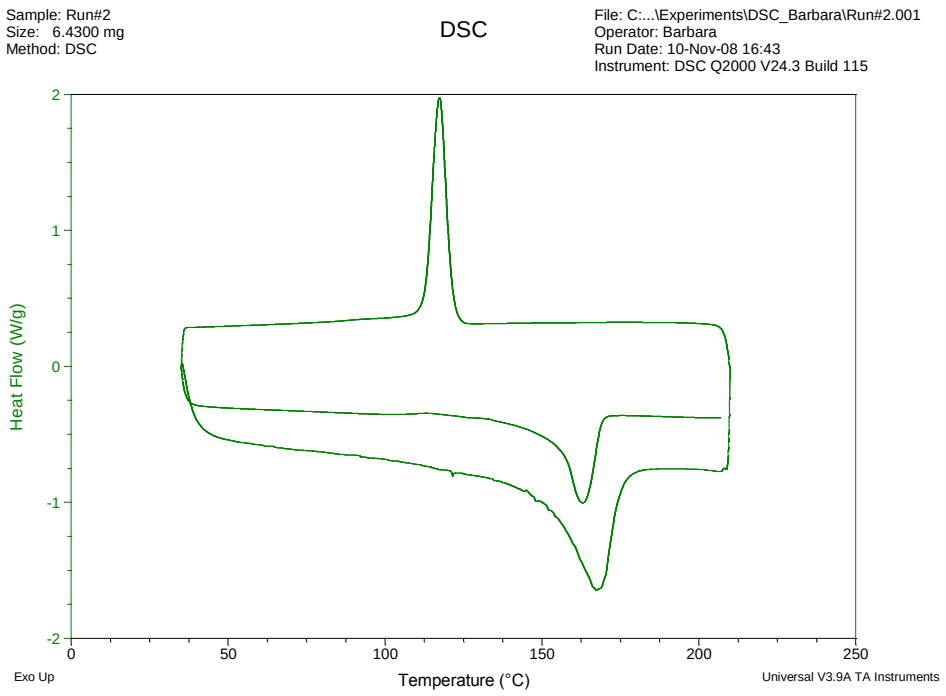

Figure 5-13 DSC curve Run # 2.

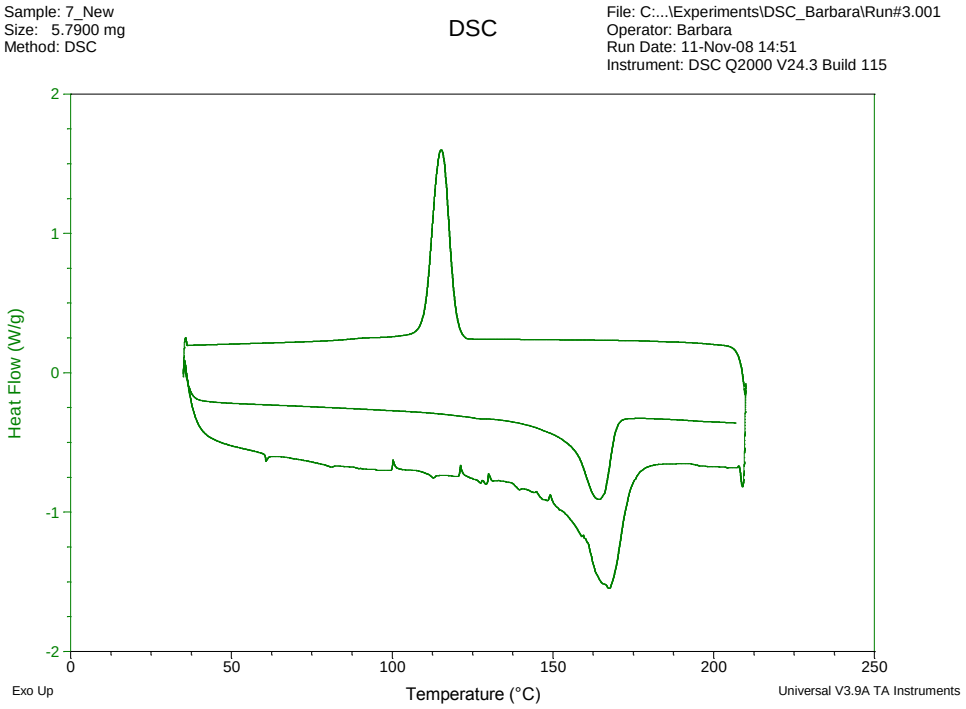

Figure 5-14 DSC curve Run # 3.

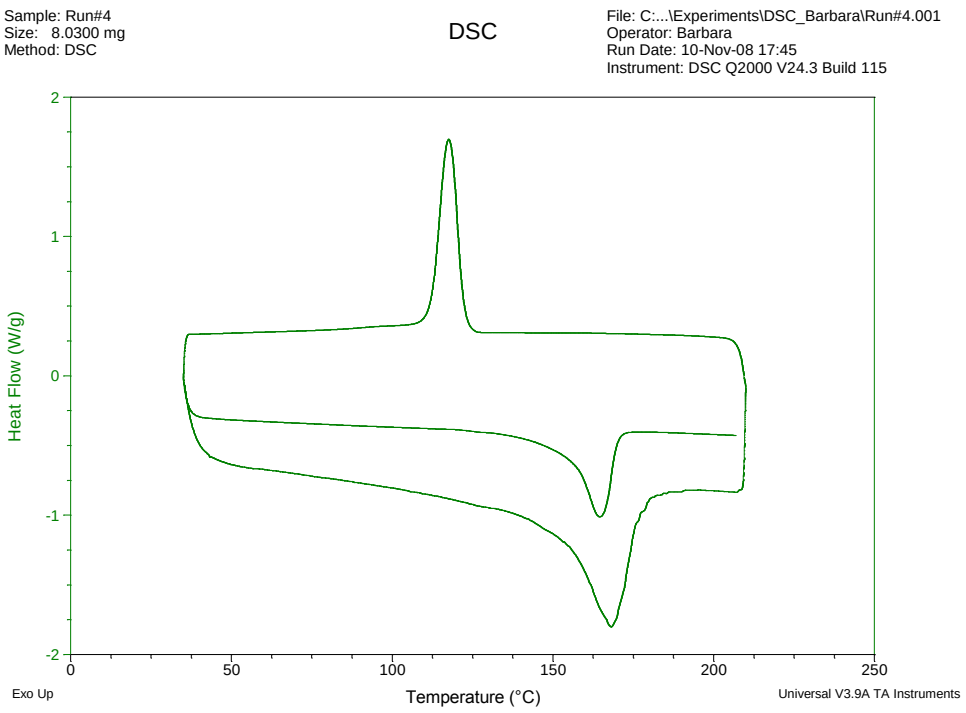

Figure 5-15 DSC curve Run # 4.

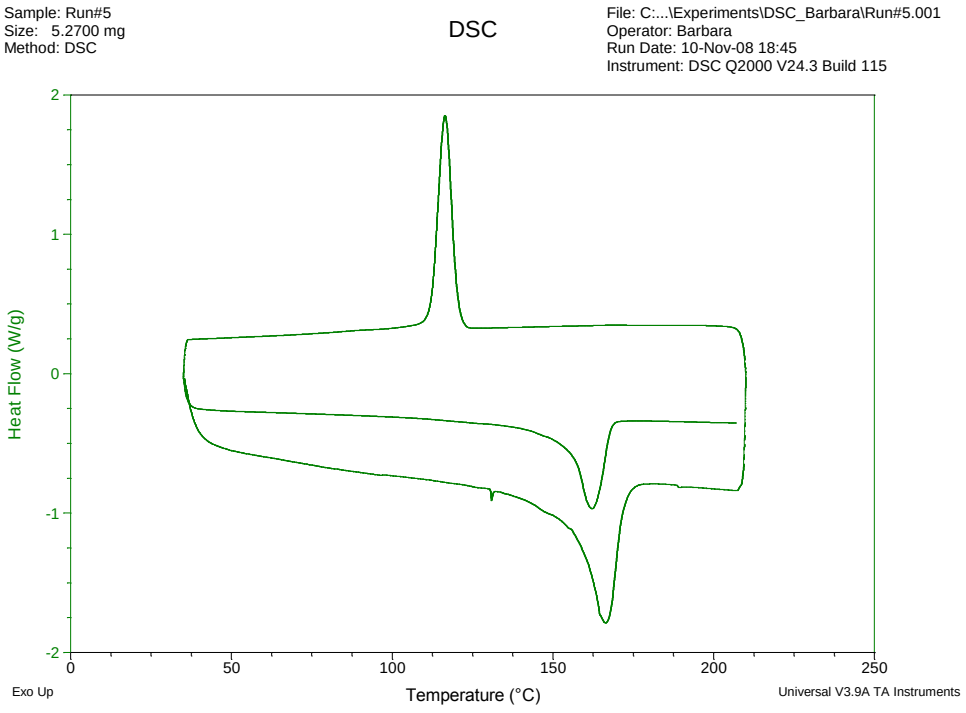

Figure 5-16 DSC curve Run # 5.

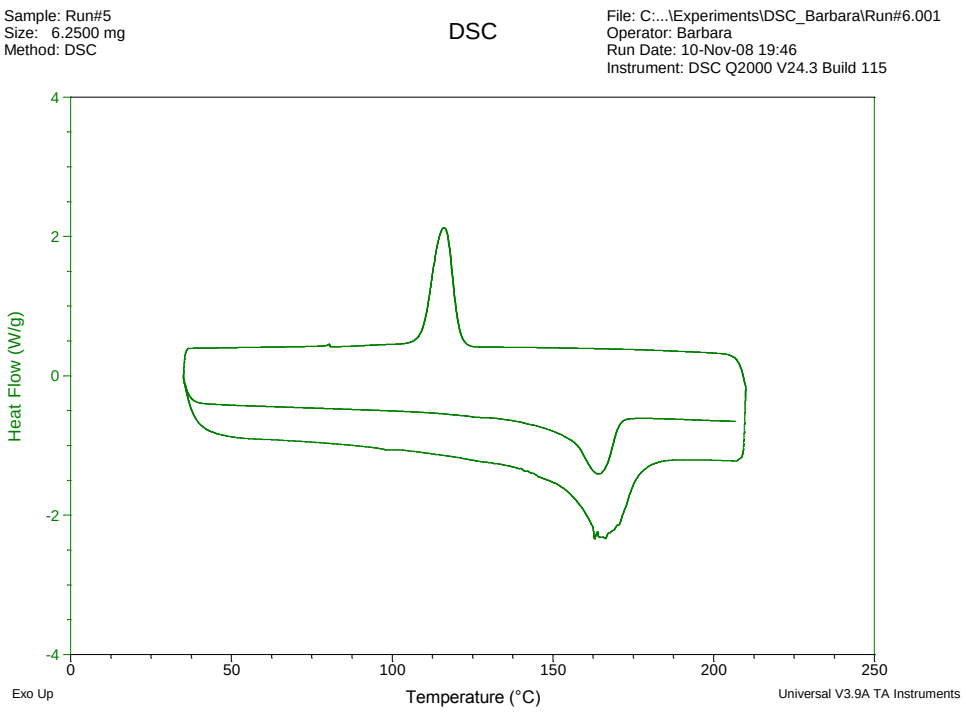

Figure 5-17 DSC curve Run # 6.

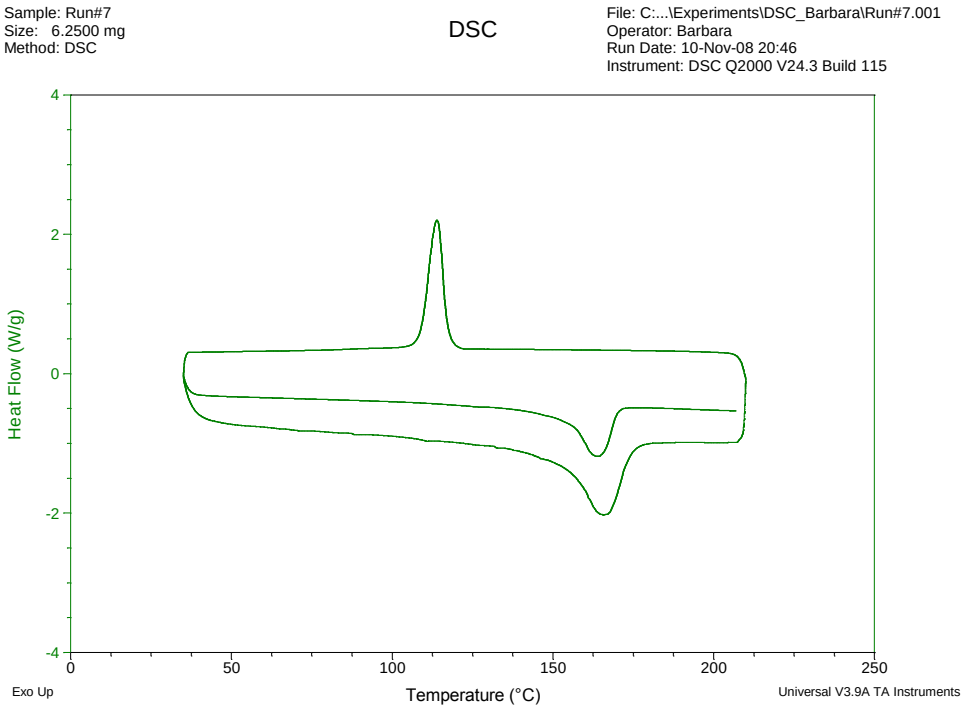

Figure 5-18 DSC curve Run # 7.

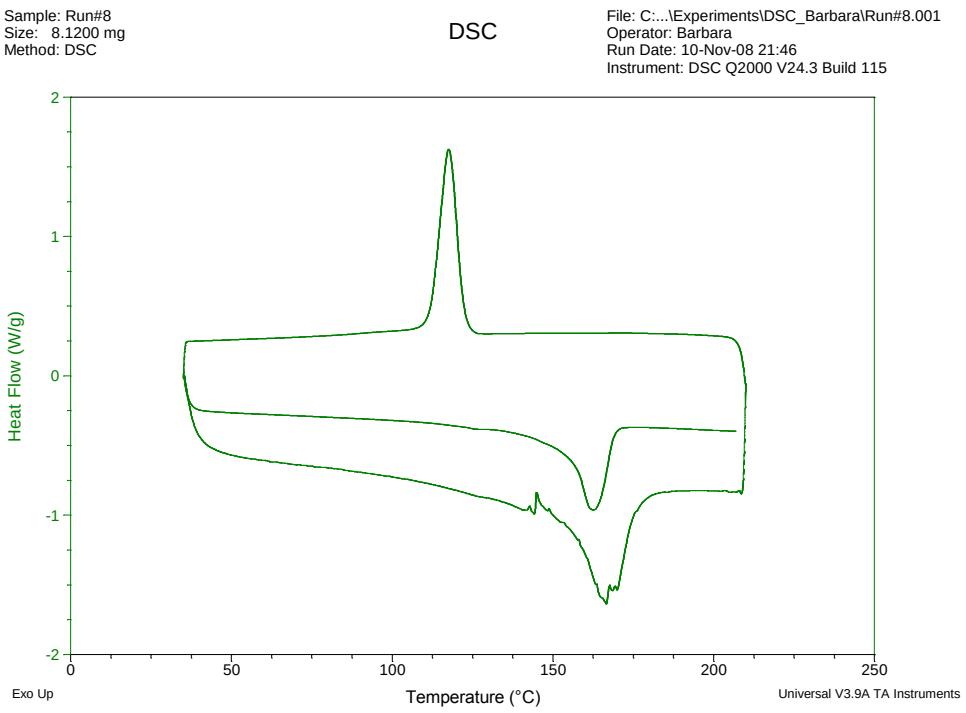

Figure 5-19 DSC curve Run # 8.

COMPOUNDING FORMULATION FOR EXTRUSION

Table 5-2 Compounding formulations for extrusion.

Run	Filler type	Filler treatment	Matrix/Coupling agent	Filler [%]	Anti-oxidant
I	None	None	PP (no extrusion)	None	None
II	None	None	PP		
III	None	None	PP		0.35 % Irganox 1010
IV	None	None	3 % MA-PP		
1	SF (Bunge)	None	PP	30	0.35 % Irganox 1010
2	SF (Bunge)	None	3 % MA-PP		
3	IS	AE in H_2O	PP		
4	IS	AE in H_2O	3 % MA-PP		
5	IS	AE in NaCl	PP		
6	IS	AE in NaCl	3 % MA-PP		
7	Soy Flour (Ford)	None	PP		
8	Soy Flour (Ford)	None	3 % MA-PP		